

MODELING OF A HIGH TEMPERATURE PEM FUEL CELL

A THESIS SUBMITTED TO
THE GRADUATE SCHOOL OF NATURAL AND APPLIED SCIENCES
OF
MIDDLE EAST TECHNICAL UNIVERSITY



BY
BERNA SEZGİN

IN PARTIAL FULFILLMENT OF THE REQUIREMENTS
FOR
THE DEGREE OF MASTER OF SCIENCE
IN
CHEMICAL ENGINEERING

NOVEMBER 2016

Approval of thesis:

MODELING OF A HIGH TEMPERATURE PEM FUEL CELL

submitted by **BERNA SEZGİN** in partial fulfillment of the requirements for the degree of **Master of Science in Chemical Engineering Department, Middle East Technical University** by,

Prof. Dr. Gülbin Dural Ünver
Dean, Graduate School of **Natural and Applied Sciences** _____

Prof. Dr. Halil Kalıpçılar
Head of Department, **Chemical Engineering** _____

Prof. Dr. İnci Eroğlu
Supervisor, **Chemical Engineering Dept., METU** _____

Assoc. Prof. Dr. Yılser Devrim
Co-Supervisor, **Energy Systems Eng. Dept., Atılım University** _____

Examining Committee Members:

Assoc. Prof. Dr. Serkan Kınca
Chemical Engineering Dept., METU _____

Prof. Dr. İnci Eroğlu
Chemical Engineering Dept., METU _____

Assoc. Prof. Dr. Yılser Devrim
Energy Systems Eng. Dept., Atılım University _____

Assoc. Prof. Dr. Görkem Külâh
Chemical Engineering Dept., METU _____

Asst. Prof. Dr. Ekin Özgirgin Yapıcı
Mechanical Engineering Dept., Çankaya University _____

Date: 07.11.2016



I hereby declare that all information in this document has been obtained and presented in accordance with academic rules and ethical conduct. I also declare that, as required by these rules and conduct, I have fully cited and referenced all material and results that are not original to this work.

Name, Last Name: Berna SEZGİN

Signature:

ABSTRACT

MODELING OF A HIGH TEMPERATURE PEM FUEL CELL

Sezgin, Berna

M.Sc., Department of Chemical Engineerin

Supervisor: Prof. Dr. İnci Erođlu

Co-Supervisor: Assoc. Prof. Yılsar Devrim

November 2016, 113 pages

High temperature polymer electrolyte membrane fuel cells (HT-PEMFC) are considered as the next generation of fuel cells since high temperature operation for PEM fuel cells has several advantages such as single phase operation, high carbon monoxide tolerance, low or zero carbon emission and removal of some equipment from the system. In order to obtain high performances, HT-PEMFC systems should be optimized in terms of dimensions, materials, operating conditions and other parameters. Modeling can help to pre-estimate the effects of different design parameters and operating conditions on the fuel cell performance, which shortens the required time for these analysis in reference to the time spent for experiments.

In this study, three-dimensional (3-D) model of HT-PEMFC is developed. The model is implemented as isothermal and steady-state. Model domains are considered for two different geometries: single flow channel and multiple flow channels. Models are simulated by using licensed software package program Comsol Multiphysics 5.0, and its Fuel Cells & Batteries module. The program has solved the governing equations by finite element method. Moreover, it is an advantage to use this program for HT-PEMFC modeling by the reason of including Fuel Cell module.

In the scope of this study, some critical parameters are prescribed as effective parameters for HT-PEMFC performance. These are inlet velocities (or flow rates) of reactant gases to the both anode and cathode inlet gas channels, conductivity of the membrane and meshing strategy. Influences of inlet velocities of reactant gases and conductivity of the membrane are studied for both single channel and multiple channel HT-PEMFC models, while influence of meshing strategy is studied for only multiple channel HT-PEMFC model. It is seen that increasing inlet velocities of reactants (hydrogen and air) enhances HT-PEMFC performance as long as enough oxygen is supplied to the system. In addition, increasing proton conductivity of the membrane provides better performance for both channel geometries. For the effect of meshing strategy, it is found that the results are more accurate for small size of mesh elements. For all models that have been developed are validated with the experimental data.

Keywords: HT-PEMFC modeling, Sensitivity analysis, Comsol Multiphysics

ÖZ

YÜKSEK SICAKLIKTA ÇALIŞAN PEM YAKIT PİLİNİN MODELLENMESİ

Sezgin, Berna
Yüksek Lisans, Kimya Mühendisliği Bölümü
Tez Yöneticisi: Prof. Dr. İnci Eroğlu
Ortak Tez Yöneticisi: Doç. Dr. Yılser Devrim

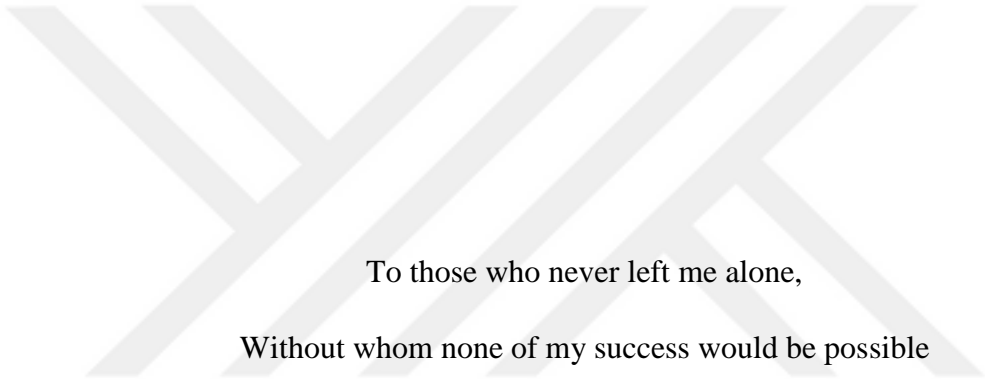
Kasım 2016, 113 sayfa

Yüksek sıcaklıkta çalışan polimer elektrolit membran yakıt pilleri (HT-PEMFC), birçok avantaj sağladığı için yakıt pillerinin gelecek nesli olarak düşünülmektedir. Yüksek sıcaklık operasyonun sağladığı avantajlar: tek fazlı operasyon, yüksek karbon monoksit toleransı, düşük ya da sıfır karbon emilimi ve bazı ekipmanların sistemden çıkarılabilmesidir. Yüksek sıcaklıkta çalışan PEM yakıt pillerinin boyutları, materyalleri, çalışma koşulları ve diğer parametreleri daha iyi performanslar elde edebilmek için optimize edilmelidir. Modelleme, farklı tasarım parametrelerinin ve çalışma koşullarının yakıt pili performansı üzerindeki etkisini öngörmeye yardımcı olmaktadır. Ayrıca, bu analizlerin modelleme ile yapılması, deneysel olarak yapılmasından daha kısa süreceği için zaman kazandırmaktadır.

Bu çalışmada, üç boyutlu yüksek sıcaklıkta çalışan PEM yakıt pili geliştirilmiştir. Model, eş sıcaklıklı ve durağan durumda gerçekleştirilmiştir. Model alanı, tek akış kanalına ve çoklu akış kanalına sahip olarak iki farklı geometride düşünülmüştür. Geliştirilen modeller, lisanslı ve paket yazılım programı olan Comsol Multiphysics 5.0 programı ile çalıştırılmış ve programın Yakıt Pilleri & Bataryalar modülü kullanılmıştır. Bu programda, korunum denklemleri sonlu element metodu ile çözülmektedir. Ayrıca, Yakıt Pilleri modülünün bulunması bu programın yüksek sıcaklıkta çalışan PEM yakıt pillerinin kullanılmasında avantaj sağlamaktadır.

Bu çalışma kapsamında bazı kritik parametreler yüksek sıcaklıkta çalışan PEM yakıt pili performansı etkileyen parametreler olarak öngörülmüştür. Bu parametreler: anot ve katot tarafına beslenen reaktant gazların giriş hızları (veya debileri), polimer membranın proton iletkenliği ve çözüm ağı stratejisidir. Reaktantların sisteme giriş hızlarının etkisi ve polimer membranın proton iletkenliğinin etkisi, hem tek akış kanalına sahip hem de çoklu akış kanalına sahip modeller için çalışılmıştır. Ancak çözüm ağı stratejisinin etkisi sadece çoklu akış kanalına sahip model için çalışılmıştır. Çalışmanın sonucunda görülmüştür ki, sisteme yeterli oksijen beslendiği sürece reaktantların sisteme giriş hızlarının artırılması performansı olumlu yönde etkilemiştir. Buna ek olarak, polimer membranın proton iletkenliğinin artırılması da daha iyi performans elde edilmesini sağlamıştır. Çözüm ağı etkisinin incelenmesinde ise görülmüştür ki çözüm elementlerinin boyutu küçüldükçe daha hassas sonuçlar elde edilmiştir. Elde edilen tüm model sonuçları, deney sonuçları ile doğrulanmıştır.

Anahtar kelimeler: HT-PEMFC modelleme, Duyarlık analizi, Comsol Multiphysics



To those who never left me alone,
Without whom none of my success would be possible

ACKNOWLEDGEMENTS

I would like to express my deepest appreciations to my supervisor Prof. Dr. İnci Erođlu for her unbroken support, great guidance and utmost contributions throughout my study. I am thankful to her for encouraging me to overcome any problem I had ever met. Without her wise approach, I would never had gained all precious knowledge and experiences in all aspects of my life. My last, but not the least appreciation for her is introducing me with fuel cells, which changes the way of my life.

I also would like to thank to my co-supervisor Assoc. Prof. Dr. Yılser Devrim for her precious guidance and supports. Her knowledge and experience are very valuable for this study. I feel spirited by her benefactor attitude towards me.

I would like to thank to Hüseyin Devrim, Tek-sis İleri Teknolojiler and Danish Power Systems for being always well-disposed to me in my personal and academic life. I owe to especially Hüseyin Devrim and Tek-sis İleri Teknolojiler for supporting me throughout my study.

I would like to present my gratitude to Assoc. Prof. Dr. Serkan Kınca for his unquestioning support for technical problems I had met while using Comsol Mutiphysics.

This study is supported by the Scientific and Technological Research Council of Turkey (TUBITAK) 1001 (Grant number: 214M301) Project. This support is gratefully acknowledged.

I would like to thank to Elsevier for the copyrights of our published paper that is included as a chapter in my M.Sc. thesis.

I would like to thank to one of my dearest friends, Dilara Gülçin Çağlayan, for being an awesome friend and partner. I am also thankful for her to being always together, that I have already missed, and trying to overcome all problems together. She is the one that I enjoyed with while learning fuel cells and Comsol Multiphysics.

I would like to present my lovely thanks to Deniz Kaya for her true friendship that I have loved to share since 2009. I also would like to thank to my beloved friends Merve Tufan, Elif Kocaman, Zeynep Sümer, Onur Yüksel, Gökhan Karabıyık, Ebru Okur and Özge Erdemir for their precious friendship and moral supports.

I would like to thank to Atalay Çalışan and Berrak Erkmen for their motivation and advices they provided. I would also like to thank to Gökçe Avcıoğlu and Emine Kayahan for their supports.

Last but not the least; I would like to present my sincerest thanks to my family; especially to my dearest mom, and my dad, aunts and cousins for their unconditional love and support under any circumstances. Throughout my whole life, they always believe me that I can success.

TABLE OF CONTENTS

ABSTRACT	v
ÖZ.....	vii
ACKNOWLEDGEMENTS	x
TABLE OF CONTENTS	xii
LIST OF TABLES	xv
LIST OF FIGURES.....	xvi
LIST OF SYMBOLS.....	xx
LIST OF ABBREVIATIONS	xxii
CHAPTERS	
1. INTRODUCTION.....	1
2. HIGH TEMPERATURE PEM FUEL CELLS	7
2.1. HT-PEMFC Operation Principles	8
2.2. HT-PEMFC Components	11
2.2.1. Membrane.....	11
2.2.2. Catalyst Layers	14
2.2.3. Gas Diffusion Layers.....	15
2.2.4. Bipolar Plates (Flow Fields).....	15
2.3. Review of PEMFC Modeling.....	18
3. MODEL DEVELOPMENT BY COMSOL MULTIPHYSICS	23
3.1. Algorithm of Comsol Multiphysics.....	23
3.2. HT-PEMFC Model Development having Single Flow Channel.....	61
3.3. HT-PEMFC Model Development having Multiple Flow Channels	64

4. MODELING AND SENSITIVITY ANALYSIS OF HIGH TEMPERATURE PEM FUEL CELLS BY USING COMSOL MULTIPHYSICS ¹	67
4.1. Introduction	67
4.2. Experimental	70
4.3. Modeling Approach.....	70
4.3.1. Modeling Instructions	70
4.3.2. Assumptions	72
4.3.3. General Equations	72
4.3.4. Boundary Conditions	73
4.3.4. 3D Comsol Multiphysics Model	74
4.4. Results and Discussions	75
4.4.1. Effect of Inlet Air Velocity on Performance of HT-PEMFC.....	75
4.4.2. Effect of Inlet Hydrogen Velocity on Performance of HT-PEMFC	78
4.4.3. Effect of Proton Conductivity of PBI Membrane on Performance of HT-PEMFC	81
4.4.4. Channel Concentration Profiles of Reactants and Products along a Single Channel	83
4.5. Conclusion.....	86
5. SENSITIVITY ANALYSIS OF HT-PEMFC.....	87
5.1. Model Validation.....	88
5.2. Effect of Proton Conductivity of the Membrane.....	94
5.3. Effect of Inlet Velocities of Reactants (Hydrogen and Air).....	95
5.4. Effect of Meshing Strategy	97
6. CONCLUSIONS	101
REFERENCES.....	103

APPENDICES

A. COMPUTER SPECIFICATIONS..... 109

B. EXPERIMENTAL SET-UP 113



LIST OF TABLES

TABLES

Table 1.1 Main characteristics of different types of fuel cells	3
Table 2.1 Comparison of PBI and PBI/SiO ₂ membrane in terms of acid doping, proton conductivity and acid leaching [14].....	14
Table 2.2 Previous studies of PEMFC modeling available in the literature	21
Table 2.3 Continuation of Table 2.2	22
Table 3.1 Parameters list embedded in Comsol Multiphysics for HT-PEMFC modeling having single flow channel.....	62
Table 3.2 Continuation of Table 3.1	63
Table 3.3 Parameters list embedded in Comsol Multiphysics for HT-PEMFC modeling having multiple flow channel.....	65
Table 3.4 Continuation of Table 3.3	66
Table 4.1 Parameter list for high temperature PEM fuel cell modeling	71
Table 5.1 Parameter list for HT-PEMFC modeling	89
Table 5.2 Different stoichiometric ratios and corresponding inlet velocities of reactants.....	95

LIST OF FIGURES

FIGURES

Figure 2.1 Typical HT-PEMFC representation and its components	9
Figure 2.2 Typical polarization curve of HT-PEMFCs [7]	10
Figure 2.3 Poly 2,2'-m-(phenylene)-5,5'-bibenzimidazole[2]	11
Figure 2.4 The synthesis of PPA doped PBI membrane [3]	12
Figure 2.5 Proton conductivity mechanism of PPA doped PBI membrane	13
Figure 2.6 Materials for bipolar plates used in HT-PEMFCs [16]	16
Figure 2.7 Different types of flow field configurations used for HT-PEMFCs (a) step-serpentine, (b) pin-type, (c) parallel, (d) interdigitated [17]	17
Figure 3.1 “ <i>Model Wizard</i> ” selection in Comsol Multiphysics	24
Figure 3.2 Selection of “ <i>Space Dimension</i> ”	24
Figure 3.3 Main physics in Comsol Multiphysics	25
Figure 3.4 Sub-physics of Electrochemistry physics	26
Figure 3.5 Sub-physics of Reacting Flow in Porous Media physics	27
Figure 3.6 Added physics for PEMFC modeling	28
Figure 3.7 Study selection in Comsol Multiphysics	29
Figure 3.8 “ <i>Definitions</i> ” tool and its sub-sections	30
Figure 3.9 “ <i>Parameters</i> ” section in Comsol Multiphysics	31
Figure 3.10 “ <i>Materials</i> ” section in Comsol Multiphysics	32
Figure 3.11 “ <i>Definitions</i> ” tool under “ <i>Component</i> ” section in Comsol Multiphysics	33
Figure 3.12 “ <i>Geometry</i> ” section in Comsol Multiphysics	34
Figure 3.13 Building steps of MEA for PEMFC modeling	35
Figure 3.14 Work Plane settings in Comsol Multiphysics	36
Figure 3.15 Geometry building in Work Plane for multiple channel geometry	37

Figure 3.16 2-D drawing of mixed serpentine flow channel geometry by Work Plane	38
Figure 3.17 Domain probes of PEMFC model	39
Figure 3.18 “Electrolyte” section and its settings in Comsol Multiphysics.....	40
Figure 3.19 “Insulation” section and its setting in Comsol Multiphysics.....	41
Figure 3.20 “Initial Values” and its settings in Comsol Multiphysics.....	42
Figure 3.21 “Porous Electrode 1” and its settings in Comsol Multiphysics	42
Figure 3.22 “Porous Electrode Reaction 1” and its settings in Comsol Multiphysics	43
Figure 3.23 “Porous Electrode 2” and its settings in Comsol Multiphysics	44
Figure 3.24 “Porous Electrode Reaction 2” and its settings in Comsol Multiphysics	45
Figure 3.25 “Electrode 1” and its settings in Comsol Multiphysics	46
Figure 3.26 “Electric Ground 1” and its settings in Comsol Multiphysics.....	46
Figure 3.27 “Electric Potential 1” and its settings in Comsol Multiphysics.....	47
Figure 3.28 “Initial Values 2” and its settings in Comsol Multiphysics.....	47
Figure 3.29 “ <i>Reacting Flow of Porous Media</i> ” physics and its sub-sections	48
Figure 3.30 “Transport Properties” section and its settings in Comsol Multiphysics	49
Figure 3.31 “No Flux” section and its setting in Comsol Multiphysics.....	50
Figure 3.32 “Wall 1” section and its setting in Comsol Multiphysics.....	50
Figure 3.33 “Initial Values 1” section and its setting in Comsol Multiphysics	51
Figure 3.34 “Porous Matrix Properties 1” section and its setting in Comsol Multiphysics	51
Figure 3.35“Porous Matrix Properties 2” section and its setting in Comsol Multiphysics	52
Figure 3.36 “Porous Electrode Coupling 1” section and its setting in Comsol Multiphysics	52
Figure 3.37 “Reaction Coefficients 1” section and its setting in Comsol Multiphysics	53
Figure 3.38 “Inflow 1” section and its setting in Comsol Multiphysics	53
Figure 3.39 “Outflow 1” section and its setting in Comsol Multiphysics	54

Figure 3.40 “Inlet 1” section and its setting in Comsol Multiphysics.....	54
Figure 3.41 “Outlet 2” section and its setting in Comsol Multiphysics	55
Figure 3.42 Sequence types of “Mesh” tool in Comsol Multiphysics	56
Figure 3.43 Mesh element sizes available in Comsol Multiphysics	56
Figure 3.44 Meshed domain of HT-PEMFC model.....	57
Figure 3.45 “Study” tool in Comsol Multiphysics	58
Figure 3.46 Solver types in “Stationary Solver”	59
Figure 3.47 “Results” tool in Comsol Multiphysics.....	60
Figure 3.48 3-D, isothermal HT-PEMFC model domain having single flow channel.....	61
Figure 3.49 3-D, isothermal HT-PEMFC model domain having multiple flow channels.....	64
Figure 4.1 Comparison of experimental polarization data with model predictions for varying air velocities; (a) Fuel cell polarization behavior, voltage vs current density, (b) Power density vs current density. Modeling conditions; 160°C, ambient pressure, H ₂ inlet velocity= 0.1 m/s, $\lambda_A=1.0$, $\kappa = 10$ S/m.	77
Figure 4.2 Comparison of experimental polarization data with model predictions for varying hydrogen and air velocities; (a) Fuel cell performance based on acid doped PBI membrane voltage vs current density, (b) Power density vs current density. Modeling conditions; 160°C, ambient pressure, Air inlet velocity= 0.8 m/s, $\lambda_C=3.2$, $\kappa = 10$ S/m.	80
Figure 4.3 Comparison of experimental polarization data with model results obtained with acid doped PBI membrane having different proton conductivities. Modeling conditions; 160°C, ambient pressure, H ₂ inlet velocity= 0.133m/s and Air inlet velocity= 0.8 m/s, $\lambda_{A/C}=1.3/3.2$ and mass fraction of hydrogen=0.99	82
Figure 4.4 Concentration profiles along anode gas channel predicted for 0.6V and $\kappa = 10$ S/m. (a) Hydrogen concentration profile, (b) Water concentration profile. Modeling conditions are same as Figure 4.3.	84
Figure 4.5 Concentration profiles along cathode gas channel predicted for 0.6V and $\kappa = 10$ S/m. (a) Oxygen concentration profile, (b) Water concentration profile. Modeling conditions are same as Figure 4.3.	85

Figure 5.1 Comparison of experimental polarization data with model result for PBI/SiO ₂ membrane	90
Figure 5.2 Membrane current density distribution at 0.6 V	91
Figure 5.3 Concentration profile for hydrogen at anode, predicted for 0.6 V with PBI/SiO ₂ membrane (mol/m ³).....	92
Figure 5.4 Concentration profile for oxygen at cathode, predicted for 0.6 V with PBI/SiO ₂ membrane (mol/m ³).....	92
Figure 5.5 Concentration profile for produced water at cathode, predicted for 0.6 V with PBI/SiO ₂ membrane (mol/m ³).....	93
Figure 5.6 Comparison of polarization curves obtained by model for PBI ($\kappa=7.11$ S/m) and PBI/ SiO ₂ ($\kappa=8.66$ S/m)	94
Figure 5.7 Effect of different inlet velocities of hydrogen and air on the high temperature PEM fuel cell performance	96
Figure 5.8 Effect of mesh strategy on the HT-PEMFC performance	98
Figure B.1 Prepared MEA including PBI/SiO ₂ membrane.....	113
Figure B.2 PEMFC test station	113

LIST OF SYMBOLS

Symbol	Definition	Unit
C	Concentration	mol/m ³
C_p	Specific heat	J/kg K
D_{ij}	Binary diffusion coefficient	m ² /s
E	Cell voltage	V
E_a	Proton conducting activation energy	J/mol K
F	Faraday's constant	96485 C
I	Current	A
i	Transfer current density	A/m ²
k	Thermal conductivity	W/m K
k_p	Permeability	m ²
M	Molar mass	kg/mol
N	Mass flux rate	kg/m ² s
P	Pressure	Pa
R	Universal gas constant	J/K mol
T	Temperature	K
u	Velocity	m/s
U_o	Thermodynamic equilibrium potential	V
x	Molar fraction	-
w	Mass fraction	-

Greek letters

α	Transfer coefficient	-
ε	Porosity	-
ϕ	Phase potential	V
μ	Dynamic viscosity	kg/m s
η	Overpotential	V
κ	Proton conductivity	S/m
ρ	Fluid density	kg/m ³

Subscripts and superscripts

a: Anode

c: Cathode

e: Electrolyte phase

eff: Effective

ex: Exchange

i, j: Species i,j

ref: Reference conditions

s: Solid phase

LIST OF ABBREVIATIONS

1-D	One-dimensional
2-D	Two-dimensional
3-D	Three-dimensional
AFC	Alkaline fuel cell
CFD	Computational fluid dynamics
CL	Catalyst layer
DBFC	Direct borohydride fuel cell
DMFC	Direct methanol fuel cell
GDL	Gas diffusion layer
HT-PEMFC	High Temperature PEM fuel cell
IPA	Isophthalic acid
LT-PEMC	Low Temperature PEM fuel cell
MEA	Membrane electrode assembly
MCFC	Molten carbonate fuel cell
OCV	Open circuit voltage
PAFC	Phosphoric acid fuel cell
PBI	Polybenzimidazole
PEMFC	Polymer electrolyte membrane fuel cell
PPA	Phosphoric acid
PTFE	Polytetrafluoroethylene
SOFC	Solid oxide fuel cell
TAB	Tetraaminobiphenyl

CHAPTER 1

INTRODUCTION

Hydrogen is considered as a promising alternative energy source comparing with the fossil fuels. For the usage of hydrogen, fuel cells can be employed as energy conversion systems. Fuel cells are the electrochemical devices that convert chemical energy into electrical energy, directly. Unlike conventional energy converters, fuel cells eliminate the energy conversion steps which makes them thermodynamically more efficient.

Fuel cells are composed of an anode and a cathode compartments which are negative and positive compartments, respectively. Hydrogen rich gaseous reactant is fed continuously to the anode compartment, while an oxidant which is generally pure oxygen or air is fed continuously to the cathode compartment. The electrochemical reaction takes places at the electrodes placed in the compartments to produce electricity.

Between anode and cathode compartments, fuel cells include an electrolyte which provides a basis for the classification of fuel cells. The proceeding of the electrochemical reaction in the cell depends on the electrolyte used in the fuel cell. According to this basis, there are different types of fuel cells. These are Alkaline fuel cells (AFC), Solid oxide fuel cells (SOFC), Molten carbonate fuel cells (MCFC), Phosphoric acid fuel cells (PAFC), Direct methanol fuel cells (DMFC), Direct borohydride fuel cells (DBFC) and Polymer electrolyte membrane fuel cells (PEMFC). Having different electrolytes changes the operating conditions of the fuel cell (such as: temperature) because of different specific properties of the

electrolyte. Various fuel cells have their own advantages and disadvantages; therefore, they are used for different applications [1].

Table 1.1 lists differences, advantages, disadvantages and applications of different types of fuel cells listed above.



Table 1.1 Main characteristics of different types of fuel cells

	Electrolyte	Operating temperature	Advantages	Disadvantages	Applications
PEMFC	Perfluoro sulfonic acid	50-100°C	Low corrosion, low temperature, quick start-up	Expensive catalyst, sensitive to fuel impurities	-Transportation -Electric utility -Mobile applications
DBFC	Anion exchange membrane Cation exchange membrane	50-100°C	High efficiency, low corrosion	Necessity of hydrogen removal, recycle of sodium metaborate	-Mobile applications
DMFC	Perfluoro sulfonic acid	50-100°C	Elimination of reformer, easy miniaturization	Methanol cross-over, production of CO ₂	-Mobile applications -Military
AFC	Aqueous solution of potassium hydroxide	50-200°C	Cathode reaction is faster in alkaline electrolyte, low cost components	Sensitive to CO ₂ in air and fuel	-Military -Space
PAFC	Phosphoric acid solution	175-200°C	Increased tolerance to fuel impurities	Expensive catalyst, long start-up time, large size	-Electric utility -Distributed generation
MCFC	Solution of lithium, sodium and potassium carbonates	600-1000°C	No noble metal is needed, fuel flexibility, high efficiency	Corrosion, low power density, long start-up time	-Electric utility
SOFC	Ceramics	600-1000°C	Usage of variety of catalysts, fuel flexibility, low corrosion, suitable for CHP	Thermal effects of cell components, long start-up time	-Auxiliary power -Electric utility

PEM fuel cells are most common type of fuel cells because they have quick start-up and shut-down which makes them easy to adapt for mobile applications like automobiles and portable electronic devices. Moreover, the simplicity and viability of PEM fuel cells are distinctive features compared to other types of fuel cells. Therefore, PEM fuel cell technology is considered to be the closest to the market, some of which are already placed in the market as commercial products.

Polymer electrolyte membrane is placed at the center of a PEM fuel cell. On both sides of the membrane, porous electrodes are placed. These electrodes should be porous because reactant gases are fed from anode and cathode sides and they should reach the interface of the membrane and the electrode. The electrochemical reactions take place at the catalyst layers (CL), which are parts of the electrodes. These electrodes are sandwiched by gas diffusion layers (GDL). Membrane electrode assembly (MEA) is known as the heart of the PEM fuel cell which consists of membrane, CLs and GDLs. Bipolar plates, which are next to the both sides of the MEA, collect and conduct electrical current [2]. Detailed functions of each component will be explained in Chapter 2.

PEM fuel cells can be divided into two categories relating with operating temperature as low temperature PEM fuel cells (LT-PEMFC) and high temperature PEM fuel cells (HT-PEMFC). Despite the categorization is based on the operating temperature, the nature of their catalyst, polymer electrolyte membrane, proton conductivity capacity and even fuel type can differ for each of them.

LT-PEMFCs are generally operated at temperatures below 100°C (<100°C). Generally, Nafion®, which is based on sulphonated polytetrafluoroethylene (PTFE), by Dupont is used as membrane for LT-PEMFCs. The reason of Nafion membrane usage is that it requires sufficiently enough liquid water content in order to provide effective proton conductivity. On the other hand, presence of liquid water makes water management complicated. Although Nafion membrane requires enough liquid water content, dehydration of the membrane and flooding of electrodes should be prevented, simultaneously. Effective water management is very critical because flooding of electrodes blocks the pores which does not allow

to gas transportation, which turns into a mass transport limitation problem. For LT-PEMFCs, carbon monoxide (CO) tolerance of the catalyst is 10-100 ppm, which is critically high amount to poison the membrane.

These problems that can be faced in case of low temperature operation can be resolved by increasing the operation temperature. HT-PEMFCs are generally operated between 120-180°C. As the best known membrane, polibenzimidazole (PBI) membrane, which has less dependency on water than Nafion, is typically used for high temperature operation. Proton conductivity of PBI membrane is generally acquired by doping of a strong acid, such as phosphoric acid, because the polymer itself has actually poor proton conductivity. As an alternative, PBI composite membranes can be used for high temperature operation. Presence of liquid water is eliminated for high temperature operation; i.e., generated water is only in gaseous phase. Thus, risk of flooding is extinguished from the MEA, which prevents the water management problem and mass transport limitation. CO tolerance of the catalyst is higher for HT-PEMFCs, up to 5%; therefore, usage of reformers can be easier in order to obtain the hydrogen from other organic sources.

Changing an operation condition, such as temperature, pressure or the fuel type, can result in different problems for PEM fuel cells. This is the point where modeling of PEM fuel cells gain importance in order to pre-estimate the effects of different parameters starting from temperature. Optimization of different parameters helps to improve the efficiency of the fuel cell. Moreover, modeling can able to diagnose many possible problems which may not be seen during the actual experiments. Therefore, it can reduce the number of experiments which helps saving the time and money. PEMFC operations involve multi-dimensions, many physics, multi-components and multi-phases. Modeling gives the opportunity to investigate each one of them individually. In addition to these, modeling does not only help to improve the efficiency, but also it can help to understand the mechanisms such as mass and momentum transports. Considering all these advantages, modeling of PEMFCs is necessary and critical for system design and optimization including all fuel cell physics while at the same time having short solution times.

The aim of this study is to develop an isothermal, three-dimensional model of HT-PEMFC in order to make sensitivity analysis to improve the efficiency of the cell. In the light of this topic, several critical parameters that may have significant effects on the cell performance are investigated. These parameters are inlet velocities of reactants fed to the anode and cathode side (hydrogen and air), proton conductivity of the membrane and mesh size. Sensitivity analysis is performed for both single and multiple channel geometries. For the modeling of HT-PEMFC having single flow channel, the properties of commercial membrane produced by Danish Power Systems are taken as basis, while for the modeling of HT-PEMFC having multiple channel in mixed serpentine geometry, the properties of membrane produced by our FCRC research group are taken as basis. For both cases, the performances are compared for modeling and experimental results to validate the models. For the simulation of developed models, licensed Comsol Multiphysics 5.0, which is a commercial software program, and its Fuel Cells & Batteries module is used. The program uses finite element method and it is applicable to wide range of engineering problems since it includes many different physics.

CHAPTER 2

HIGH TEMPERATURE PEM FUEL CELLS

PEM fuel cells are most common type of fuel cells because of their suitability to many different applications [3]. They provide high power density, low corrosion, quick start-up, and high efficiency; therefore, they are promising clean and alternative energy sources [4]. Current PEMFCs are operated in the temperature range of 50-100°C because of the operation temperature of the polyelectrolyte membrane (generally Nafion) [5]. However, high temperature operation for PEMFCs are relatively new field and considered as the next generation of PEMFCs.

In recent years, high temperature PEM fuel cells (temperature range from 100-200°C) have been recognized as a promising solution in order to remove many challenges which are surveyed during the low temperature operation (refers to the temperatures below 100°C). HT-PEMFC technology is more desirable because of several advantages. First of all, it is operated above the boiling temperature of water hence the generated water is only in one phase. Removal of liquid water from the cell simplifies the water management of system design and operation. More importantly, CO tolerance of the catalyst is much higher than low temperature operation. CO poisoning of the membrane is a very critical problem of the PEM fuel cells and higher CO tolerance can eliminate membrane separator from the system for CO cleaning of the membrane. Moreover, it enhances the usage of reformers, which makes possible not only pure hydrogen, but also other types of fuels including hydrogen. Another advantage is that reaction kinetics for

both anode and cathode electrodes are faster for high temperature operation, while oxygen reduction kinetics at the cathode side very slow for low temperature operation. In addition, gases do not need to be humidified before entering the system which also eliminates the usage of external humidification. All these eliminations of equipment would dramatically simplify the system design, cost, weight and size. Furthermore, higher value of heat recovery can be obtained for high temperature operation.

The following subsections cover operation principles and components of HT-PEMFCs, and a literature survey based on HT-PEMFC modeling.

2.1. HT-PEMFC Operation Principles

The main components of PEM fuel cells having high temperature operation are polymer electrolyte membrane, catalyst layers, gas diffusion layers and bipolar plates. The membrane is located at the center of the cell, which divides the cell into anode and cathode compartments. Three structures (membrane, CLs and GDLs) compose MEA and it is squeezed with two bipolar plates. Figure 2.1 shows a typical representation of PEM fuel cell and its components.

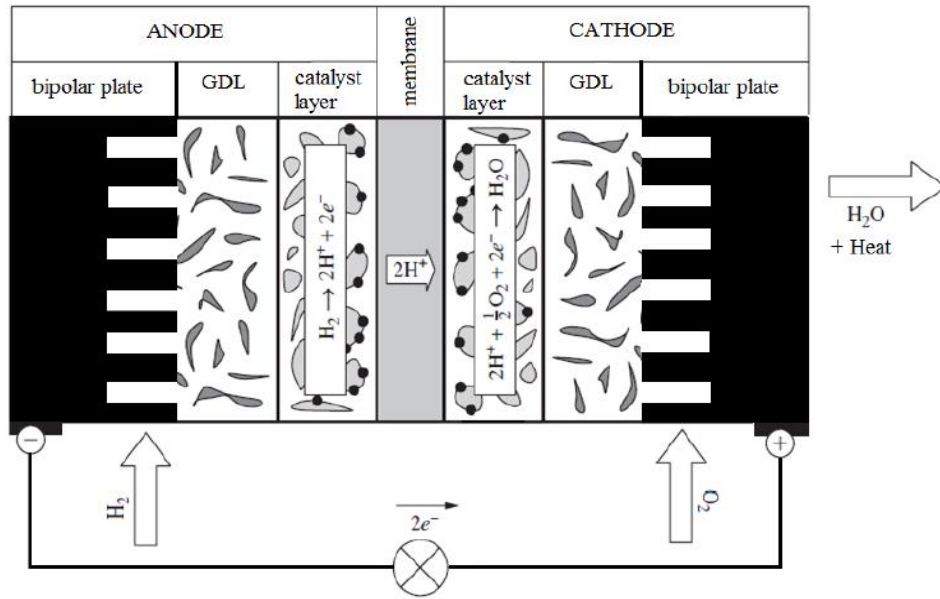
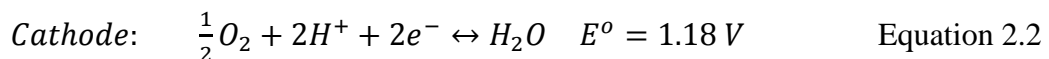


Figure 2.1 Typical HT-PEMFC representation and its components

The electrochemical reactions occur at both anode and cathode side of a PEM fuel cell. At the anode side, hydrogen splitting reaction takes place at the surface of the catalyst layer. Hydrogen splitting reaction have primary constituents as proton and electrons. Protons are immigrated through the membrane from anode to cathode side, while electrons are immigrated from electrodes since the polymer electrolyte membrane cannot conduct electrons, but only protons. At the cathode side, water formation reaction takes place in the presence of oxygen. Generated water is carried out of the cell by excess flow of oxygen. At the end of these simultaneous reactions, electrical current is obtained as product by the travel of electrons through an external circuit as well as water generated by electrochemical reaction.

The anode and cathode side reactions of a PEM fuel cell are shown below in equation 2.1, 2.2 and 2.3.



The overall HT-PEMFC potential E^o is equal to 1.18 V, which is the maximum cell potential, called as open circuit voltage. This value corresponds when the produced water is in gaseous phase. However, the overall potential E^o is equal to 1.229 V for LT-PEMFCs when the produced water is in liquid phase. These values are theoretical values obtained at normal conditions (Temperature=298.15 K, P=1 atm); but in practice, the fuel cell can generally provide 0 to 1.0 volts because there can be losses depending upon operating conditions [6]. Three different types of losses (activation, ohmic and mass transfer losses) are indicated in Figure 2.2.

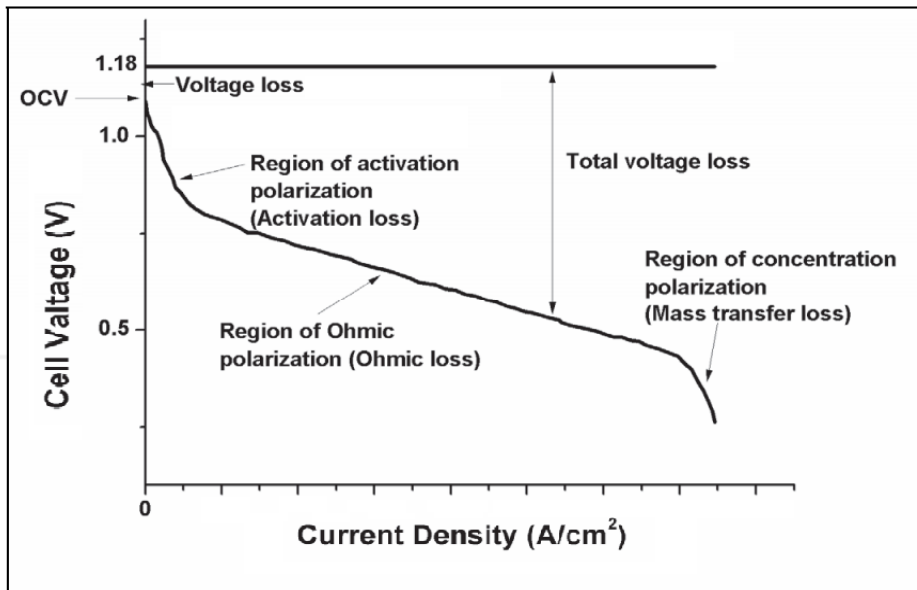


Figure 2.2 Typical polarization curve of HT-PEMFCs [7]

Activation losses are caused by the reaction kinetics. When the reaction which takes places at the interface of membrane and the electrode has slow kinetics, activation losses are inevitable to form. Especially for low current densities, these losses become more important. Ohmic losses are caused by the resistance to the travel of electrons through electrodes and travel of ions through the membrane. Mass transfer losses are caused by the diffusion of ions, which creates negative concentration gradient and it affects the speed of transport. Activation losses and mass transport losses are strongly nonlinear, while ohmic losses is linear in the

performance curve of a HT-PEMFC. Within this range of voltage, a simple HT-PEMFC is operated at its nominal range 0.5-0.7 V [6].

2.2. HT-PEMFC Components

2.2.1. Membrane

Many studies are adapted to develop proton conducting membranes for high temperature operation, above 100°C, of PEM fuel cells [3]. PBI membrane, proposed by Litt and investigated by Savinell, Wainright et al., has been studied as a promising electrolyte for HT-PEMFCs [8]. Figure 2.3 shows the chemical structure of PBI.

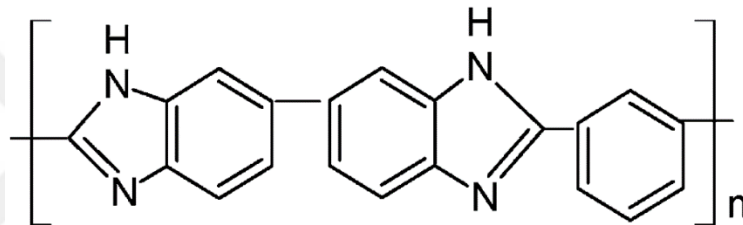


Figure 2.3 Poly 2,2'-m-(phenylene)-5,5'-bibenzimidazole[2]

PBI membranes should be doped with a strong acid such as; sulphuric acid (H_2SO_4), phosphoric acid (H_3PO_4), nitric acid (HNO_3), hydrochloric acid (HCl), perchloric acid (HClO_4) in order to gain proton conductivity. Savagado and Xing [9] compared the conductivity values of PBI membranes doped with different acids and they found that $\text{H}_2\text{SO}_4 > \text{H}_3\text{PO}_4 > \text{HClO}_4 > \text{HNO}_3 > \text{HCl}$. Since sulphuric acid damages the stability of PBI membrane, phosphoric acid doped PBI membranes are the most commonly used membrane for HT-PEMFCs. Synthesis of phosphoric acid doped PBI membrane is shown in Figure 2.4. Tetraaminobiphenyl (TAB) and isophthalic acid (IPA) are used for the synthesis as in the form of homogeneous solution and phosphoric acid (PPA) is used as solvent.

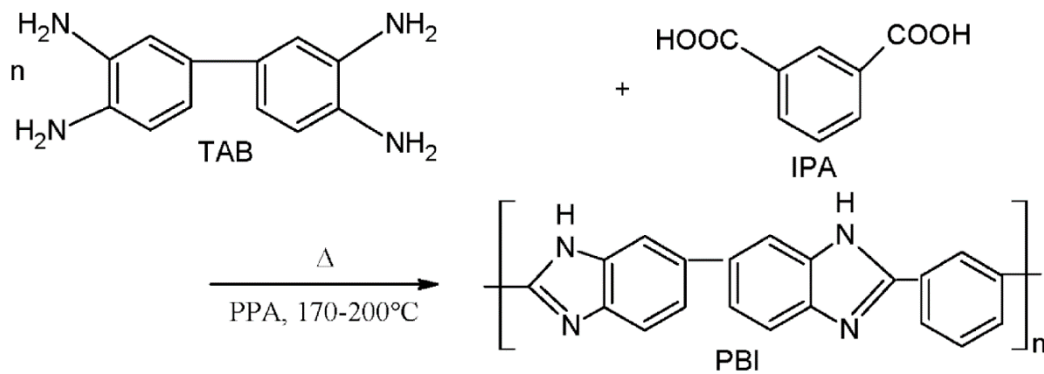


Figure 2.4 The synthesis of PPA doped PBI membrane [3]

The proton conductivity of an acid doped PBI membrane is strongly depend on acid doping level of the membrane as well as operating temperature, relative humidity and the molecular weight of the membrane. For example, PPA acid PBI membrane has the proton conductivity of 2 S/m for acid doping level of 5-6 at 160°C, while it is 10 S/m for acid doping level of 10 at 160°C [10]. As another example, PPA doped (acid doping level=7.3) PBI membrane has the proton conductivity as 2 s/m at 100°C, while it is 5 S/m at 180°C. Moreover, PPA doped (acid doping level=7.3) PBI membrane at 100°C at 10% and 20% relative humidity have proton conductivities as 3 S/m and 4.5 S/m, respectively [11].

Figure 2.5 shows the proton conduction mechanism of PPA doped PBI membrane. For low level of acid doping, proton conduction is acquired between N-H sites and PPA anions by proton hopping because of high levels of protonation. However, for high level of acid doping to the PBI membrane, free acids are present in the polymer which can provide high proton conductivity values[12].

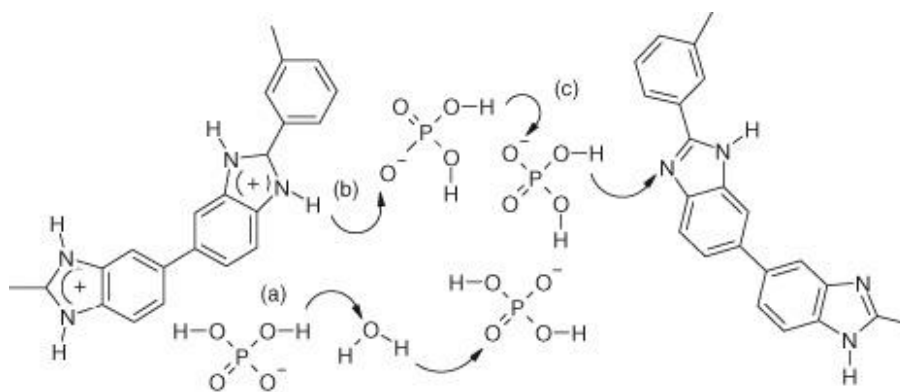


Figure 2.5 Proton conductivity mechanism of PPA doped PBI membrane

Acid doped PBI membranes provide high stability and high conductivity, yet acid leaching and catalyst degradation are serious problems PBI membranes having higher acid doping level. Higher acid doping with PBI membrane causes leaching of unbound acid from the membrane by the flow of water and it leads that the membrane have lost its mechanical strength. Because of these reasons, HT-PEMFC performance dramatically decreases during the operation. In order to overcome this problem, PPA doped PBI membranes can mixed with inorganic filler which would eliminate acid leaching and stability problems. This type of membranes called as PBI-based composite membranes. Higher stability of the PBI based composite membranes can be explained by the sorption of additional PPA on the particle surface [13]. Several types of inorganic fillers can be employed such as hygroscopic oxides (SiO_2 , TiO_2 , ZrO_2 , and Al_2O_3), clays and zirconium phosphates (ZrP). Among these inorganic fillers, SiO_2 has strong H-bonding capability to acids, which can remove acid leaching and improve proton conductivity. Moreover, its cost is relatively cheaper than other inorganic fillers [14].

Table 2.1 shows the comparison of PPA doped PBI membrane and PBI/SiO₂ composite membrane. Acquired proton conductivity values are obtained at an operation temperature of 165°C.

Table 2.1 Comparison of PBI and PBI/SiO₂ membrane in terms of acid doping, proton conductivity and acid leaching [14]

Membrane	Membrane Doping Level*	Proton Conductivity (S/m)	Acid Leaching Degree (wt.%)
PBI	11	7.65	41.5
PBI/SiO ₂	10	8.66	36.3

*Molecules of PPA acid/repeating unit of PBI

2.2.2. Catalyst Layers

For a HT-PEMFC, there is a catalyst layer which is placed at both anode and cathode compartments. These catalyst layers are separated by the polymer electrolyte membrane and at the other side of these catalyst layers, GDLs are in contact with them. These layers should provide transfer of electrons and protons in order to support electrochemical reactions. Each half reaction (oxidation and reduction) takes place at these layers and the layers are able to decrease the activation energy of the reactions. Therefore, electrochemical reactions can proceed faster or at a lower temperature.

Catalyst layer includes porous electrochemical support, which is usually an electroactive metal. Porosity of the catalyst provides the layer to transfer water and reactant gases, as well as providing active sites for the layer. The most common used metal is platinum (Pt) because of its high electrocatalytic activity, high resistance to corrosion and oxidation. In spite of Pt's good performance, it is a precious metal with high cost. In order to reduce the amount of Pt loading, many researches are focused on alternative ways to decrease the amount of Pt loading by increasing the utilization of Pt [15].

In order to increase the surface area and the utilization of the catalyst, two different paths are followed. During the MEA preparation, either the catalyst is dispersed on GDL (carbon paper or carbon cloth) and then sandwiched with the membrane, or it is dispersed on the membrane and then sandwiched with GDLs.

2.2.3. Gas Diffusion Layers

GDLs are porous layers in contact with the catalyst layers for both anode and cathode compartments. GDLs are the current collectors squeezed between bipolar plates and CLs. An ideal GDL should possess to transport of reactants toward CLs and to have good electrical and thermal conductivities. Electrical conductivity is needed in order to transfer electrons, while thermal conductivity is needed for the transfer of heat from catalysts to other components. GDLs are critical for the removal of generated water from the cell. Produced water at the catalyst layer is transferred via GDLs through the outlet gas channels of the cell. This feature of GDL has crucial role for the water management, which helps the cell to prevent flooding.

The structure of GDL is generally carbon based product such as carbon paper, carbon cloth or carbon fiber. Carbon based products are preferable because they provide good gas permeability which eases the transport of reactants, good electronic conductivity, good compressibility and stability in acid environment [16]. .

2.2.4. Bipolar Plates (Flow Fields)

Bipolar plates are the backbones of HT-PEMFCs. They collect and conduct electrons and they provide the flow of reactants, hydrogen and oxygen. Bipolar plates cover the large fraction of fuel cell weight, volume and cost. In order to be able to show these properties, several of materials can be proposed as the structure of them. Since they support the MEA, they should be mechanically strong and durable. Recently, graphite bipolar plates are considered as the standard material for small volume manufacturing or lab-scale studies. Graphite has high resistance

to corrosion and low surface resistance. Although graphite is very suitable and shows good performance, it is very brittle and lacks mechanical strength, especially for high volume manufacturing. For this reason, metal bipolar plates are preferable for high volume manufacturing in terms of mechanical stability with higher cost effectiveness. However, the major drawbacks of metal bipolar plates are the low resistance to corrosion and weight [17]. Alternatively, composite bipolar plates can be used. They can be based on graphite. Graphite-based composite plates are advantageous since they are mechanically strengthened by addition of composites with low cost. Moreover, they show good resistance to corrosion and they are lighter than metal plates. Figure 2.6 represents the materials that are generally used for bipolar plates for HT-PEMFCs.

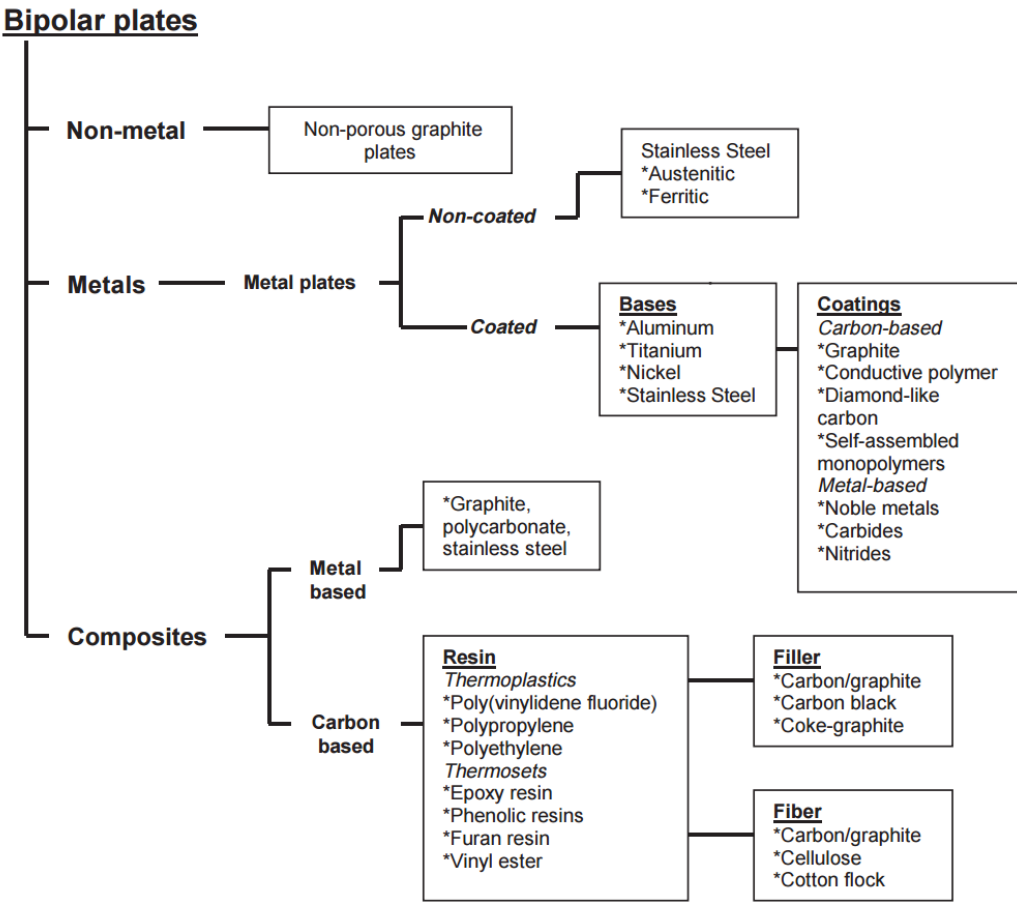


Figure 2.6 Materials for bipolar plates used in HT-PEMFCs [18]

The design of flow fields is a critical parameter because HT-PEMFC performance can be optimized by different flow channel geometries. In order to keep the performance high, the distribution of reactant gases through the flow channel should be uniform. There are several types of flow field pattern configurations, the most commonly used types are parallel, step-serpentine, pin-type and interdigitated. Figure 2.7 shows flow field patterns of most commonly used types for HT-PEMFCs.

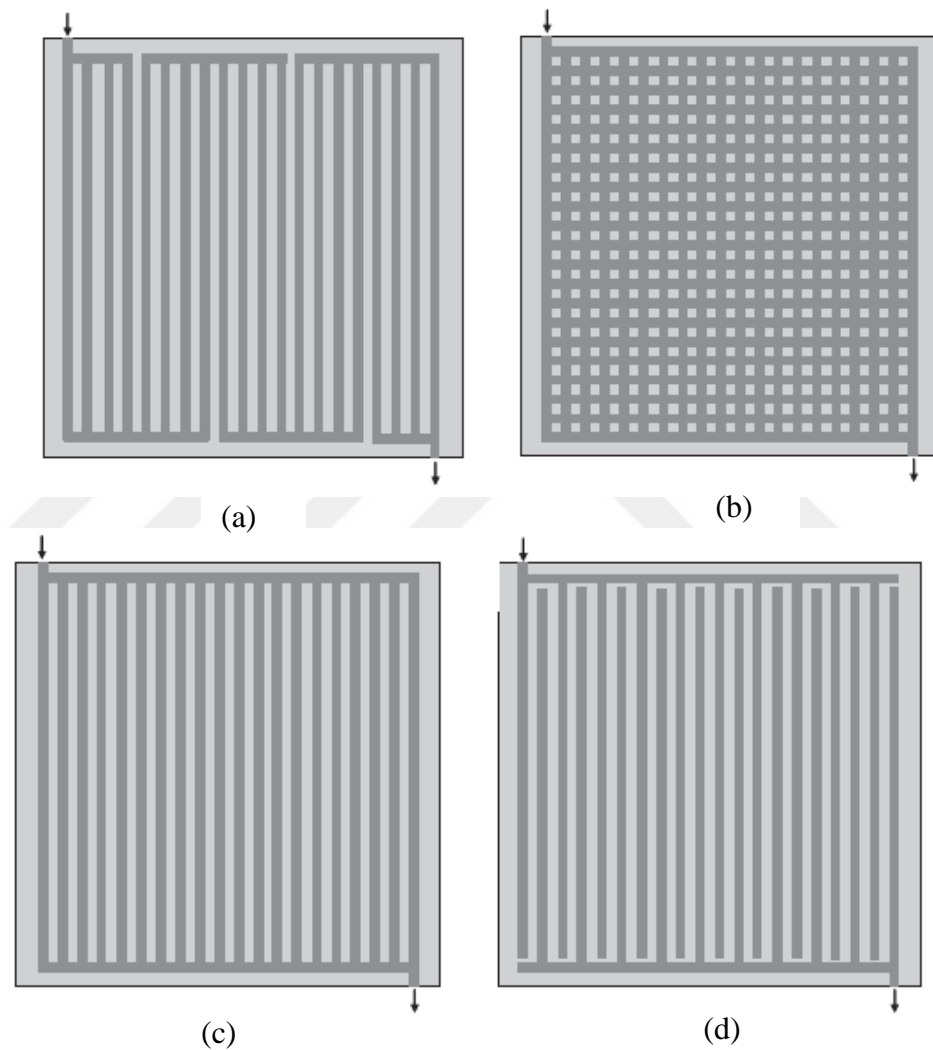


Figure 2.7 Different types of flow field configurations used for HT-PEMFCs (a) step-serpentine, (b) pin-type, (c) parallel, (d) interdigitated [19]

2.3. Review of PEMFC Modeling

In last two decades, researches upon HT-PEMFC have gain interest. There are few numbers of studies, especially on HT-PEMFC modeling. Cheddie and Munroe revealed the first publication on this topic. They developed one-dimensional (1-D) model of HT-PEMFC using PBI membrane. The model was assumed as steady-state and non-isothermal and the modeling results were compared with the experimental data results reported by Wang et al [20]. They compared the performances of HT-PEMFC for the cases of pure oxygen and air as the oxidant and oxygen had showed better performance for both modeling and experimental results. Moreover, they investigated the effect of inlet gas flow rates. Three different flow rates, which were reduced by the factor of 10 and 100, were chosen for both anode and cathode. They concluded that there would be no distinct mass transport region if sufficient reactants provided to that electrochemical reaction could proceed completely. Other parameter that they studied was conductivity of the PBI membrane. Three conductivity values were considered: 1.87 S/m, 9.6 S/m and 17 S/m. They observed that increasing proton conductivity produced observable increase in performance curve [21].

The same group published another study on three-dimensional (3-D) modeling of HT-PEMFCs operating with PBI membrane. The model was developed as non-isothermal and the modeling results were compared with the experimental results reported by Wang et al., same with their first publication [20]. They compared their 3-D model result with their own 2-D model result and they found that 3-D model can predict greater ohmic contribution. Since their model accounted all the transport phenomena, the oxygen depletion was investigated by Cheddie and Munroe. They reported that the oxygen depletion was mostly occurred in the cathode catalyst layer under the ribs. Temperature distribution was seen as increasing along the channel [22].

Shamardina et al., had developed pseudo 2-D, steady state and isothermal HT-PEMFC model to understand the properties of the cell. They compared model results with their own experimental results which were in a good agreement. They performed a parametric analysis including the effect of composition of the reactant gases, conductivity of the membrane, flow rate of reactant gases and operating temperature. For the investigation of reactant gases (only for cathode side), air and pure oxygen were chosen and it was seen that pure oxygen came out with better performance than air. Three different membranes which had different conductivities formed by adding different additives showed different performances, yet the results were too close to each other. For different flow rates of reactants, the study was performed for only cathode side. They kept the flow rate of anode side constant, while flow rate of the reactant at the cathode side was changed three times. Lastly, it was found out that increasing temperature provided increasing HT-PEMFC performance [23].

Flow channel geometry influence was studied by Lobato et al. 3-D, half-cell HT-PEMFC model having 50 cm² active area was built. Computational Fluid Dynamics (CFD) was applied for the model. Three different geometries had been investigated: 4-step serpentine, parallel and pin-type configurations. The best results were obtained for 4-step serpentine geometry, while the worst results belonged to parallel flow field. The model results were validated with experimental results which were performed by the same group. Moreover, inlet flow rate of reactants and the operating temperature were also investigated in this study [24].

Çağlayan et al. had modeled a 3-D HT-PEMFC model having single cell in order to investigate the effect of different operation temperatures on the cell performance, under the assumption of isothermal operation. Different operating temperatures between 100-180°C were considered in the scope of this study. The model was applied to be solved by Comsol Multiphysics 5.0. Model results had been compared by the experimental results including temperature dependency of proton conductivity of PBI membrane and the performance of HT-PEMFC [25].

Table 2.2 and Table 2.3 summarize the studies related with PEMFC modeling available in the literature. Studies are listed in regard to their operation type; LT-PEMFC, HT-PEMFC and DMFC. It can be seen from the tables that 1-D and 2-D models were generated in the early stages of PEMFC modeling. However, 3-D modeling of PEMFC can include all mass, momentum and current transports which cannot be completely taken into account for 1-D and 2-D models. Therefore, 3-D model developments have gain interest in the following years for PEMFCs. Among these studies, many of the models were limited by the consideration of half-cell model. They generally modeled the cathode side of the cell, by neglecting the anode side. This consideration may be accepted for LT operation for PEMFCs, but complete model development for HT-PEMFC should be considered, including both anode and cathode compartments.

In this study, 3-D HT-PEMFC model is developed in order to investigate the key parameters affecting the cell performance. The originality of the study comes from the consideration of complete fuel cell model and its solution technique. Anode compartment of HT-PEMFC is also taken into account for the pre-estimation of effect of different inlet hydrogen velocities (i.e., flow rates) on the FC performance. It may be a wrong consideration to neglect anode side effect on the performance since increasing flow rate of hydrogen may lead to have insufficient flow rate of oxygen, which causes to have incomplete electrochemical reaction through the operation. Moreover, the solution technique, Comsol Multiphysics 5.0, is relatively new software package program with its latest version. There are few HT-PEMFC models which are applied to be solved by Comsol Multiphysics 5.0 in the available literature.

Table 2.2 Previous studies of PEMFC modeling available in the literature

Authors	Year	Dimension	Operation	Time Dependency	Solution Technique
Springer et al. [26]	1991	1D	LT-PEM	Steady state	-
Wöhr et al.[27]	1998	1D	LT-PEM	Quasi-steady state	Numerical solution
Gurau et al. [28]	1998	2D	LT-PEM	Steady state	-
Siegel et al. [29]	2003	2D	LT-PEM	Steady state	CFDesign®
Hu et al. [30]	2003	3D	LT-PEM	Steady state	FORTRAN
Nguyen et al. [31]	2004	3D	LT-PEM	Steady state	VTC Algorithm
Sousa Jr & Gonzalez [32]	2005	2D	LT-PEM	Steady state	CFD Algorithm
Le & Zhou [33]	2008	3D	LT-PEM	Unsteady state	FLUENT 6.2
Cheddie & Munroe [21]	2005	1D	HT-PEM	Steady state	Runge-Kutta method
Cheddie & Munroe[22]	2006	3D	HT-PEM	Quasi-steady state	FEMLAB 3.1i
Scott et al. [34]	2007	1D	HT-PEM	Steady state	Comsol Multiphysics
Shamardina et al. [23]	2009	2D	HT-PEM	Steady state	Analytical solution
Ubong et al. [35]	2009	3D	HT-PEM	Steady state	Comsol Multiphysics
Lobato et al. [24]	2010	3D	HT-PEM	Steady state	Comsol Multiphysics 3.5
Kvesić et al. [36]	2012	3D	HT-PEM	Steady state	ANSYS-Fluent

Table 2.3 Continuation of Table 2.2

Authors	Year	Dimension	Operation	Time Dependency	Solution Technique
Su et al. [37]	2012	2D	HT-PEM	Steady state	Comsol Multiphysics
Chippar & Ju [38]	2013	3D	HT-PEM	Steady-state	FLUENT
Çağlayan et al. [25]	2016	3D	HT-PEM	Steady-state	Comsol Multiphysics 5.0
Sezgin et al. [39]	2016	3D	HT-PEM	Steady state	Comsol Multiphysics 5.0
Quellette et al. [40]	2015	3D	DM	Steady state	SIMPLE & Thomas Algorithm
Quellette et al. [41]	2015	1D	DM	Steady state	Comsol Multiphysics 4.2
Atacan et al.[42]	2016	2D	DM	Steady state	Comsol Multiphysics 5.0

CHAPTER 3

MODEL DEVELOPMENT BY COMSOL MULTIPHYSICS

In the scope of this thesis, all developed models are simulated by using licensed software package program, Comsol Multiphysics 5.0 and its Fuel Cells & Batteries module. The program is implemented to solve by using finite element method. The model includes transport of reactants gases for both anode and cathode sides, diffusion in the catalyst layers, the transport of water and the transport of electrons in the solid phase.

This section summarizes the algorithm of Comsol Multiphysics to build a mathematical model and 3-D, isothermal models developed in the scope of this thesis. Details of all governing equations, assumptions and boundary conditions will be explained in Chapter 4.

3.1. Algorithm of Comsol Multiphysics

In order to develop a mathematical model by Comsol Multiphysics, several tools should be used with respect to an ordered algorithm. The first step of the algorithm starts with the selection of “*Model Wizard*” as shown in Figure 3.1. This step is followed by the selection of “*Space Dimension*”. Comsol Multiphysics allows to build a zero-dimensional (0-D), one dimensional (1-D), axisymmetric 1-D, two-dimensional (2-D), axisymmetric 2-D or three-dimensional (3-D) model. Figure 3.2 shows the selection of “*Space Dimension*” in Comsol Multiphysics.

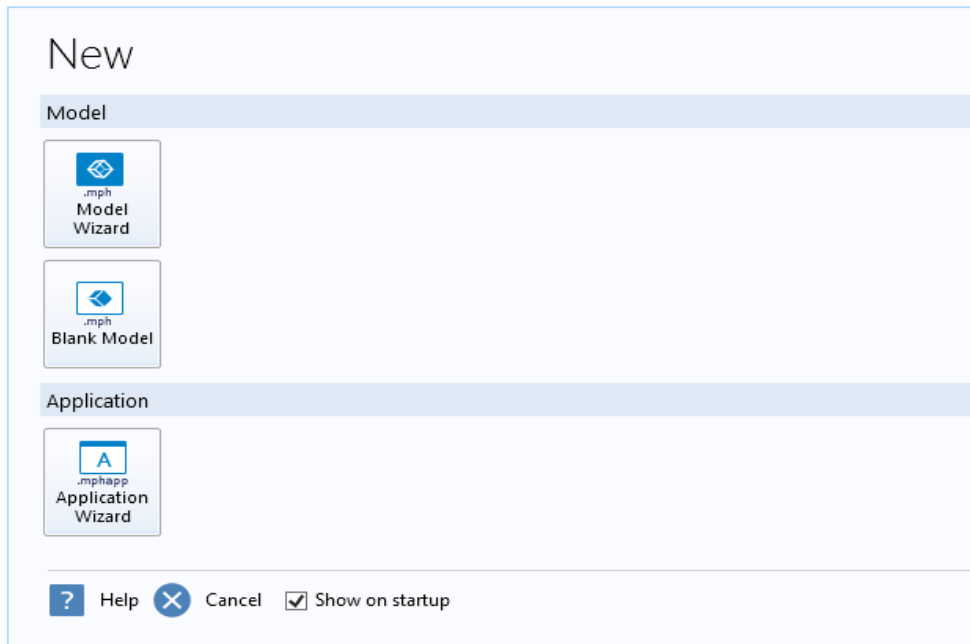


Figure 3.1 “*Model Wizard*” selection in Comsol Multiphysics

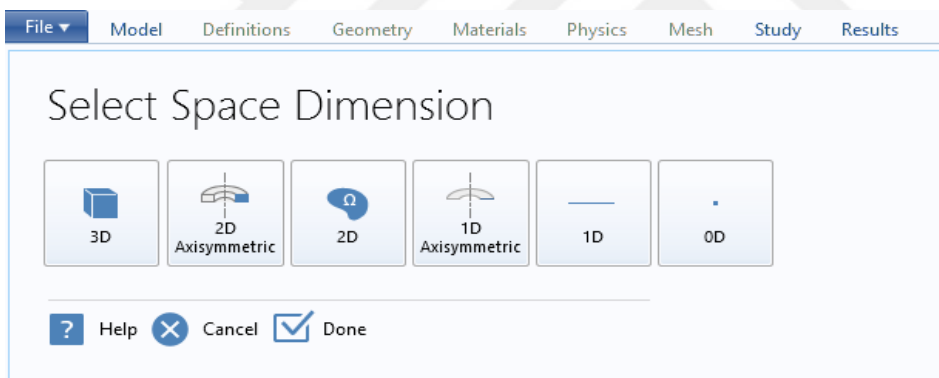


Figure 3.2 Selection of “*Space Dimension*”

Once the dimension of the model is selected, the physics that will be used for the simulation should be chosen. This step of the algorithm is very critical since each physics includes the equations to be solved for the valid model. The main physics are AC/DC, Acoustics, Chemical Species Transport, Electrochemistry, Fluid Flow, Heat Transfer, Optics, Plasma, Radio Frequency, Semiconductor, Structural Mechanics and Mathematics. These main physics include sub-physics which helps to narrow down the selection of the most appropriate physics. Figure 3.3 shows the list of main physics in Comsol Multiphysics.

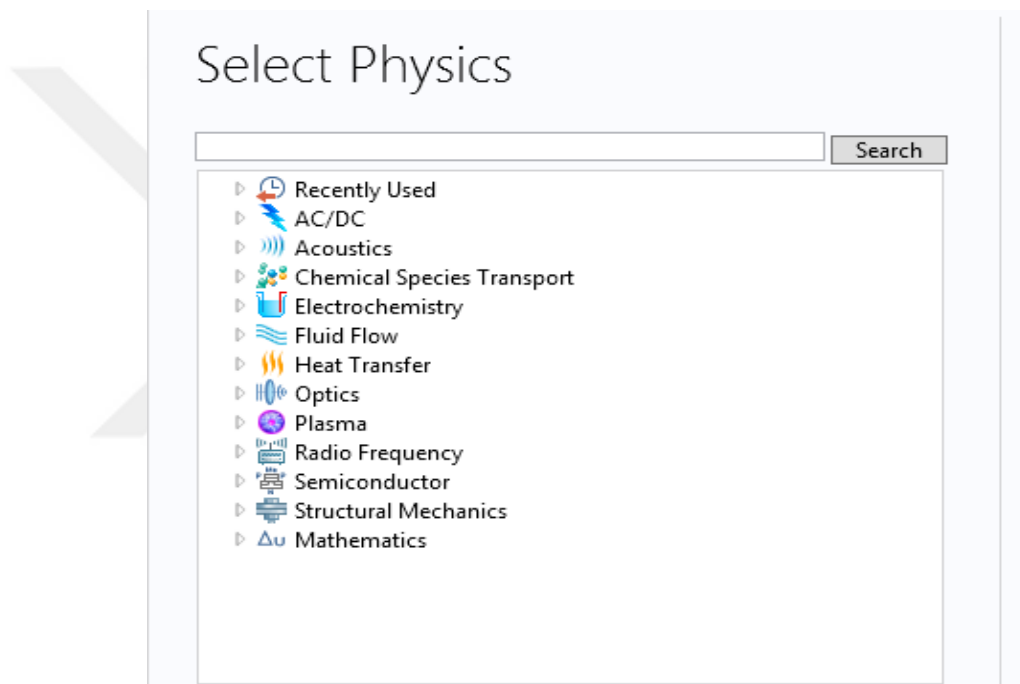


Figure 3.3 Main physics in Comsol Multiphysics

For HT-PEMFC modeling, two of the main physics are employed: Electrochemistry and Chemical Species Transport. Figure 3.4 shows the sub-physics of Electrochemistry physics. Within the sub-physics of Electrochemistry, “*Secondary Current Distribution*” physics, which includes Butler-Volmer and Tafel equations in order to obtain current distribution of the cell, is added for HT-PEMFC modeling. Moreover, this physics employs Ohm’s law in order to describe conduction of currents by charge balance.

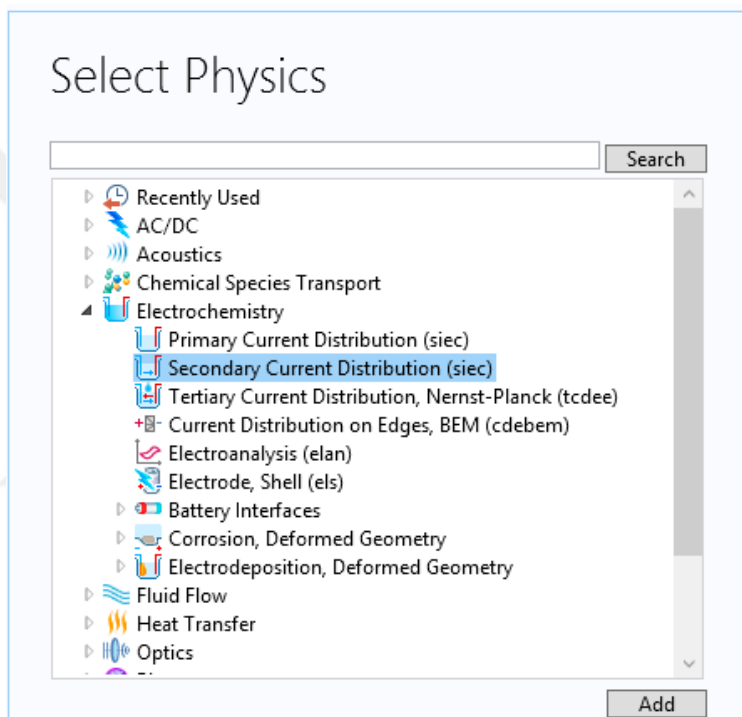


Figure 3.4 Sub-physics of Electrochemistry physics

Chemical Species Transport physics has many sub-physics including Reacting Flow in Porous Media. This physics is used for the description of the movement of a fluid through a porous medium. “*Transport of Concentrated Species*” physics, which is added for HT-PEMFC modeling, is placed under the sub-sections of Reacting Flow in Porous Media. The physics employs Brinkman equation is used for the solution of fluid momentum in porous media. In free-flow regions, Navier-Stokes equation is replaced for the solution of fluid momentum. Figure 3.5 shows sub-physics of Chemical Species Transport and Reacting Flow in Porous Media in Comsol Multiphysics.

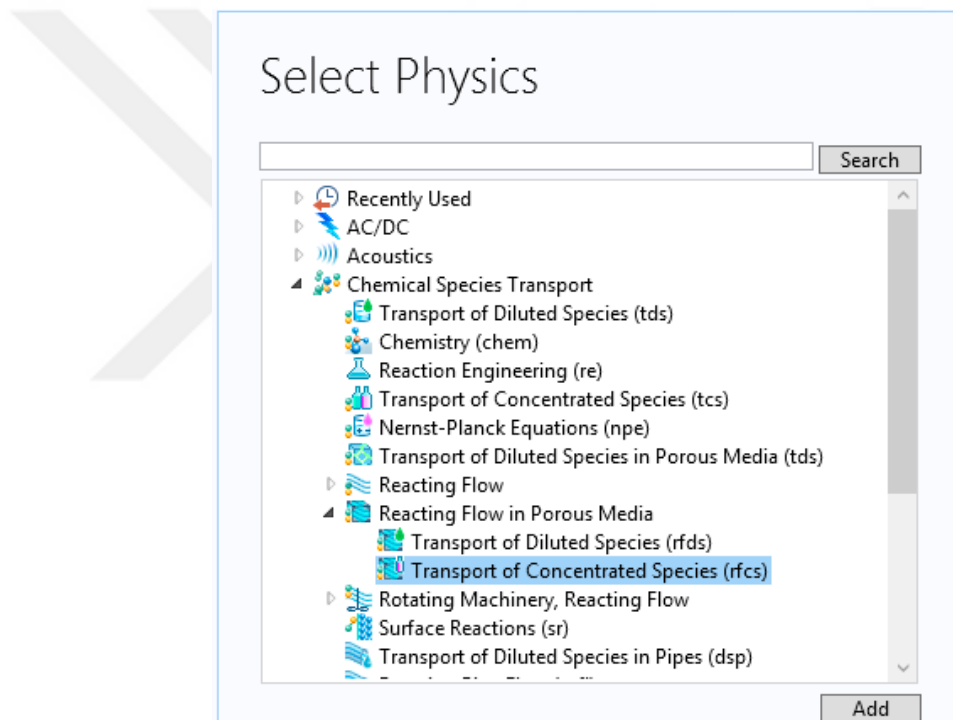


Figure 3.5 Sub-physics of Reacting Flow in Porous Media physics

“Transport of Concentrated Species” physics is added for two times for both anode and cathode compartments because anode compartment has hydrogen as fluid and cathode compartment has water and oxygen. Figure 3.6 indicates the added physics for HT-PEMFC modeling in Comsol Multiphysics.

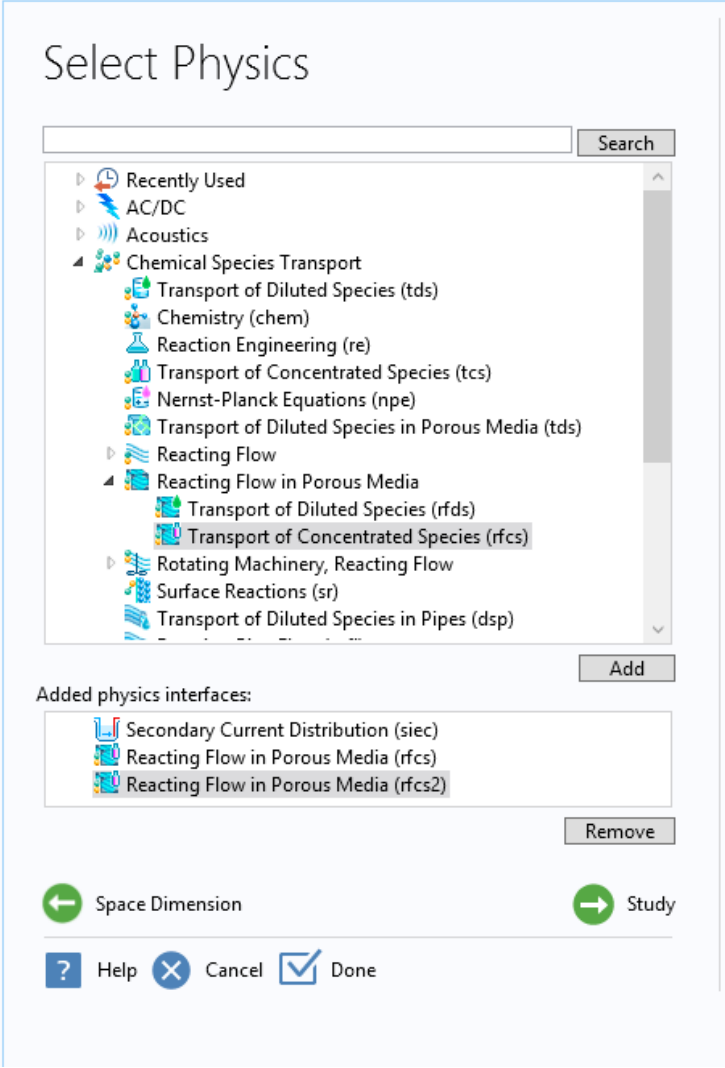


Figure 3.6 Added physics for PEMFC modeling

After the dimension and the physics selections are performed, time dependency of the study should be chosen as the next step of the algorithm. The study may be chosen as AC impedance stationary, AC impedance time dependent, stationary or time dependent. Figure 3.7 presents the different types of study selections available in Comsol Multiphysics. In the scope of HT-PEMFC modeling, study is chosen as “*Stationary*”.

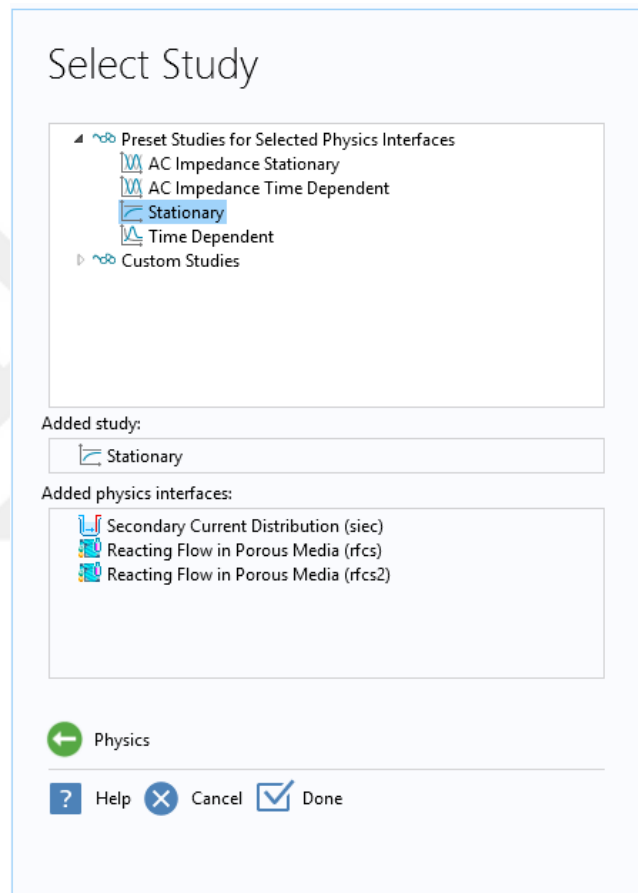


Figure 3.7 Study selection in Comsol Multiphysics

In Comsol Multiphysics, “*Model Builder*” tool is used in order to develop a complete model. “*Definitions*” tool is used for identification of parameters, variables and functions. In this section, required parameters can be embedded to the program as well as different variables can be defined to the program. Moreover, equations that are not included in Comsol Multiphysics program can be expressed in this section. Figure 3.8 shows “*Definitions*” tool and its sub-sections.

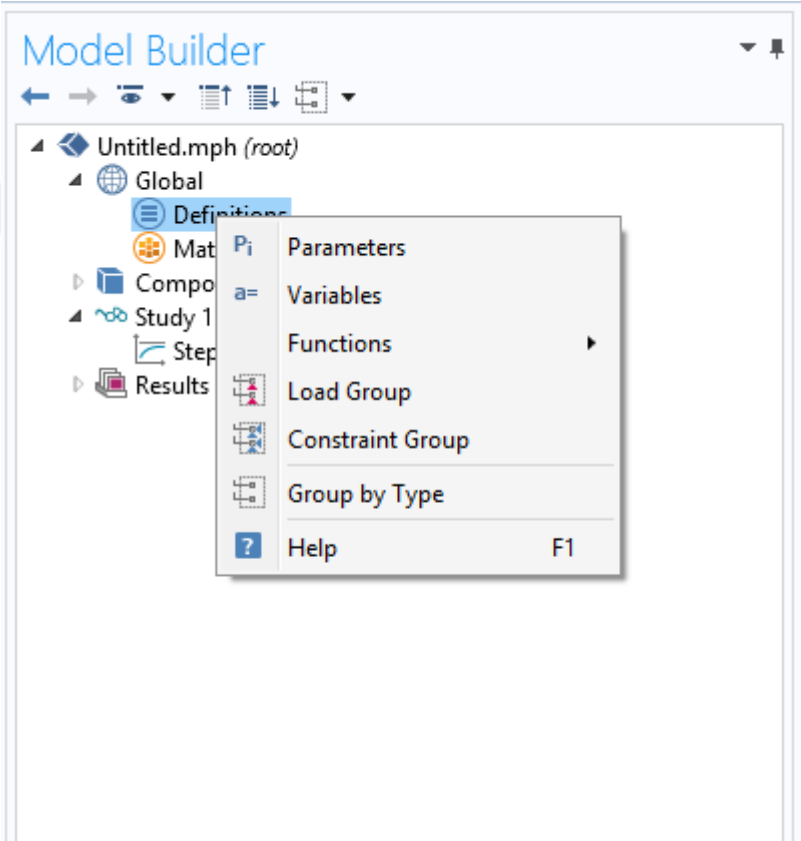


Figure 3.8 “*Definitions*” tool and its sub-sections

For HT-PEMFC modeling, thirty three different parameters are introduced to the program including cell dimensions, component and material properties. There is no variable nor function needed to be introduced in the scope of this study. Figure 3.9 shows the interface of “Parameters” section in Comsol Multiphysics.

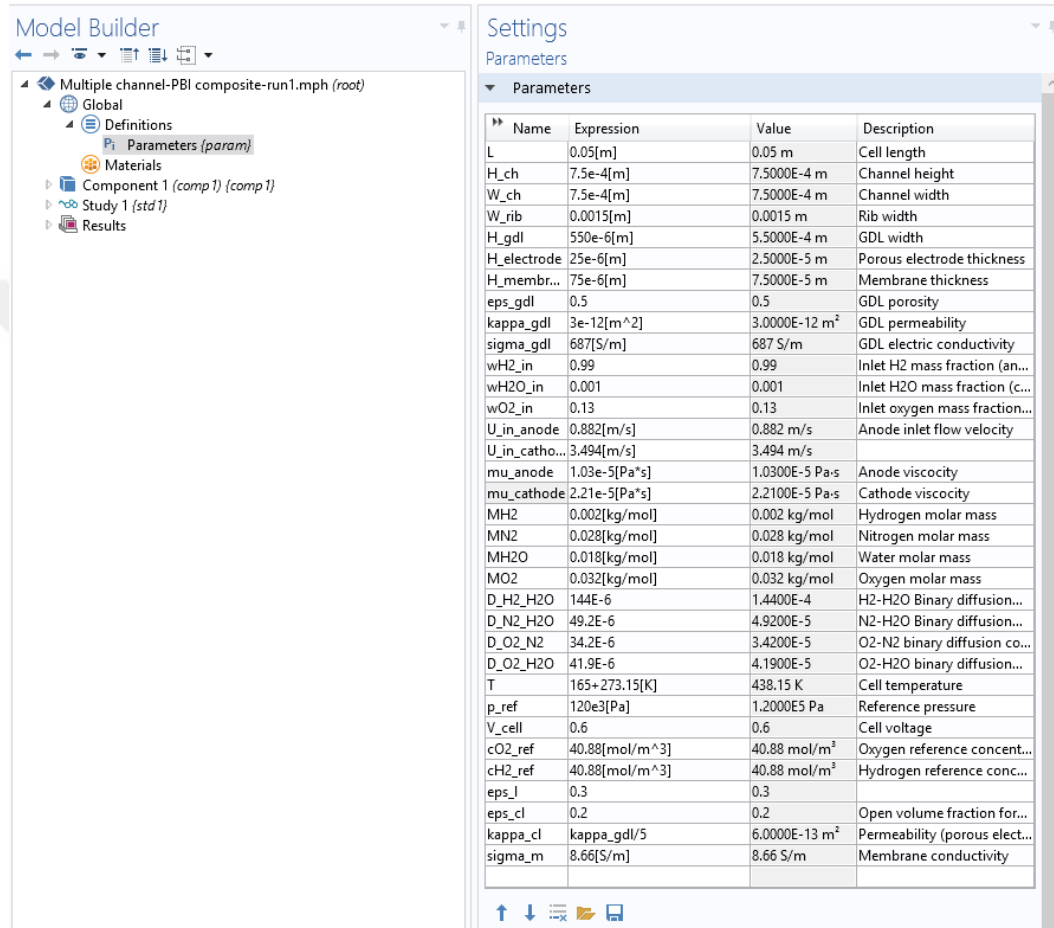


Figure 3.9 “Parameters” section in Comsol Multiphysics

Next step of the algorithm is the selection of materials which will be used in the built model. There are many chemical materials embedded to the program like organic and inorganic chemicals. However, Comsol Multiphysics allows users to define any material that is not available in the program. Material definition can be performed by integrating its chemical and physical properties as parameters. For HT-PEMFC modeling, required materials are hydrogen, oxygen and water. Although these materials are available in the material list of the program, properties of the materials are introduced as parameters such as their viscosities and molecular weights. Figure 3.10 presents the “Materials” section of the program.

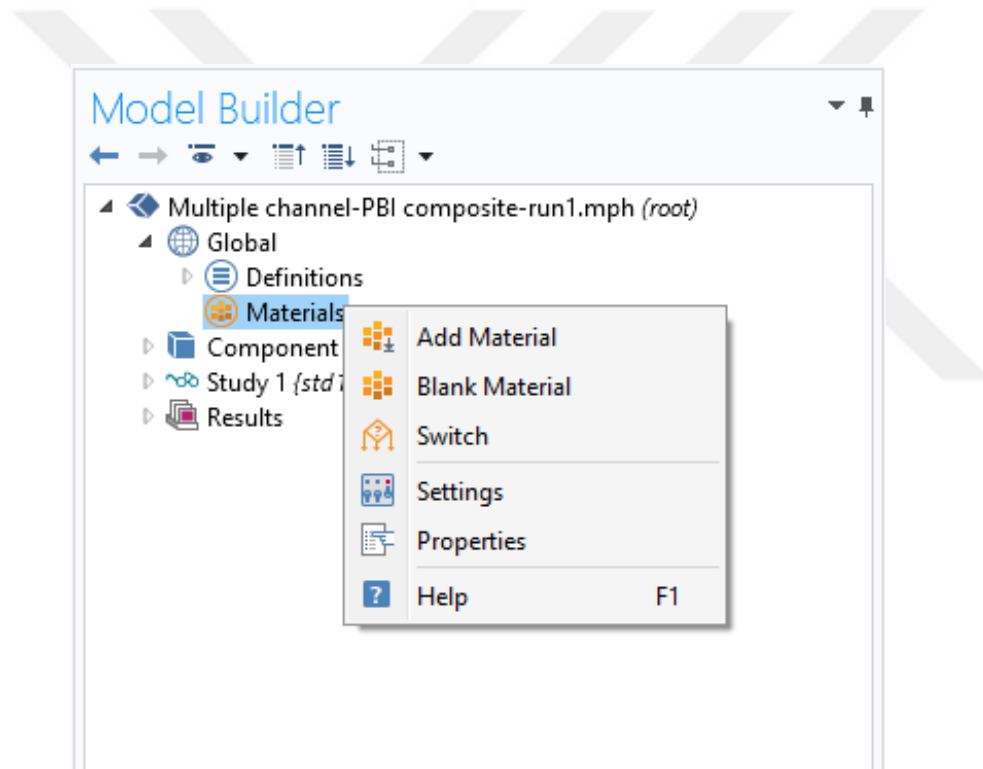


Figure 3.10 “Materials” section in Comsol Multiphysics

“*Component*” section is the most critical part of the algorithm to develop a model in Comsol Multiphysics because this section includes geometry building, the model domain definition, applied physics with respect to assumptions and boundary conditions. The first sub-section of “*Component*” section is “*Definitions*”. This tool is used to define each domain, boundary, edge or point of the model geometry. However, in order to make this identification, the geometry of the domain should be developed firstly. The interface of “*Definitions*” tool under “*Component*” section is shown in Figure 3.11.

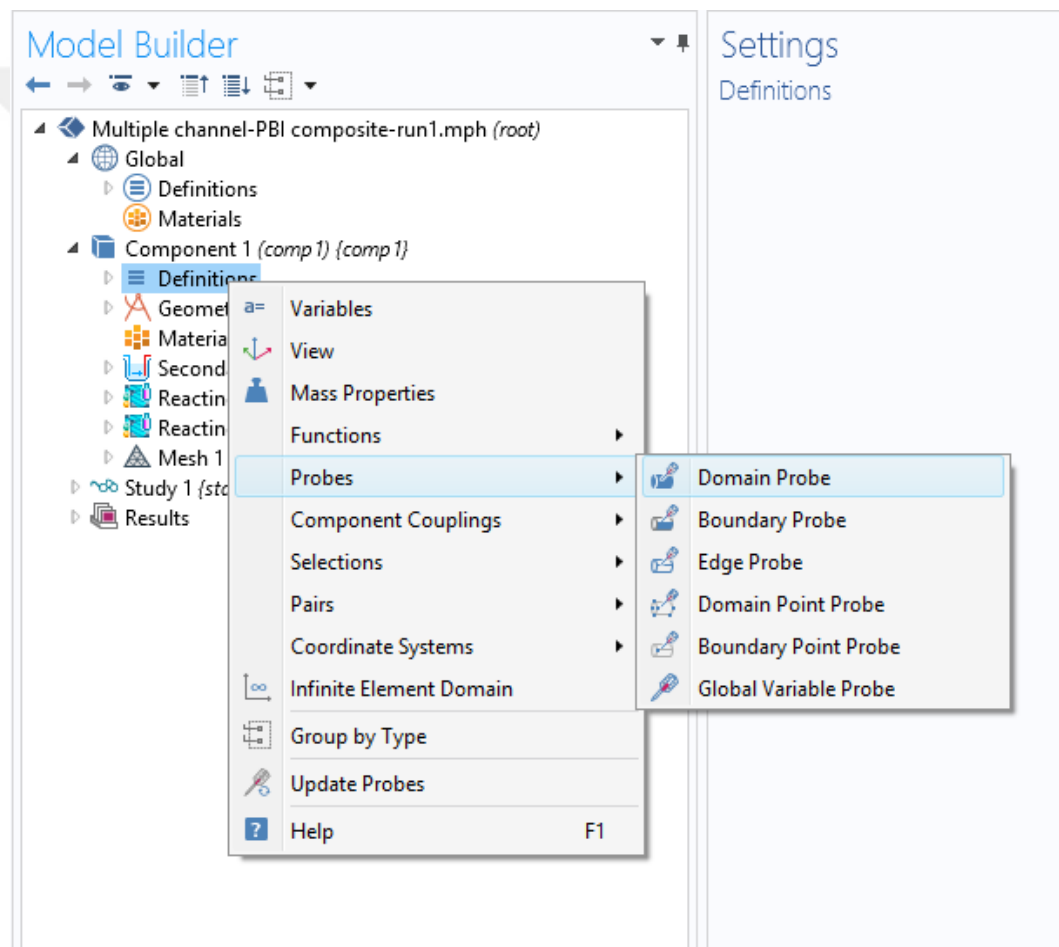


Figure 3.11 “*Definitions*” tool under “*Component*” section in Comsol Multiphysics

The “Geometry” tool is the backbone of the model building in Comsol Multiphysics. Components of a model can be built in the shape of block, cone, cylinder, sphere and more. For more complex geometries, “Work Plane” tool can be used as 2-D drawing. Then, it can be extruded with respect to the model height to make the geometry 3-D. Moreover, many operations can be performed as Booleans and Partitions, Transforms and Conversions in order to build the geometry easier. The “Geometry” section and its sub-sections are presented in Figure 3.12.

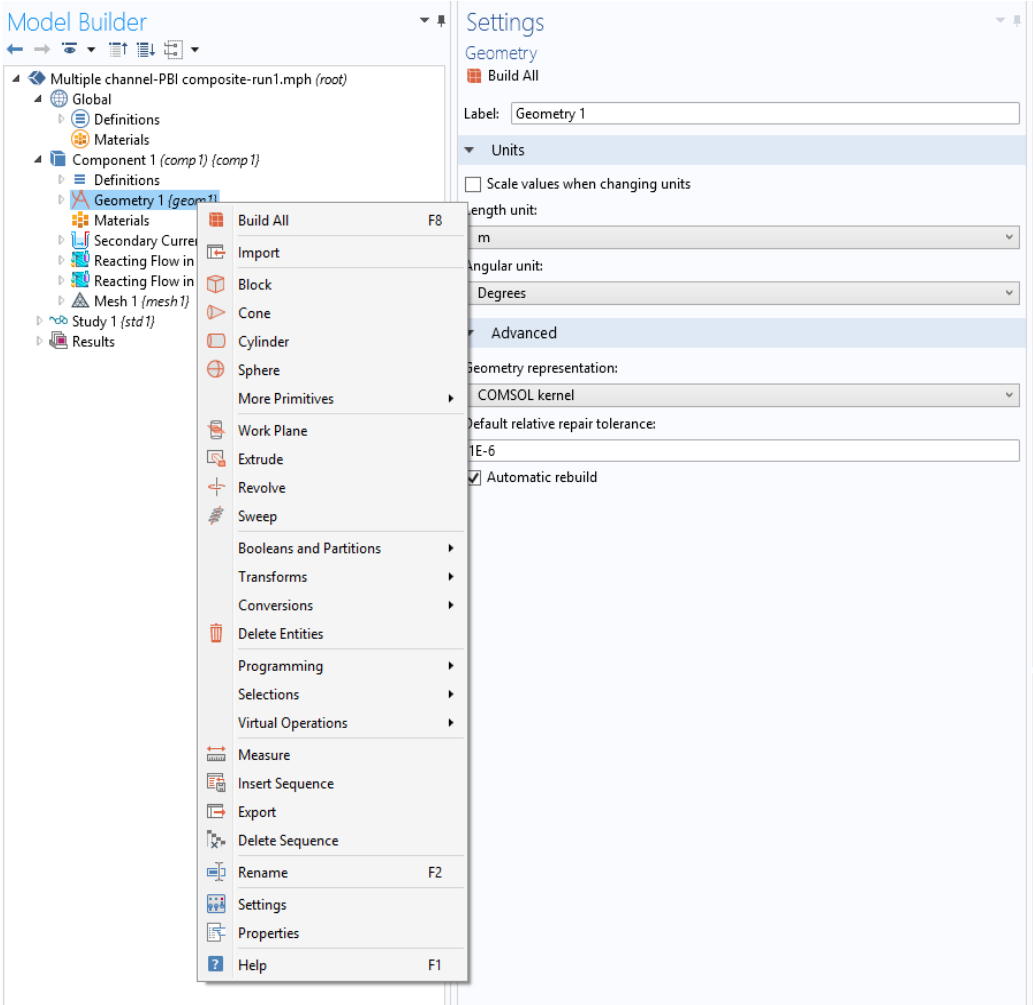


Figure 3.12 “Geometry” section in Comsol Multiphysics

For HT-PEMFC modeling, components of the MEA is built by using blocks. These blocks are built with respect to the parameters embedded to the programs including dimensions. Flow channels are built by work planes for multiple channel geometry since it includes numbers of channels in mixed serpentine type. Then they are extruded according to their height. Figure 3.13 represents the steps of HT-PEMFC model building including blocks to built MEA.

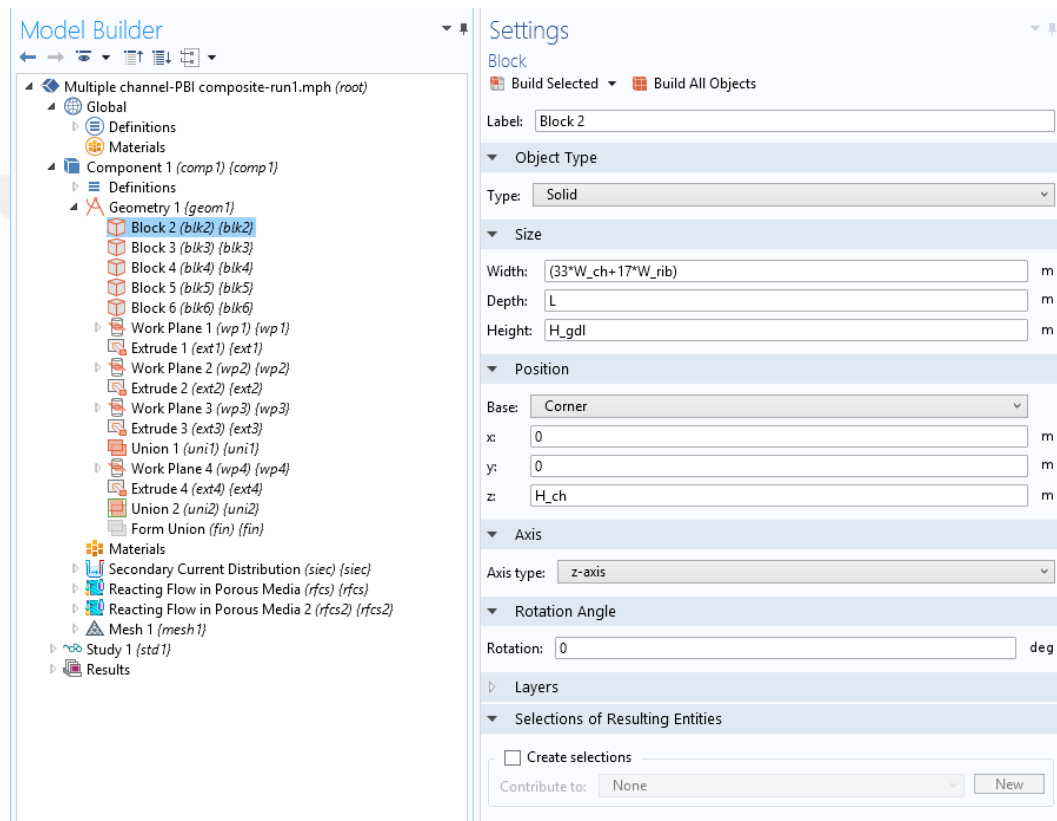


Figure 3.13 Building steps of MEA for PEMFC modeling

Once the MEA is built by using blocks, flow channels of the cell are needed to be built. For multiple flow channels, “Work Plane” tool is used to draw the domain as 2-D. The plane face can be identified as face parallel, edge parallel and so on. In this model development, “Face parallel” plane is chosen. Figure 3.14 shows the “Work Plane” settings in Comsol Multiphysics.

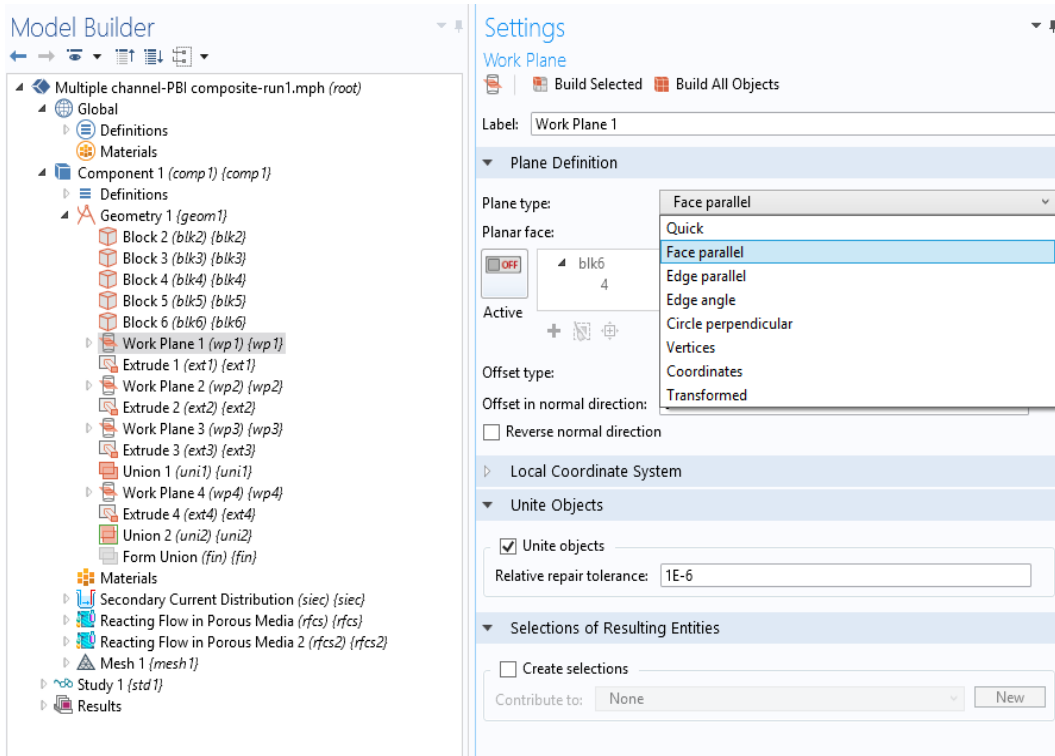


Figure 3.14 Work Plane settings in Comsol Multiphysics

Figure 3.15 shows the required geometry selections for drawing 2-D multiple flow channel geometry in mixed serpentine type. Rectangles are used for the flow channels and Fillet is used for the connection of flow channels. The complete drawing of 2-D multiple channel geometry in mixed serpentine type for HT-PEMFC modeling is shown in Figure 3.16.

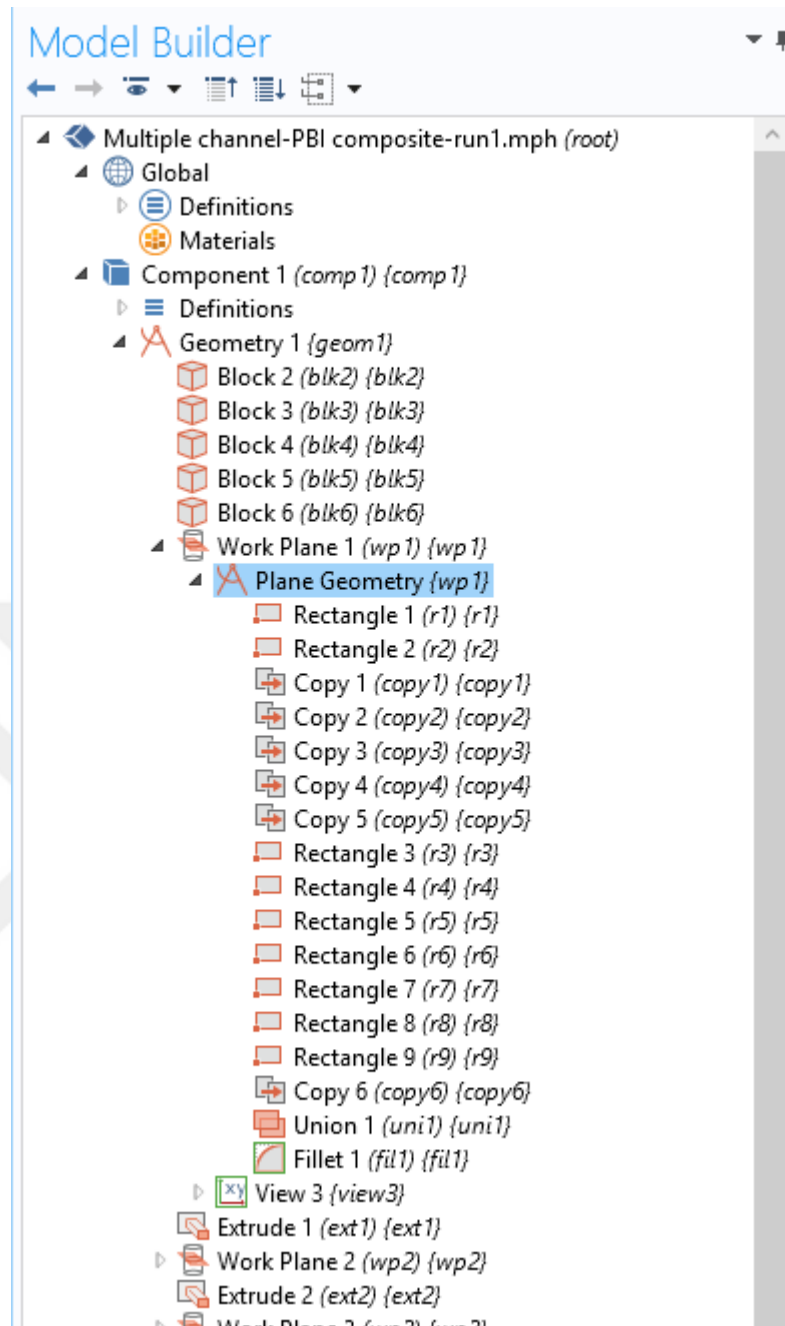


Figure 3.15 Geometry building in Work Plane for multiple channel geometry

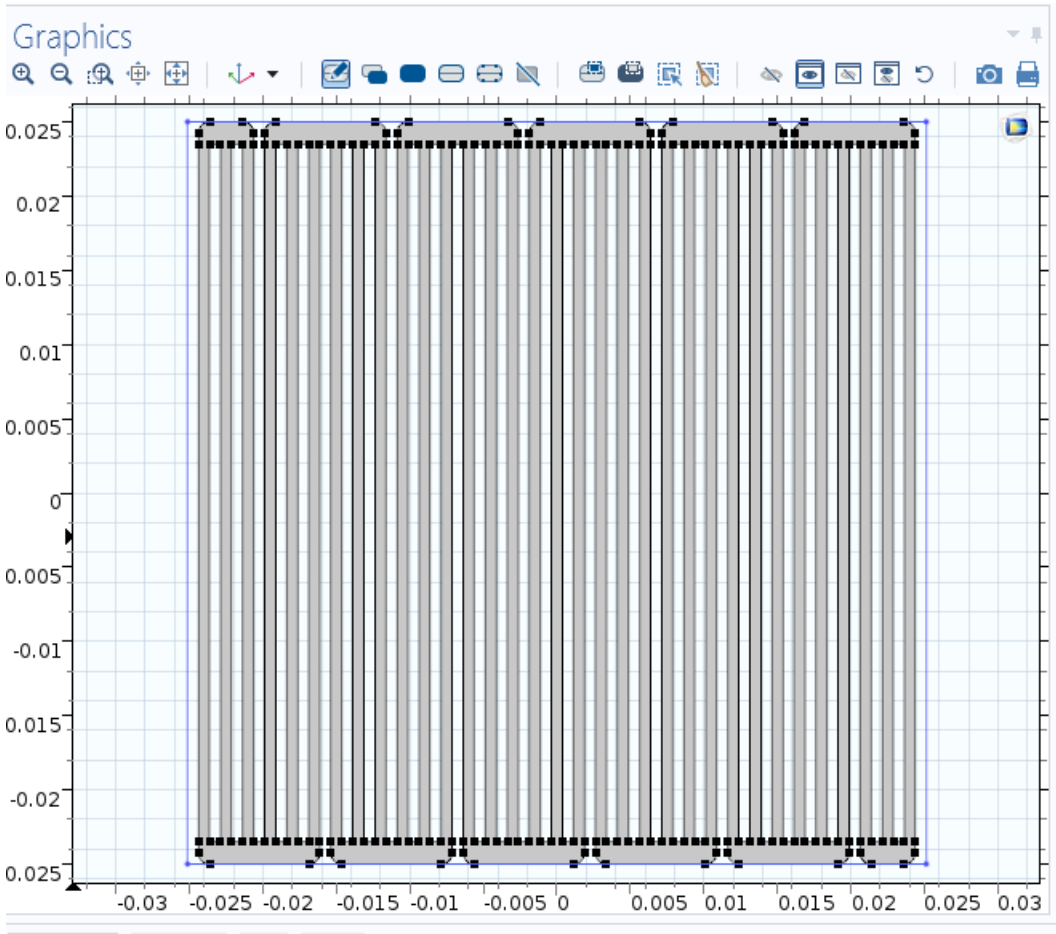


Figure 3.16 2-D drawing of mixed serpentine flow channel geometry by Work Plane

After the geometry building is finished, “Definitions” tool, which is shown in Figure 3.11, can be completed. For PEMFC modeling, seven different domain probes are defined in this section: anode channel, anode GDL, anode electrode, membrane, cathode electrode, cathode GDL and cathode channel. Moreover, anode compartment is defined as including anode channel, anode GDL and anode electrode as well as cathode compartment is defined as including cathode channel, cathode GDL and cathode electrode. Figure 3.17 indicated the identified probes for HT-PEMFC modeling.

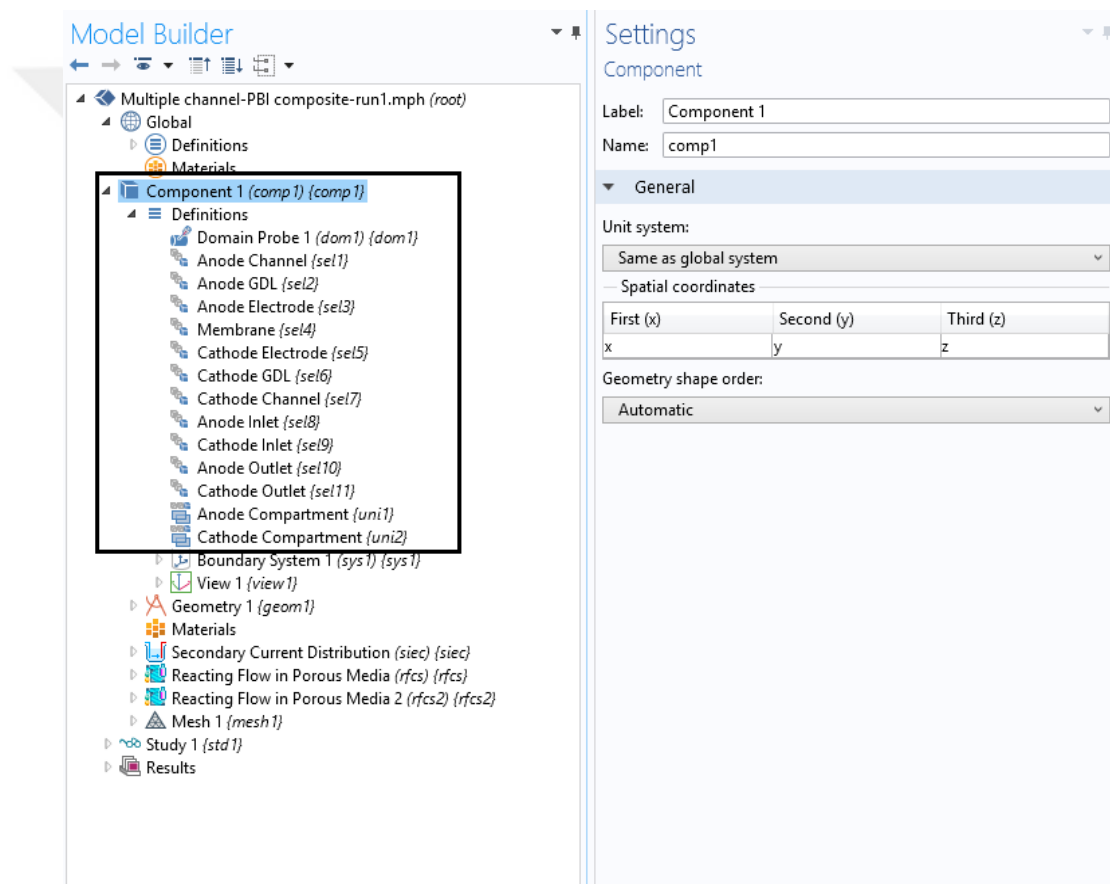


Figure 3.17 Domain probes of PEMFC model

Model development algorithm is followed by the making the details of added physics appropriate for the model. For HT-PEMFC modeling, “Secondary Current Distribution” physics is starting point that begins with “Electrolyte”. The domain of electrolyte can be chosen from the settings of “Electrolyte” section. Equations are given by the program itself. Figure 3.18 represents the “Electrolyte” section and its settings in Comsol Multiphysics.

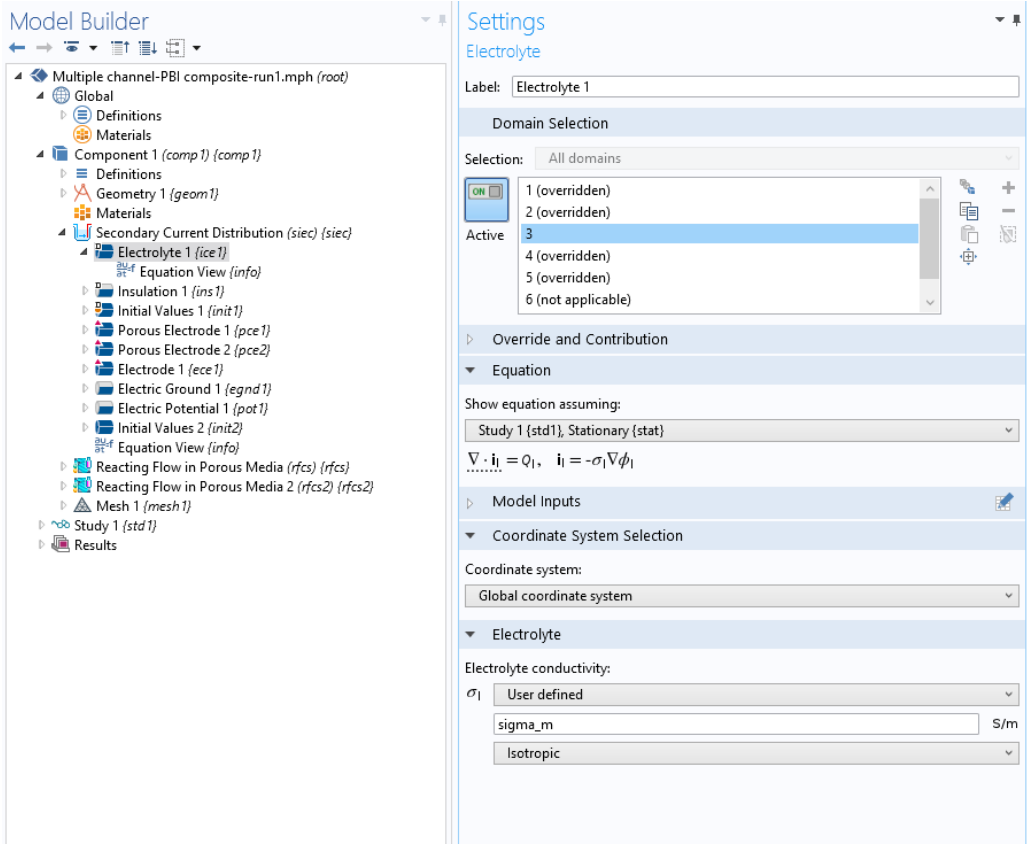


Figure 3.18 “Electrolyte” section and its settings in Comsol Multiphysics

“Insulation” is another sub-section of “*Secondary Current Distribution*” physics. According to the assumptions that are determined for the valid model, boundaries of the model that are insulated should be chosen carefully. For this model, all boundaries of the MEA as chosen as insulated from the environment. Figure 3.19 indicates the “Insulation” section and its setting in Comsol Multiphysics.

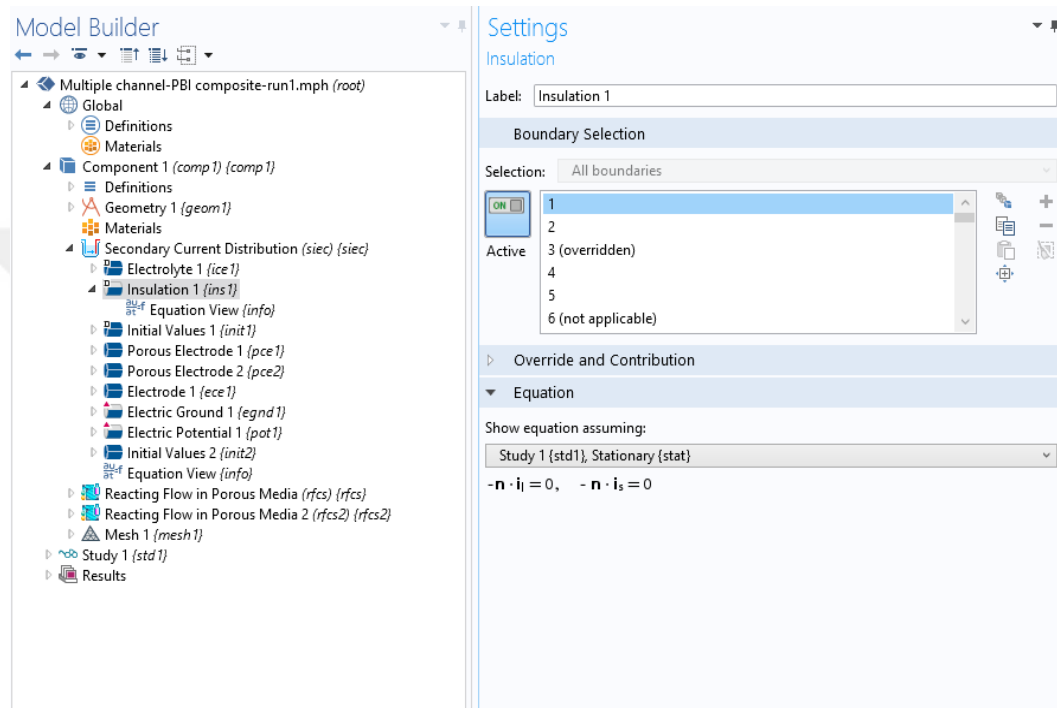


Figure 3.19 “Insulation” section and its setting in Comsol Multiphysics

The following sub-sections of “*Secondary Current Distribution*” physics are in the same logic with the previous sub-sections. For the present section of the physics, applicable domain or boundary should be chosen in order to define which parts of the domain are solved by the embedded equations. Following figures, Figure 20-28, show the sub-sections and their setting in “*Secondary Current Distribution*” physics.

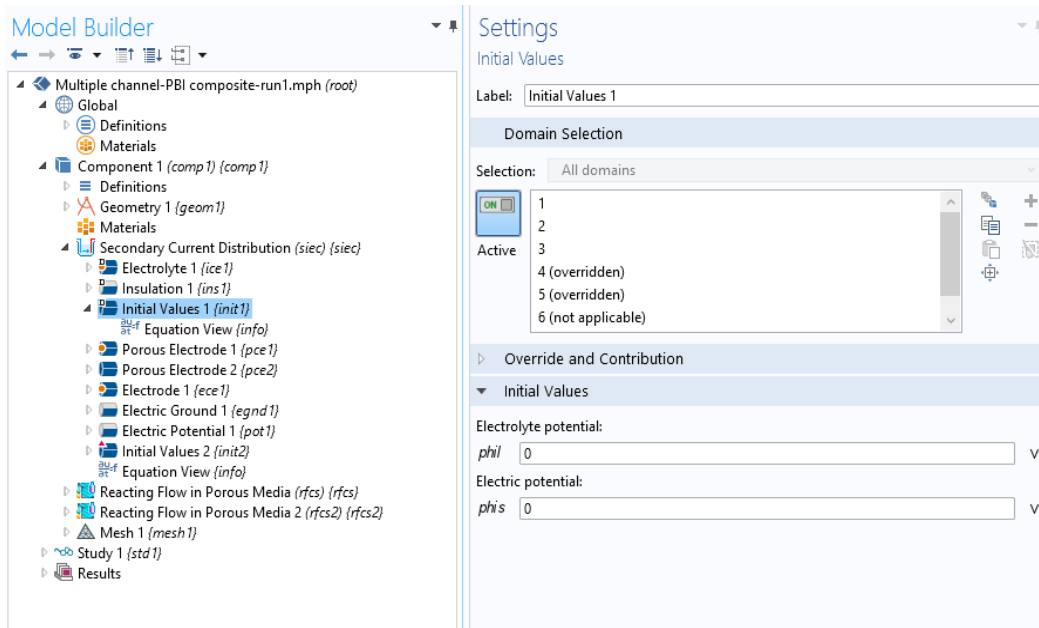


Figure 3.20 “Initial Values” and its settings in Comsol Multiphysics

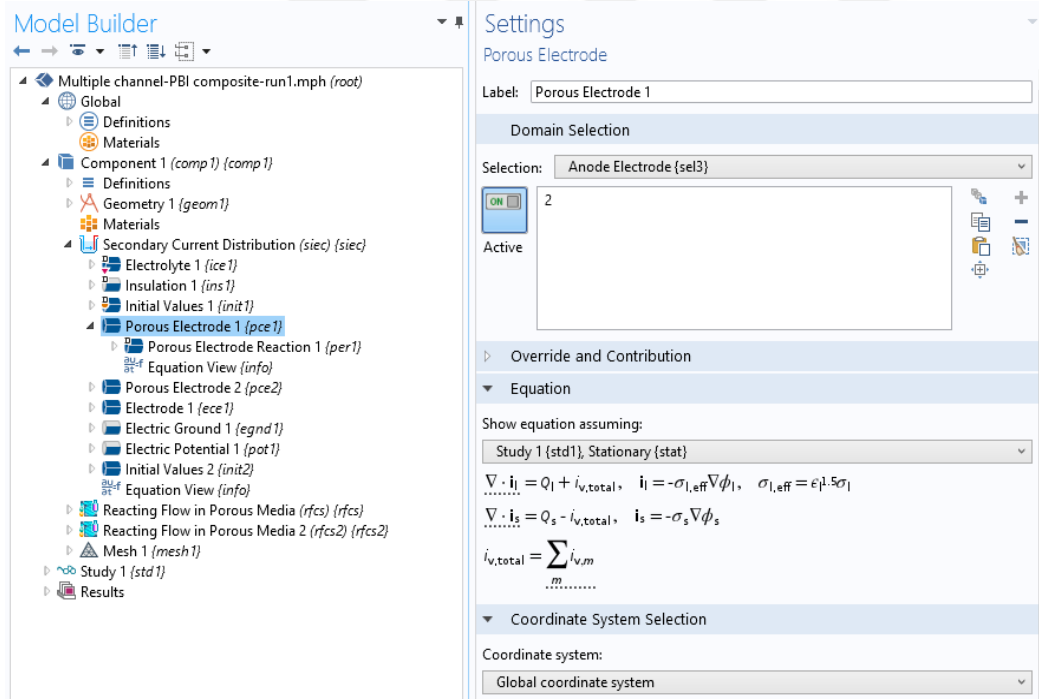


Figure 3.21 “Porous Electrode 1” and its settings in Comsol Multiphysics

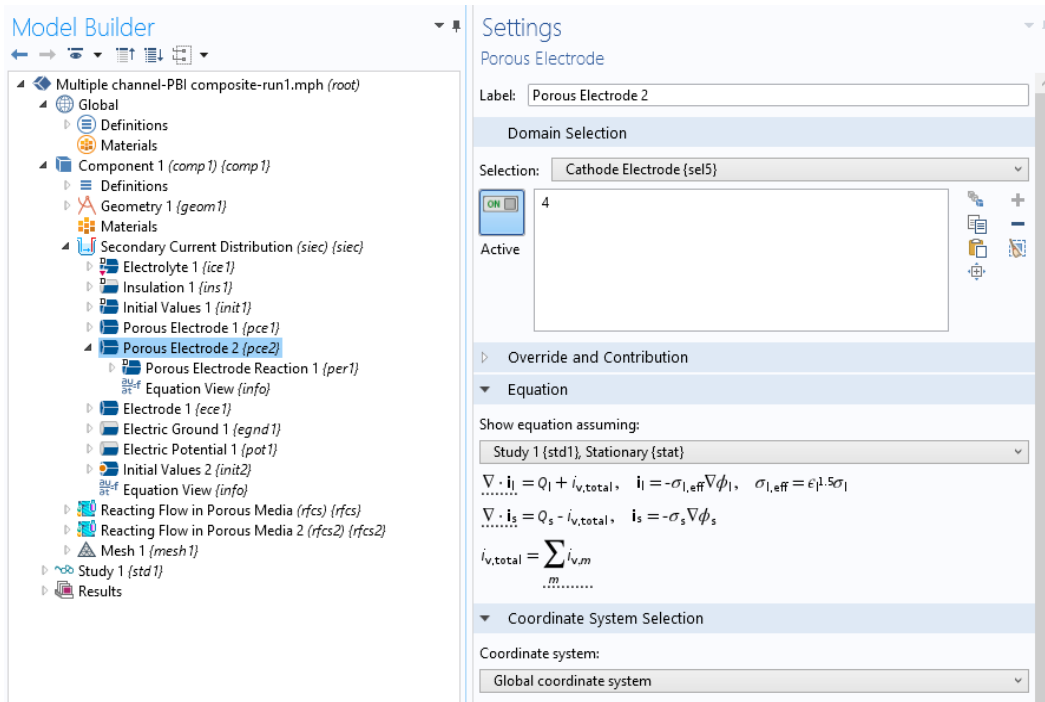


Figure 3.23 “Porous Electrode 2” and its settings in Comsol Multiphysics

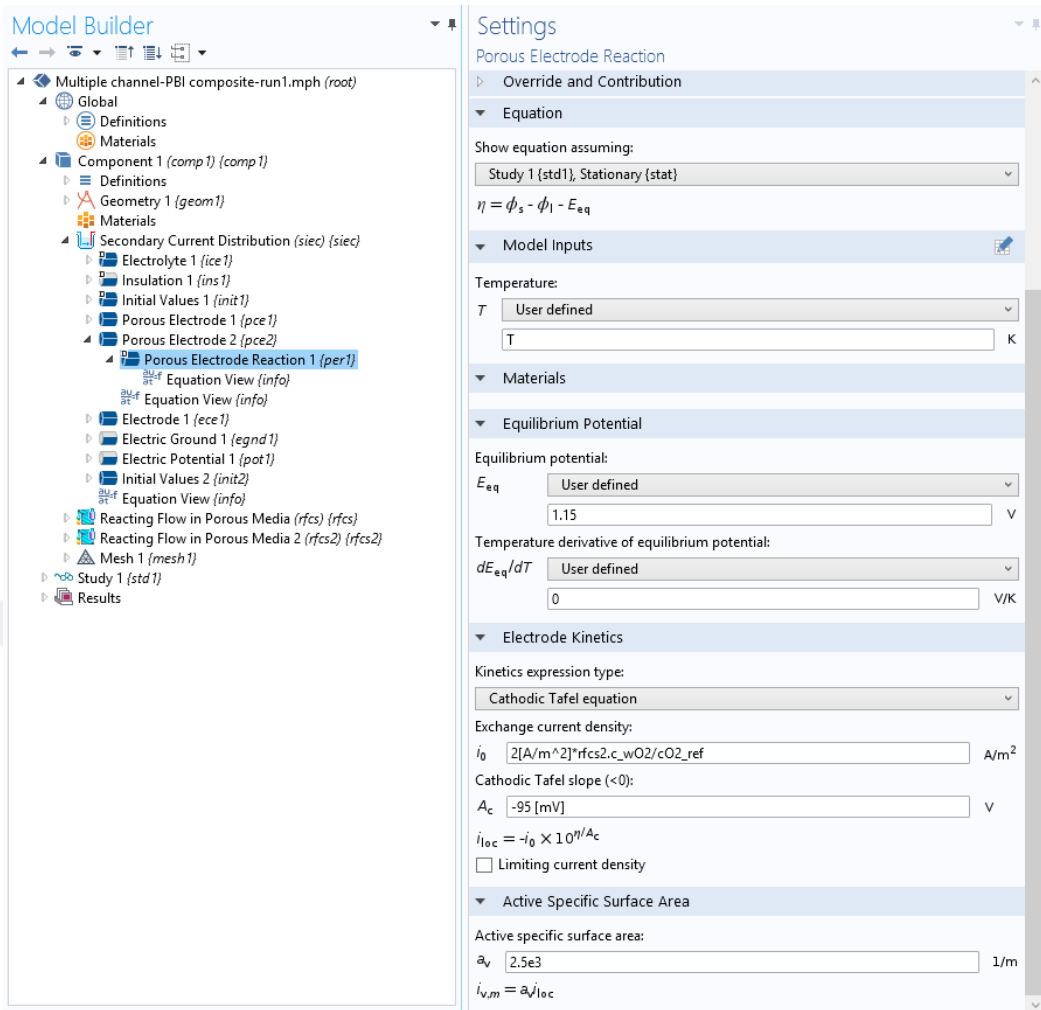


Figure 3.24 “Porous Electrode Reaction 2” and its settings in Comsol Multiphysics

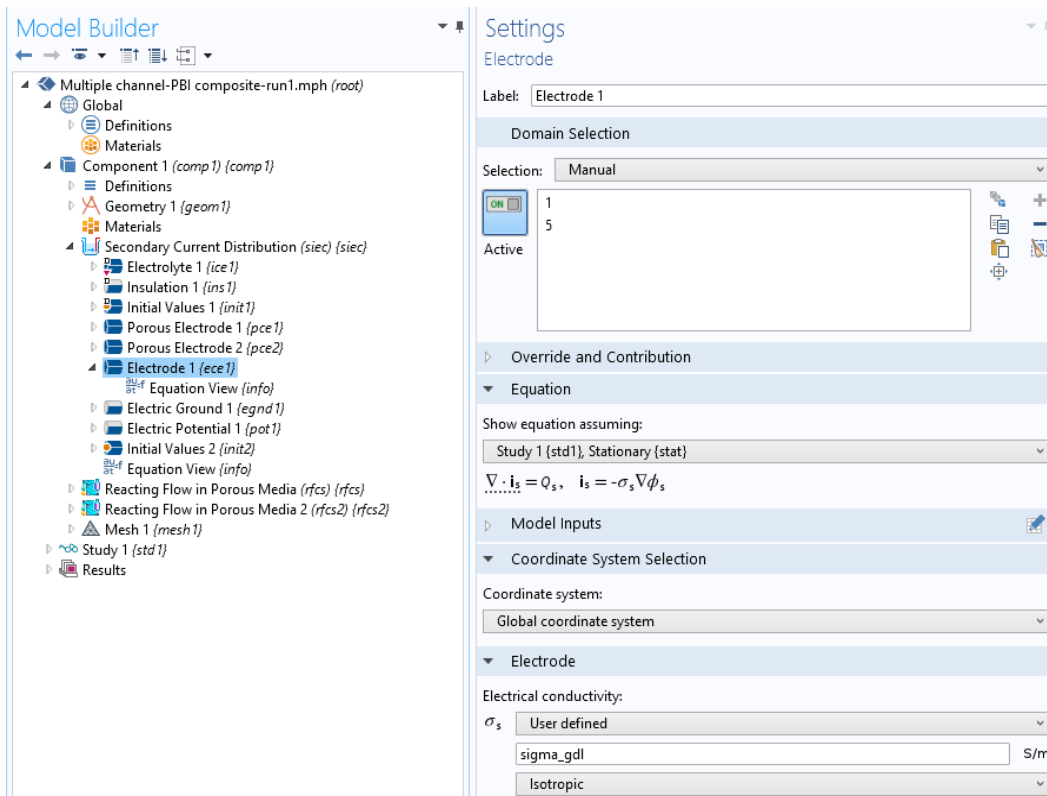


Figure 3.25 “Electrode 1” and its settings in Comsol Multiphysics

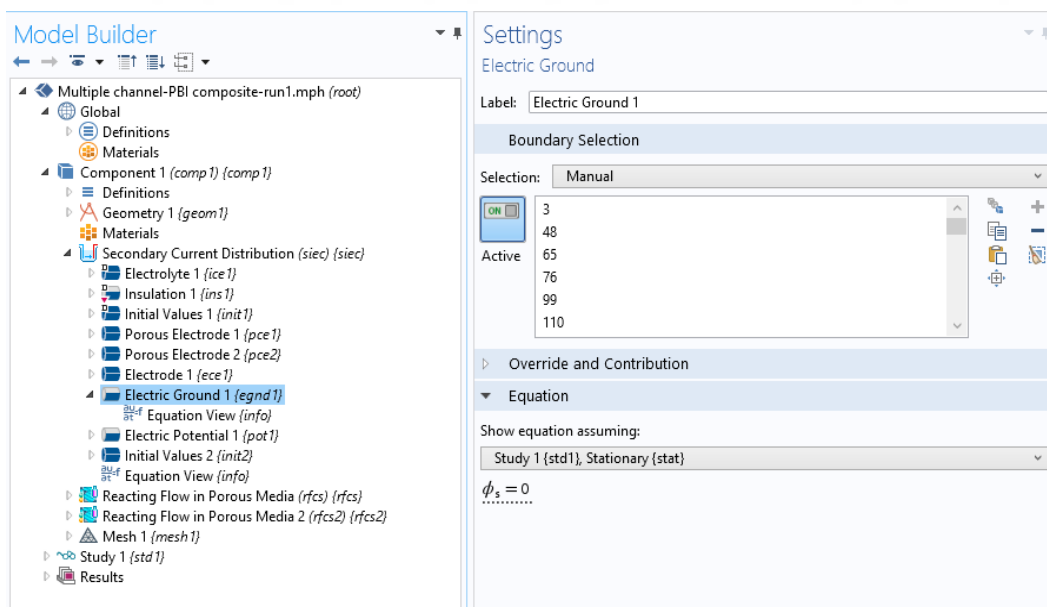


Figure 3.26 “Electric Ground 1” and its settings in Comsol Multiphysics

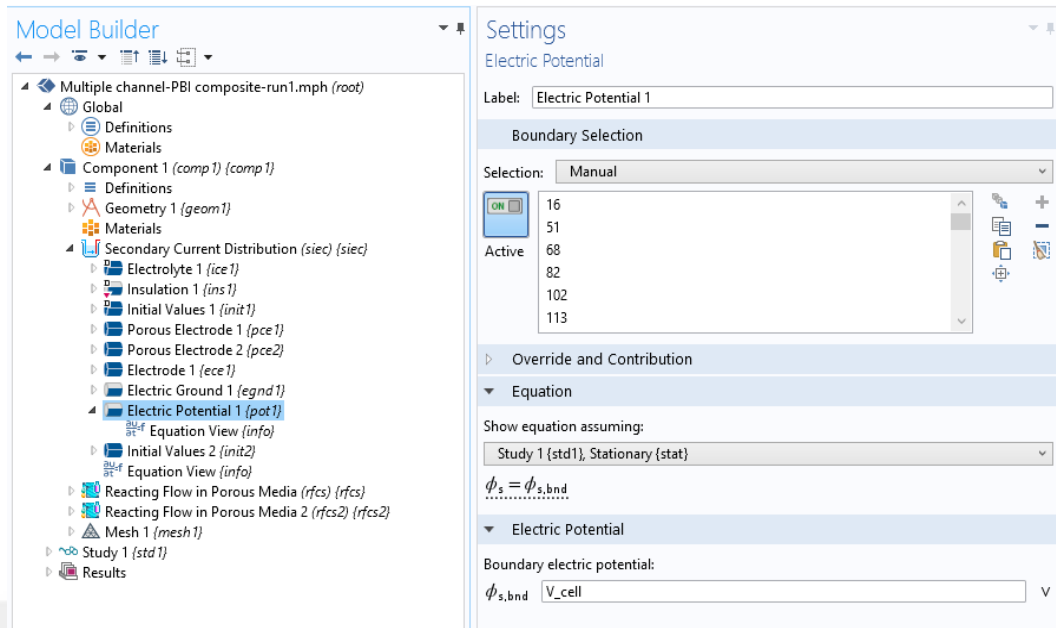


Figure 3.27 “Electric Potential 1” and its settings in Comsol Multiphysics

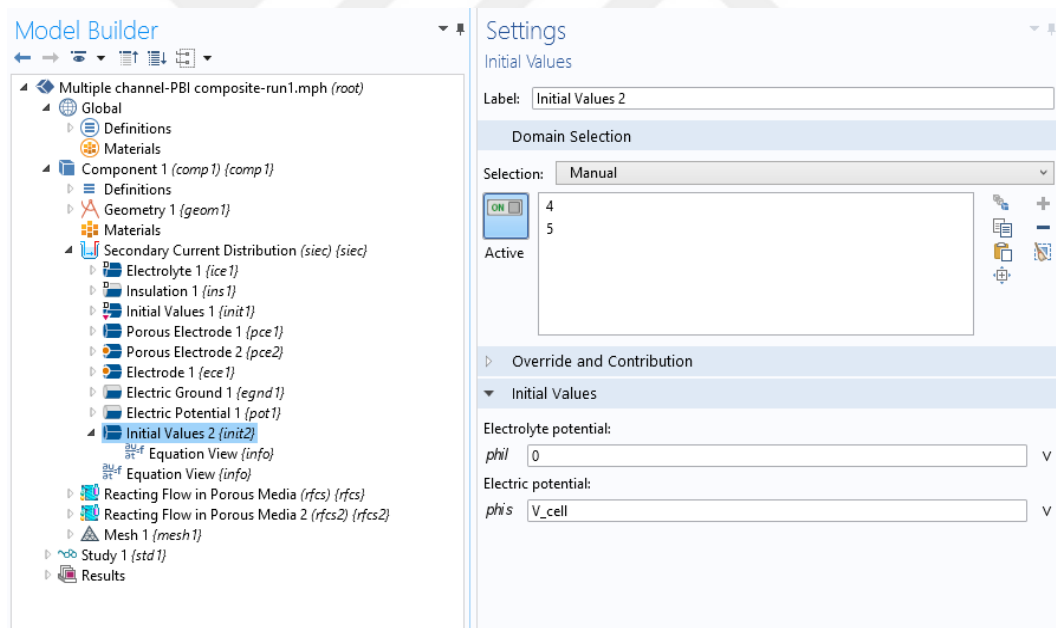


Figure 3.28 “Initial Values 2” and its settings in Comsol Multiphysics

The next step of the algorithm is followed by “*Reacting Flow of Porous Media*” physics needed to be defined appropriately according to the developed model specifications. This physics is firstly applied for anode compartment. Figure 3.29 shows the interface of this physics and settings section which includes the domain selection and equations.

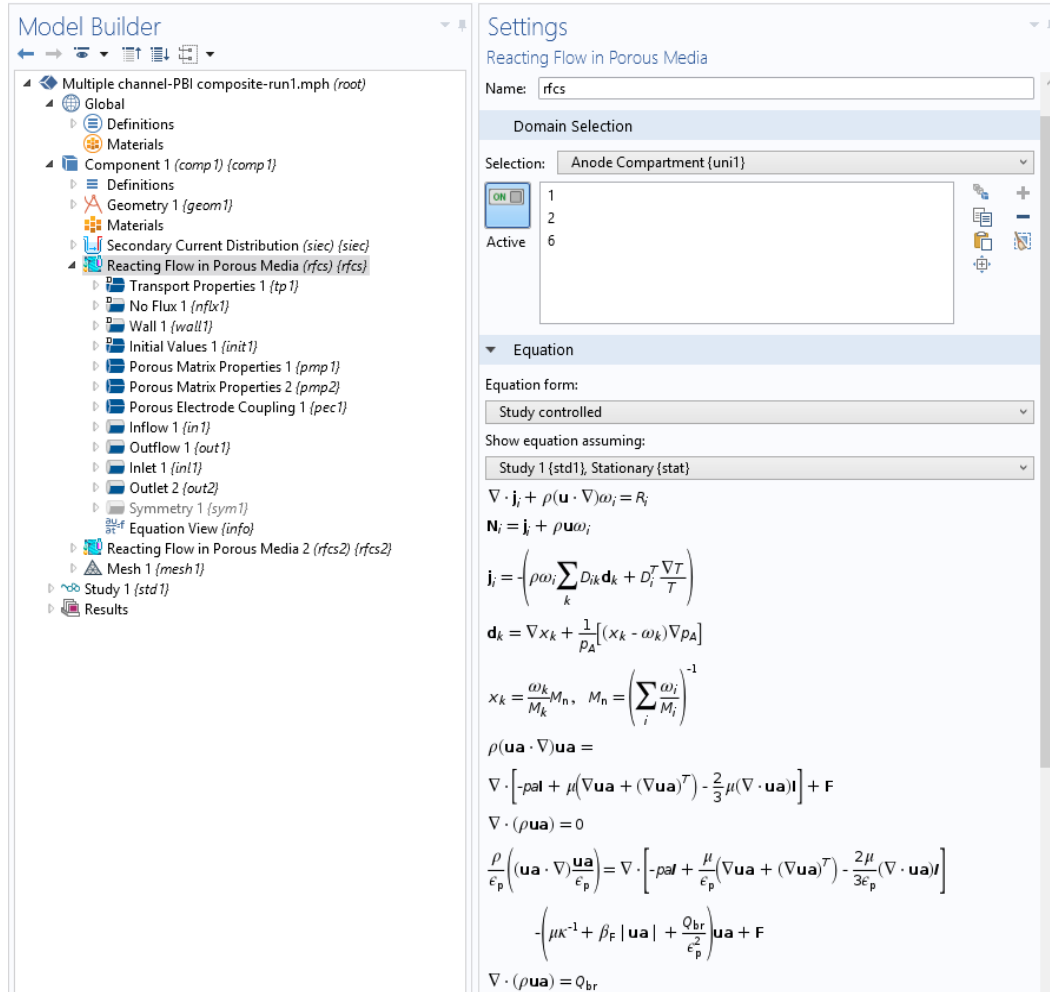


Figure 3.29 “*Reacting Flow of Porous Media*” physics and its sub-sections

“Transport Properties” is the first sub-section of this physics. In settings section, model inputs and fluid properties should be integrated to the program either by entering mathematical inputs or parameter names. Figure 3.30 demonstrates the “Transport Properties” section and its settings in Comsol Multiphysics.

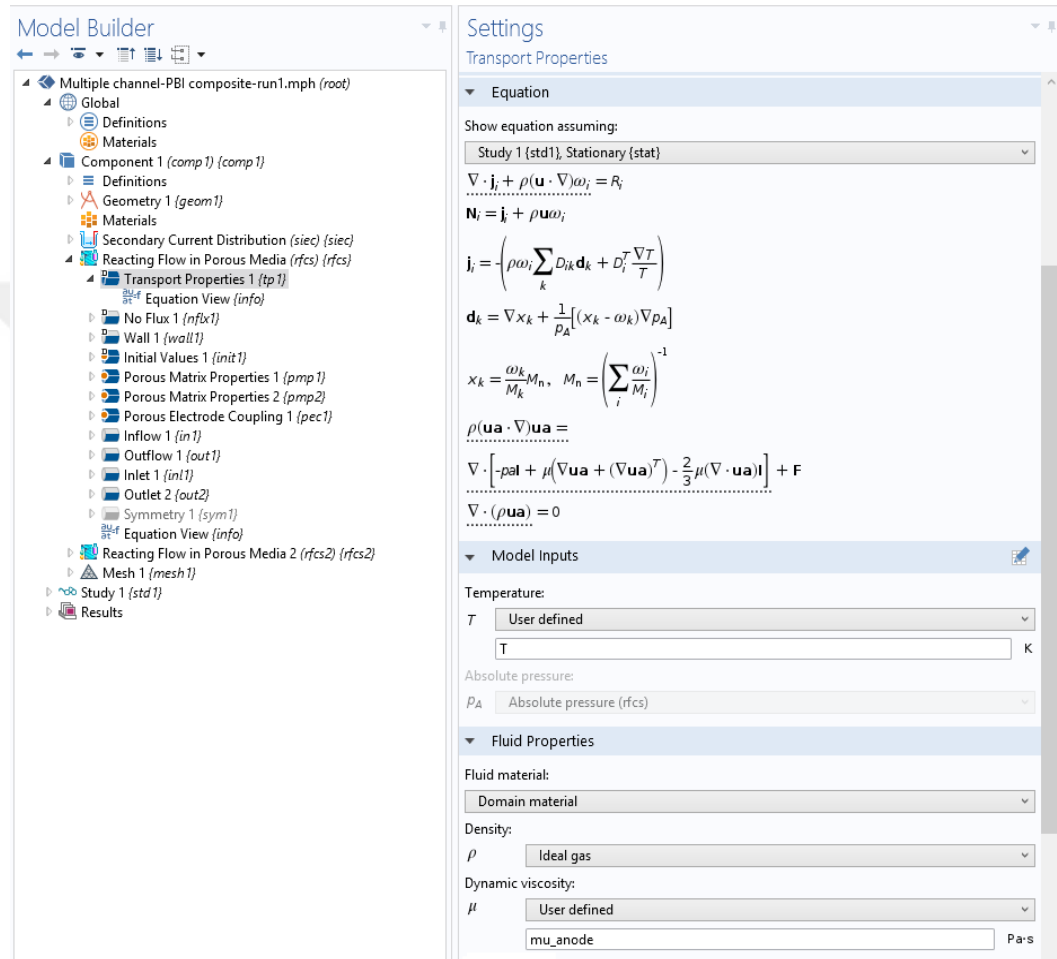


Figure 3.30 “Transport Properties” section and its settings in Comsol Multiphysics

The following figures, Figure 31-40, show the remaining sub-sections of “Reacting Flow in Porous Media” physics. Boundary or domain selection is the first step that should be determined for these sub-steps.

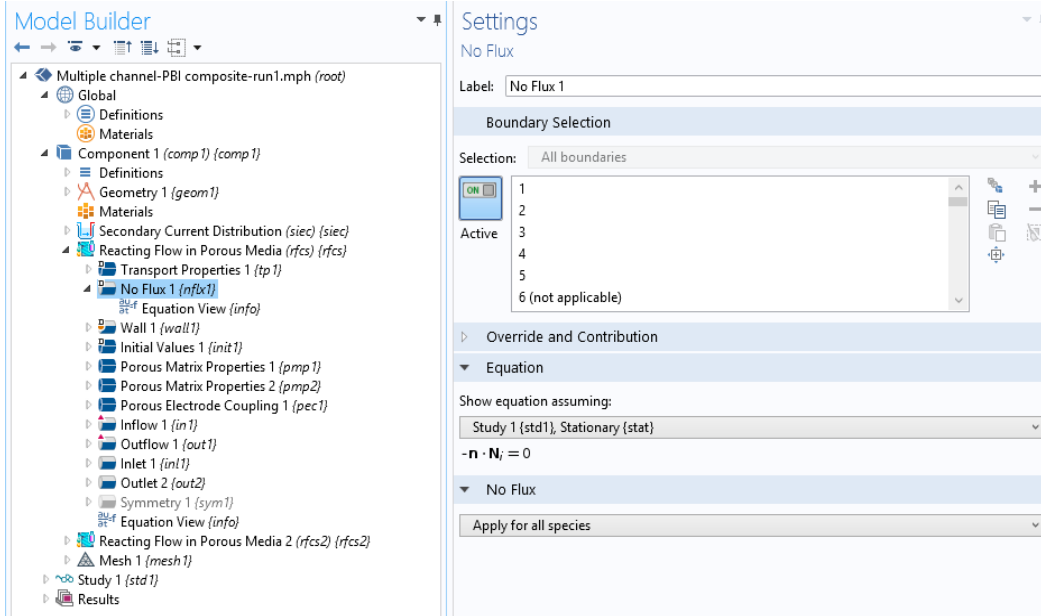


Figure 3.31 “No Flux” section and its setting in Comsol Multiphysics

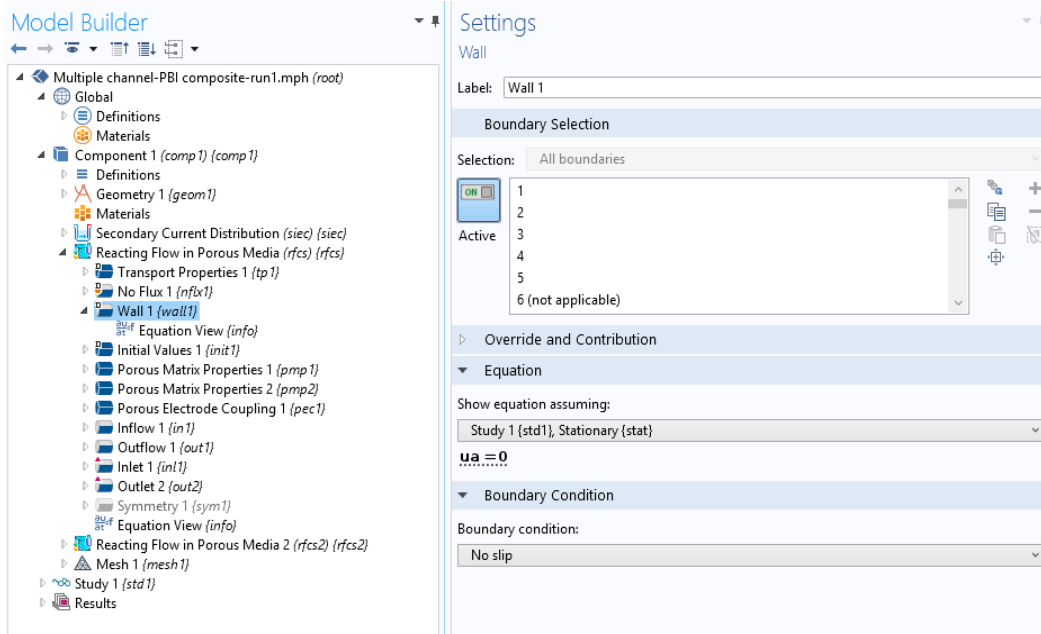


Figure 3.32 “Wall 1” section and its setting in Comsol Multiphysics

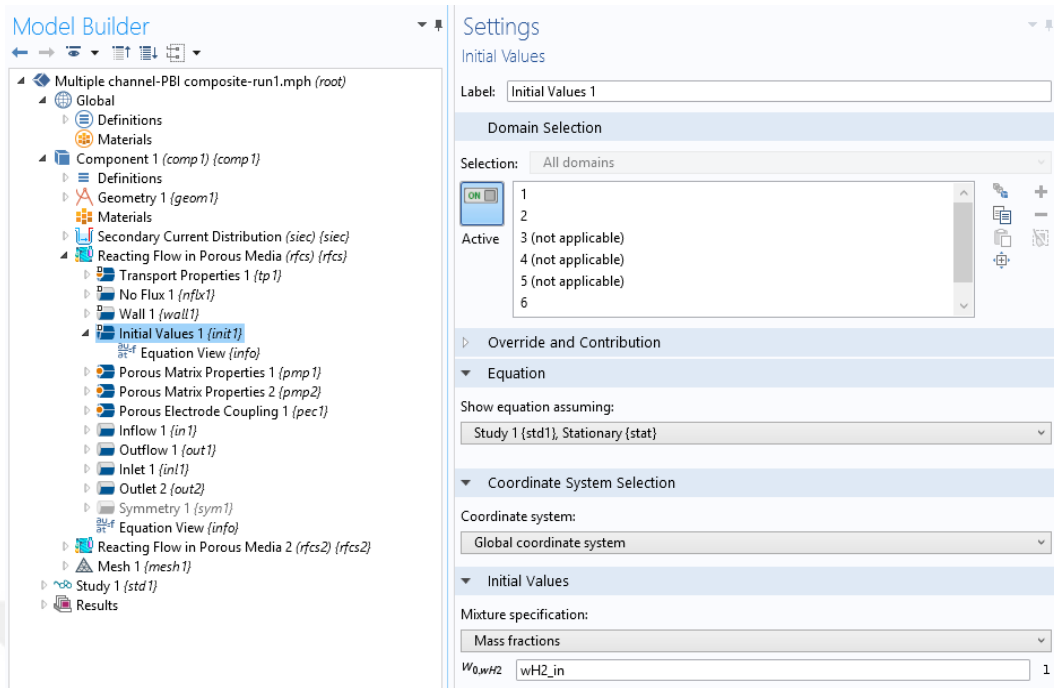


Figure 3.33 “Initial Values 1” section and its setting in Comsol Multiphysics

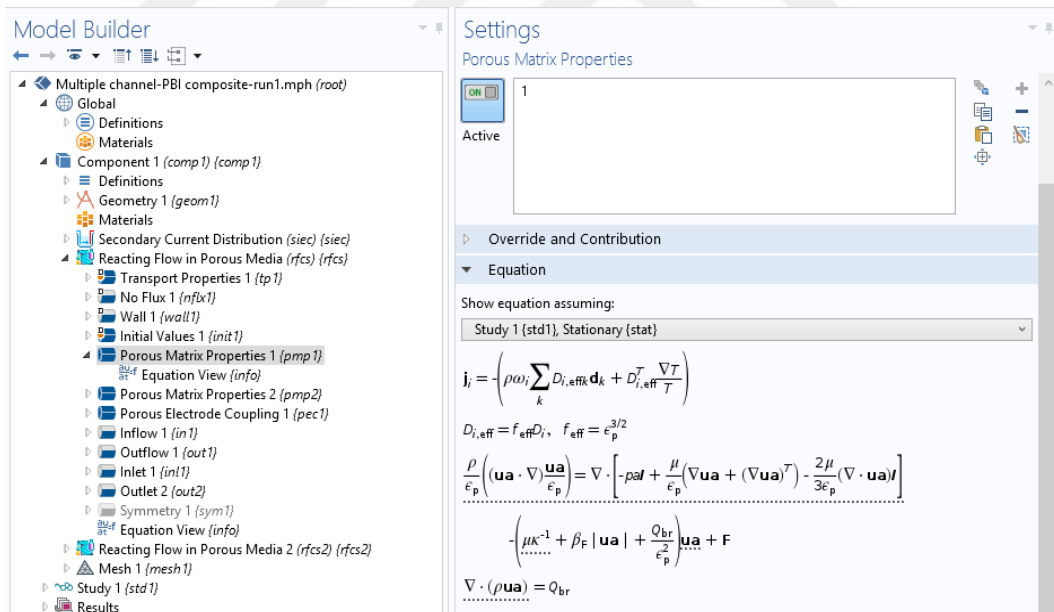


Figure 3.34 “Porous Matrix Properties 1” section and its setting in Comsol Multiphysics

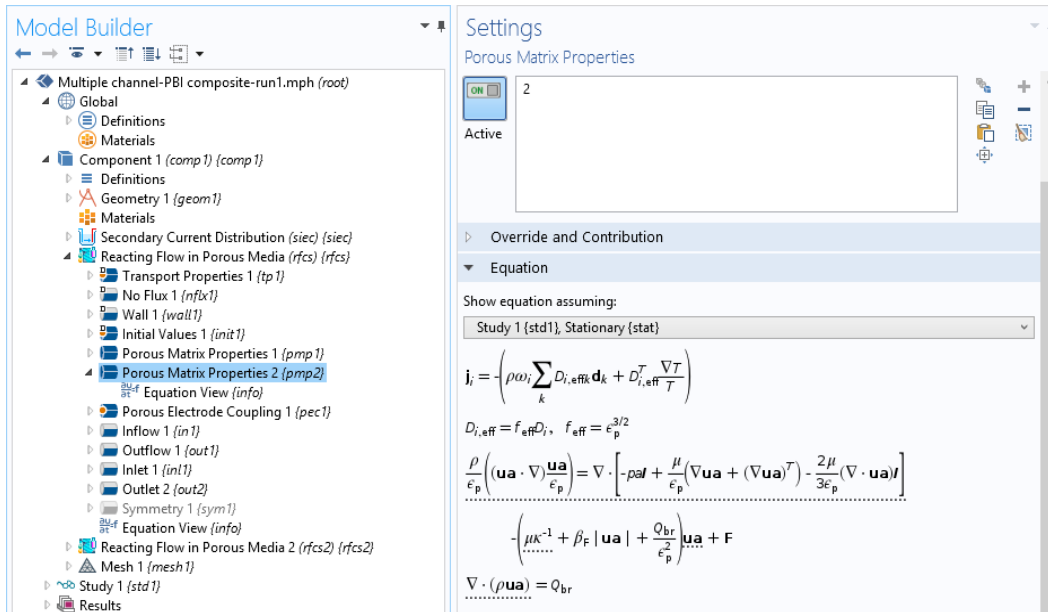


Figure 3.35 “Porous Matrix Properties 2” section and its setting in Comsol Multiphysics

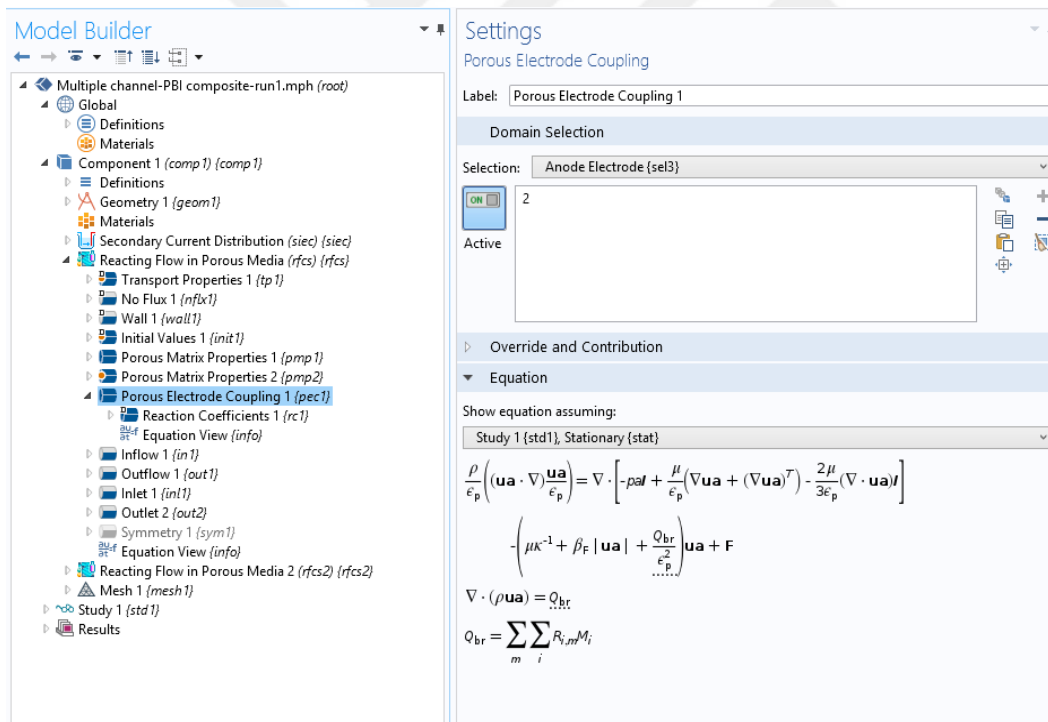


Figure 3.36 “Porous Electrode Coupling 1” section and its setting in Comsol Multiphysics

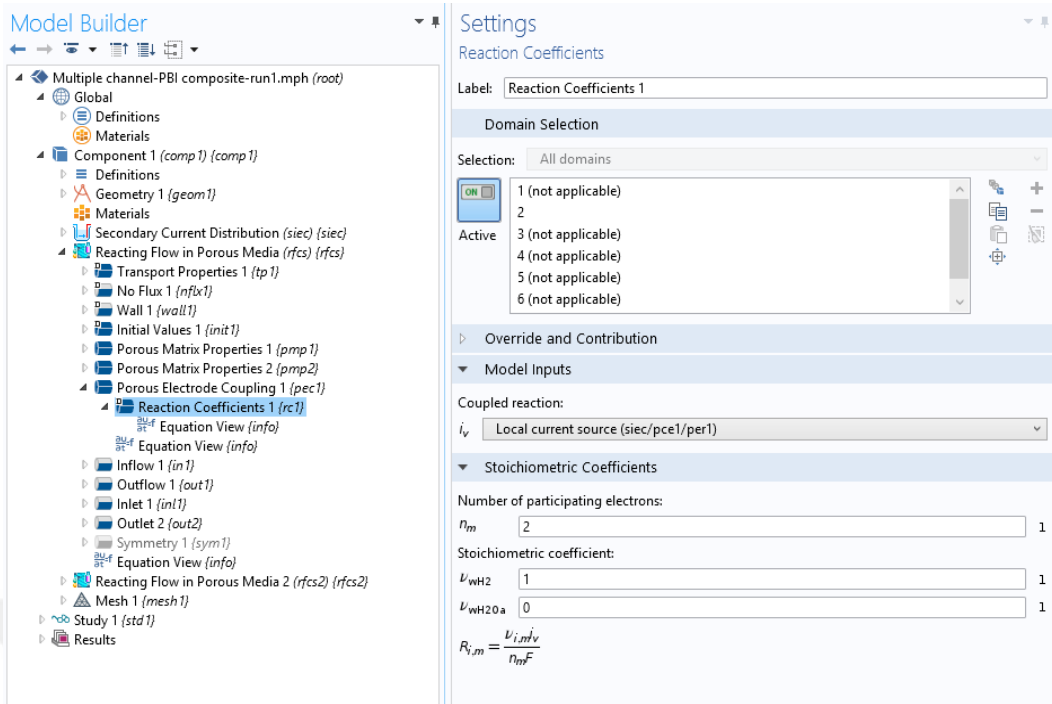


Figure 3.37 “Reaction Coefficients 1” section and its setting in Comsol Multiphysics

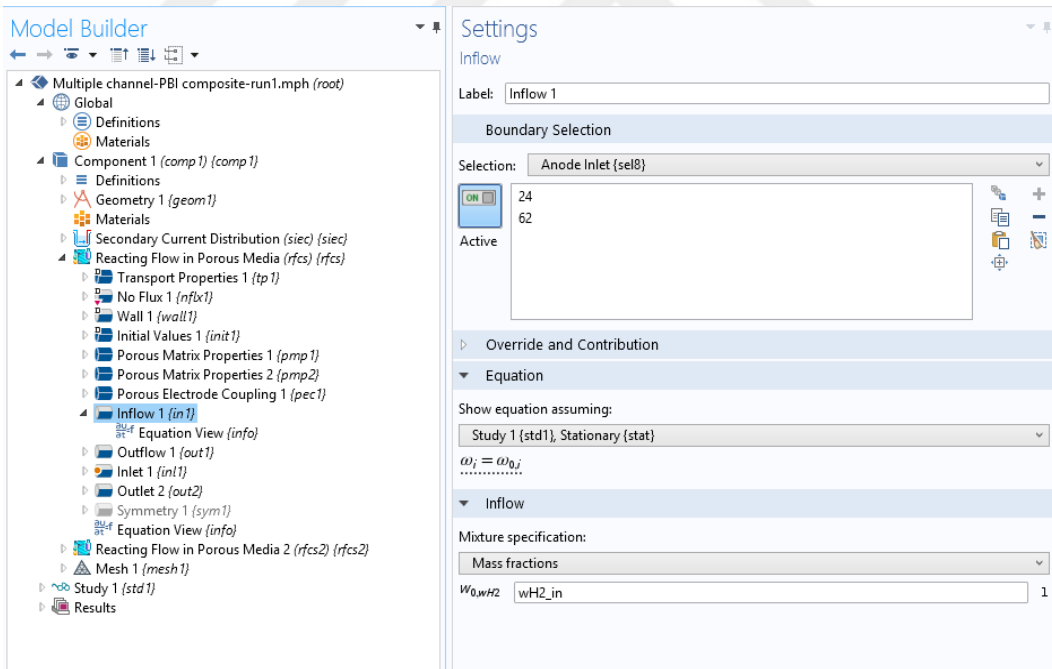


Figure 3.38 “Inflow 1” section and its setting in Comsol Multiphysics

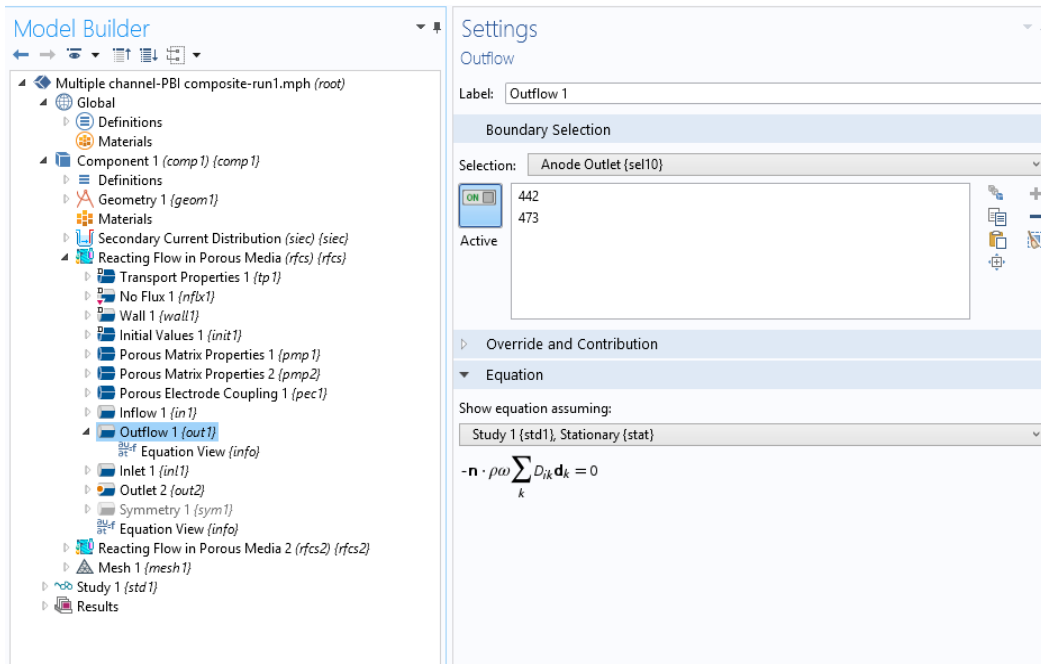


Figure 3.39 “Outflow 1” section and its setting in Comsol Multiphysics

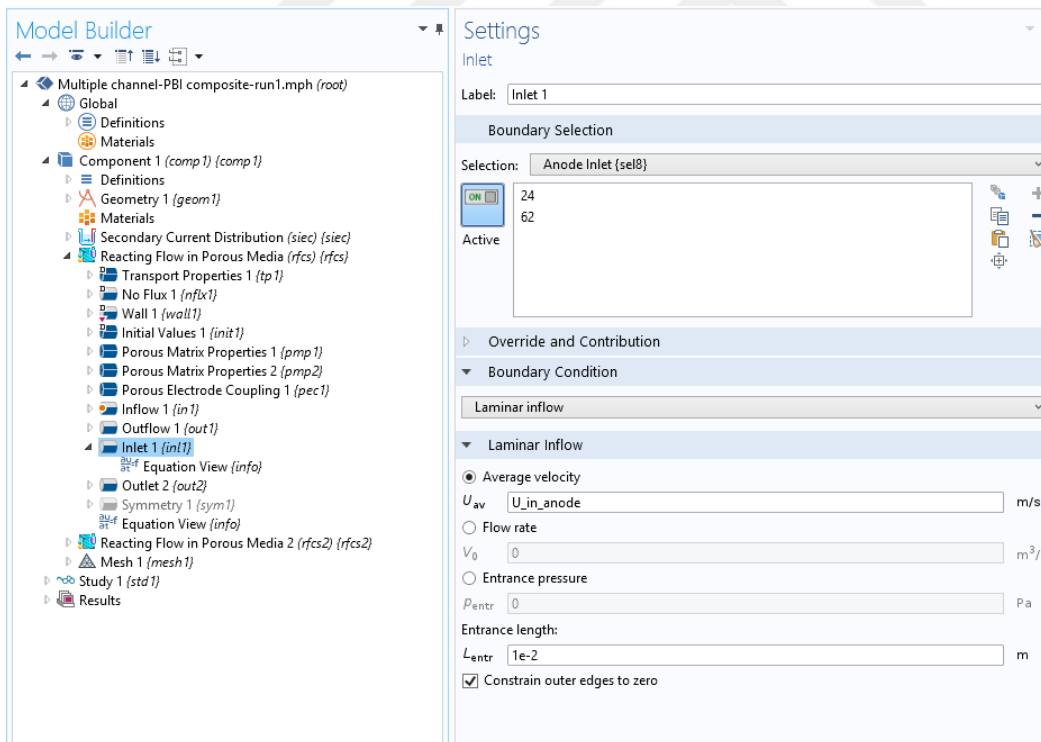


Figure 3.40 “Inlet 1” section and its setting in Comsol Multiphysics

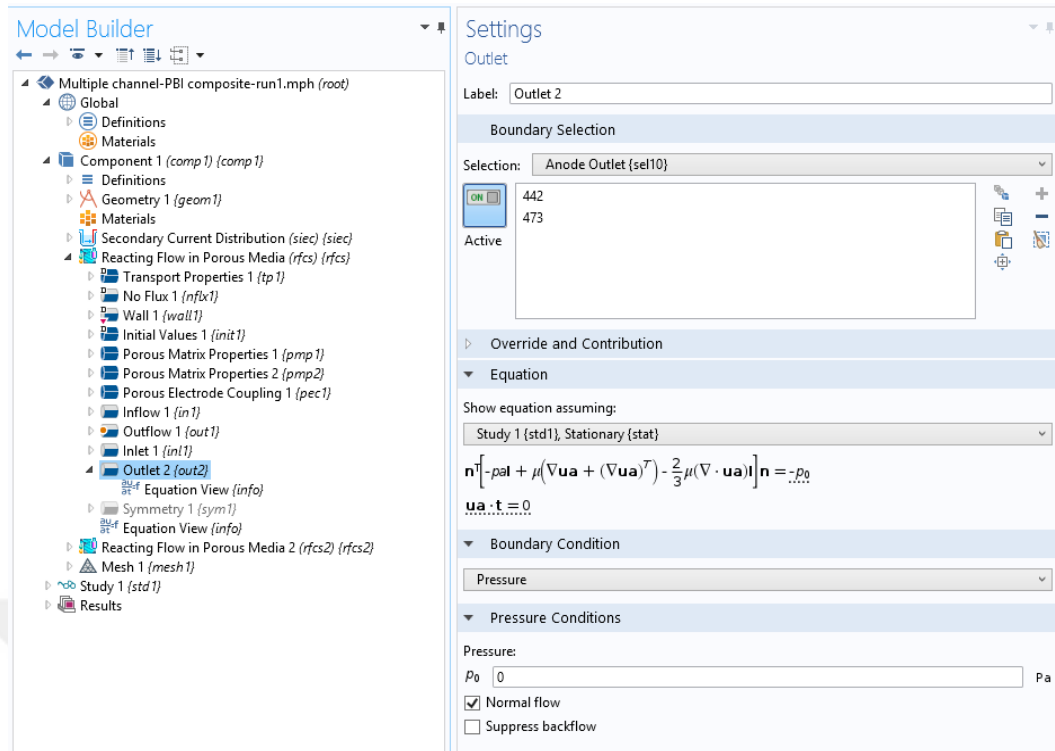


Figure 3.41 “Outlet 2” section and its setting in Comsol Multiphysics

In “Mesh” tool, the built domain is divided into small elements according to the mesh size. The sequence of type of meshing can be selected as either “User controlled” or “Physics controlled”, which is shown in Figure 3.42. For complex geometries, “User controlled” type of mesh can be very difficult to apply for each boundaries and edges. Therefore, “Physics controlled” mesh type is selected to be performed for HT-PEMFC modeling. Extremely fine mesh divides the domain into very small elements, while extremely coarse divides bigger elements. However, it should be noted that mesh size have an impact on the accuracy of the results. For HT-PEMFC model, thickness of the components of the cell differs. While flow channels and GDLs are thicker as 7.5E-4 and 5.5E-4 meters, respectively; catalyst layers and the membrane are thinner as 2.5E-5 and 7.5E-5 meters, respectively. Therefore, even it would be complex to build “User Controlled” mesh type, it is suggested to be preferred in order to optimize the meshes. In Figure 3.43, “Mesh” tool and mesh sizes in Comsol Multiphysics are shown.

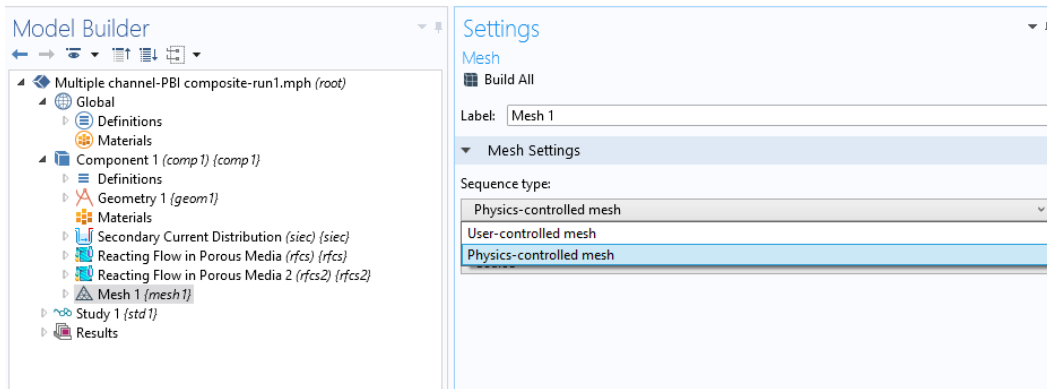


Figure 3.42 Sequence types of “Mesh” tool in Comsol Multiphysics

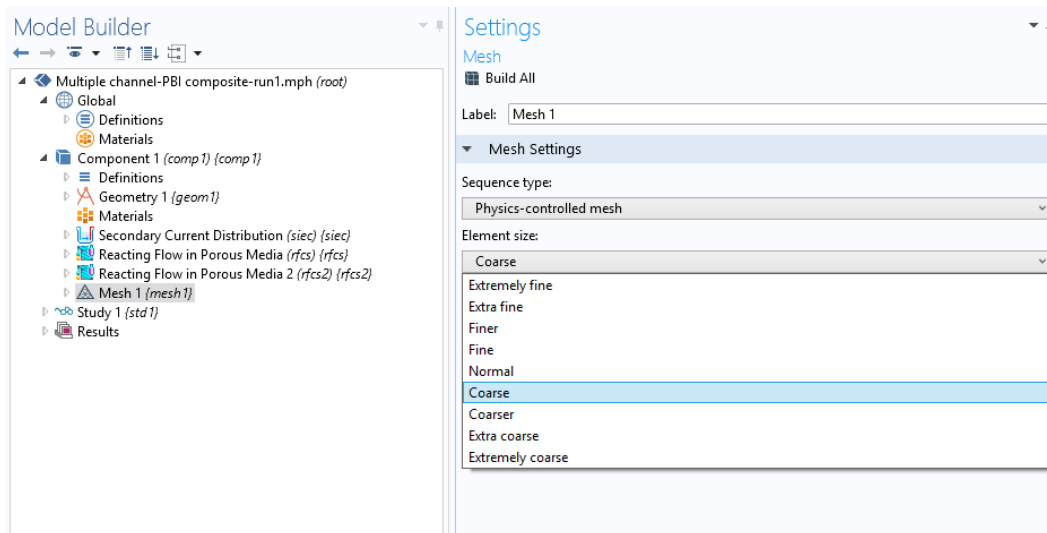


Figure 3.43 Mesh element sizes available in Comsol Multiphysics

Figure 3.44 shows the meshed domain of 3-D HT-PEMFC model in mixed serpentine geometry developed by Comsol Multiphysics. The mesh size is chosen as “Coarse”.

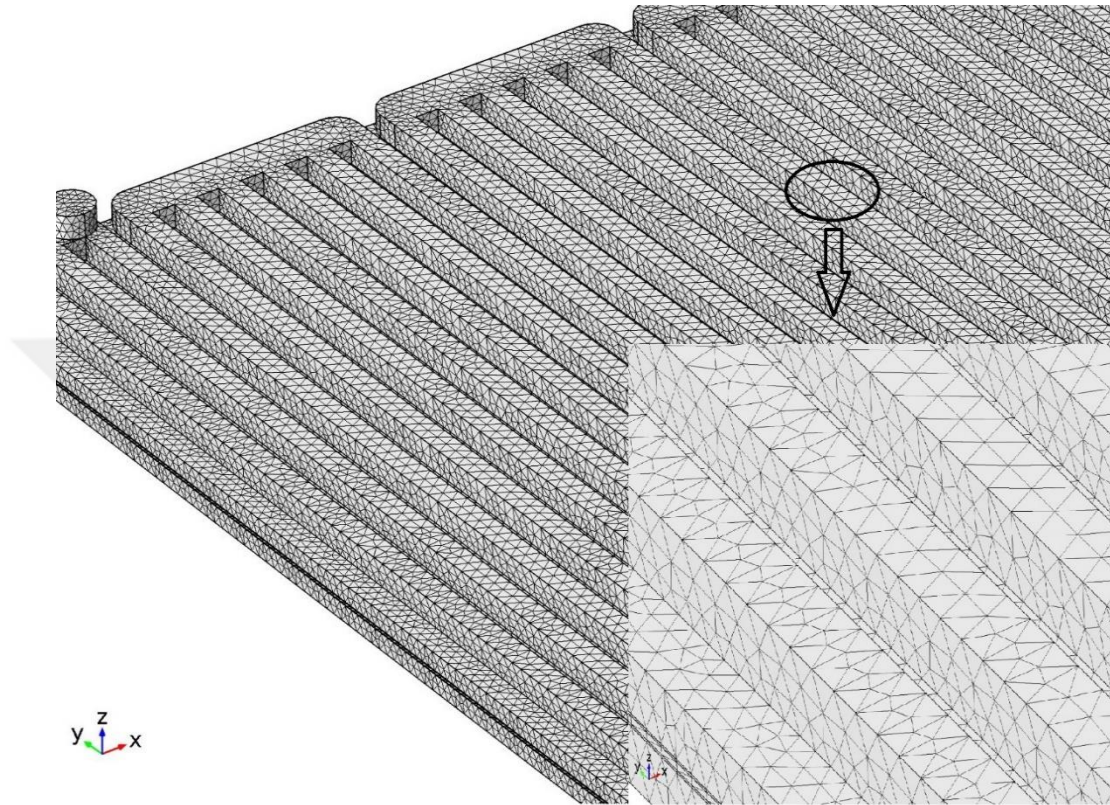


Figure 3.44 Meshed domain of HT-PEMFC model

After the meshed domain is obtained, the model is completely developed by Comsol Multiphysics. The next step of the algorithm is to add “Study” tool in order to start the simulation and obtain required results for the model. In this study, the system is chosen as stationary, not time dependent since the operation is assumed as steady-state. Figure 3.45 shows the “Study” tool including auxiliary sweep section. This section is used in order to acquire current density distribution at voltages from 0.4 to 0.9 V, by increasing 0.1 V.

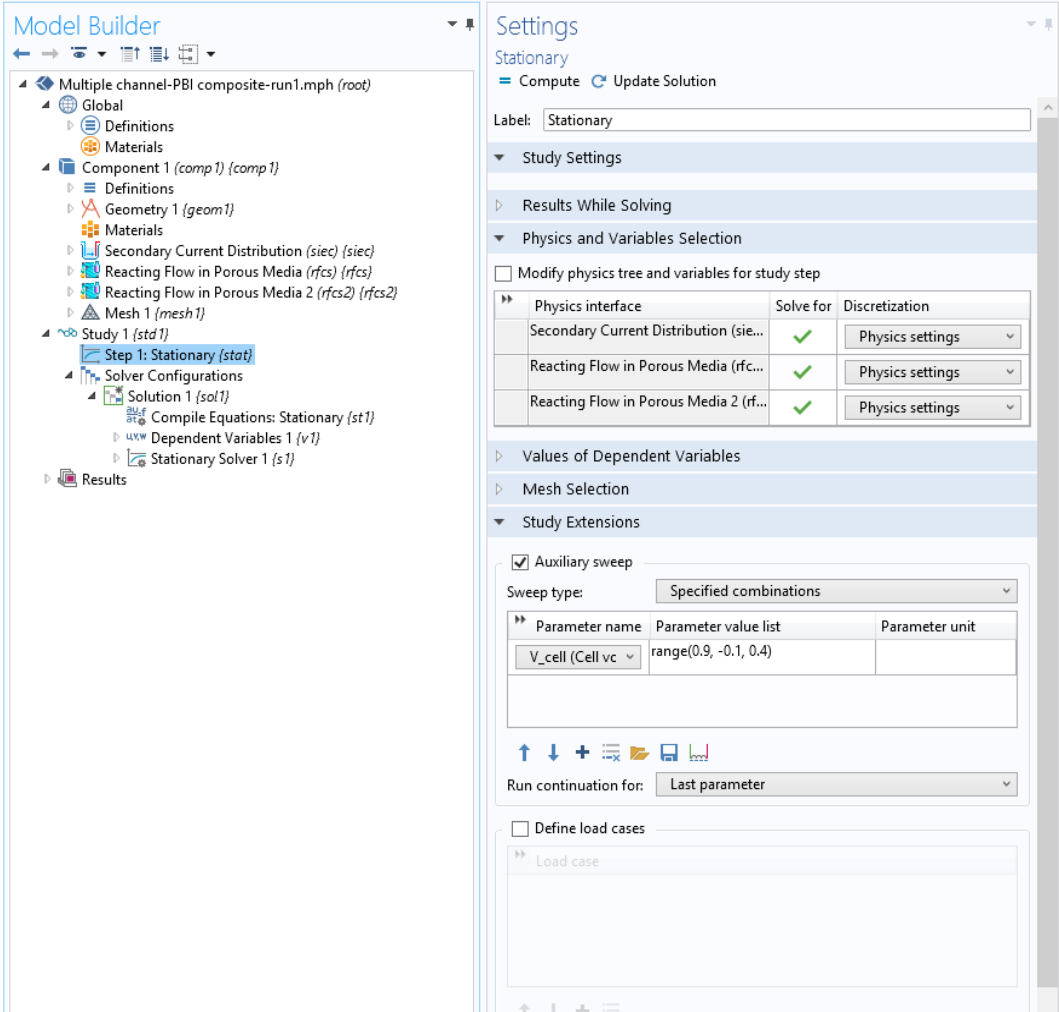


Figure 3.45 “Study” tool in Comsol Multiphysics

Figure 3.46 demonstrates the “Stationary Solver” section including its sub-sections. This solver is based on Direct Method solver. In settings section, different solver types are offered for the users by Comsol Multiphysics. These types are MUMPS, PARDISO and SPOOLES, which are based on Lower Upper (LU) decomposition. This decomposition solves a numerical analysis as matrix by using lower and upper triangular matrices. Each type of these solvers will come up with the same answer for a developed model. For well-conditioned finite element problems, it is not important which one of direct solvers to be chosen from the point of view of the solution. The differences between these solvers are the relative speeds of simulations to get results. While PARDISO is the fastest solver, SPOOLES is the slowest solver because it uses the least memory. Despite all the solvers need a lot of RAM, MUMPS and PARDISO can store some of the problem onto the hard disk. For the simulation of HT-PEMFC model, “MUMPS” solver is preferred because it uses less memory than PARDISO and much faster than SPOOLES.

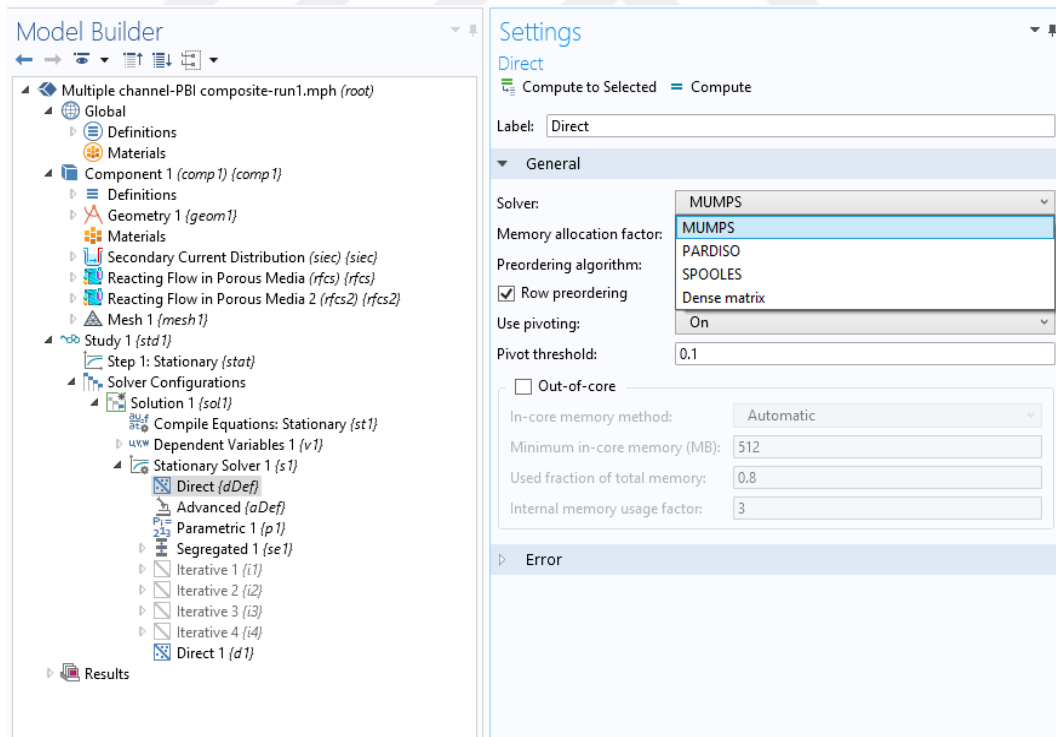


Figure 3.46 Solver types in “Stationary Solver”

The program has run several hours according to the complexity of the developed model and added physics. Once the simulation of the model is finished, the results can be obtained easily by the usage of “Results” tool. Results can be drawn as 1-D, 2-D or 3-D. For HT-PEMFC modeling, membrane current density result is acquired as 2-D, while concentration profiles of materials are obtained as 3-D. Figure 3.47 demonstrates the list of results that can be obtained at the end of HT-PEMFC model simulation.

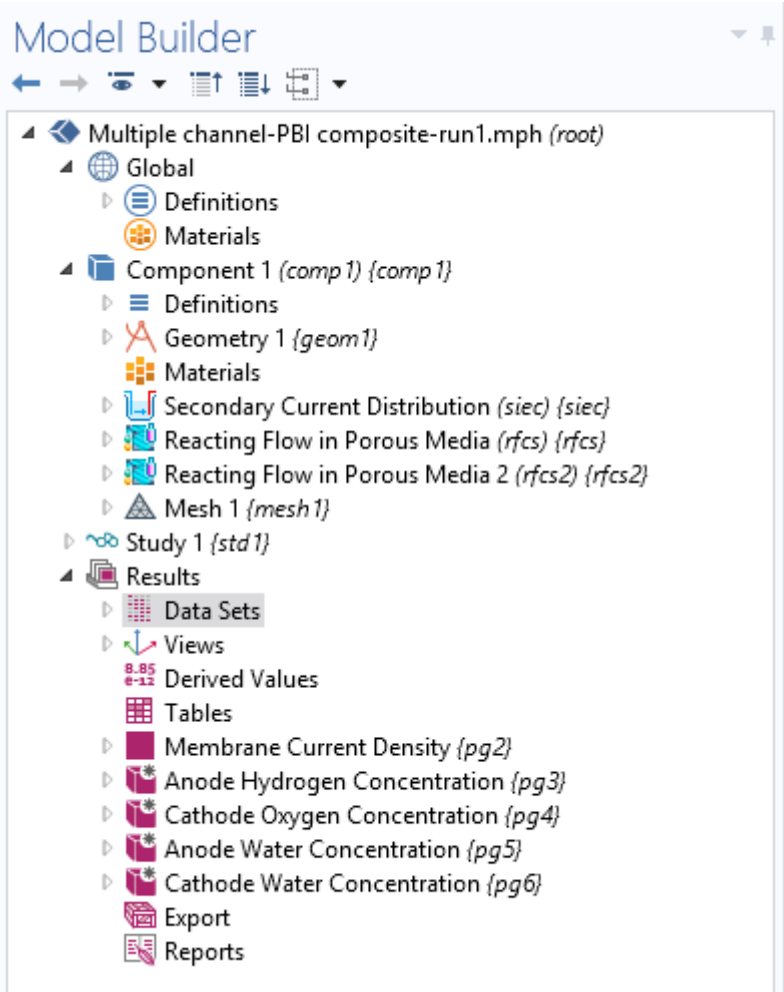


Figure 3.47 “Results” tool in Comsol Multiphysics

3.2. HT-PEMFC Model Development having Single Flow Channel

Three-dimensional, steady state HT-PEMFC model having a single flow channel is developed in order to understand the properties of the cell that affects the performance. This single channel modeling is considered as the primary step of modeling of multiple channel HT-PEMFC modeling. At this step, chemical and physical properties of phosphoric acid doped PBI membrane are used. This membrane is produced by Danish Power Systems, their commercial membrane named as Dapozol[®]. Synthesis of Dapozol[®] membrane will be explained in Chapter 4 in detail.

Figure 3.48 shows the representation of the 3-D HT-PEMFC model domain, obtained by Comsol Multiphysics, having single flow channel.

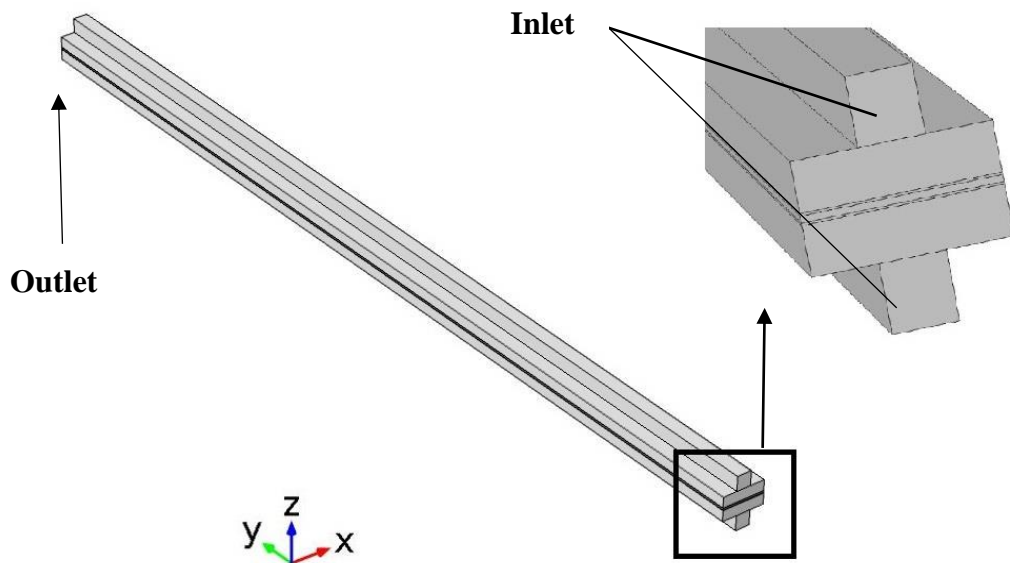


Figure 3.48 3-D, isothermal HT-PEMFC model domain having single flow channel

In order to develop a mathematical and systematic model in Comsol Multiphysics program, numbers of parameters should be integrated to the program. The program needs at least thirty three different parameters as default. These parameters include dimensions of the cell, chemical and physical properties of the components and reactants and operating conditions. Table 3.1 summarizes these parameters embedded for isothermal HT-PEMFC model having single flow channel. Table 3.2 represents the continuation of Table 3.1.

Table 3.1 Parameters list embedded in Comsol Multiphysics for HT-PEMFC modeling having single flow channel

Parameter	Symbol	Value
Cell Length (m)	L	0.04
Channel Height (m)	H_ch	7.5e-4
Channel Width (m)	W_ch	7.5e-4
Rib Width (m)	W_rib	0.0015
GDL Width (m)	H_gdl	550e-6
Porous Electrode Thickness (m)	H_electrode	25e-6
Membrane Thickness (m)	H_membrane	75e-6
GDL Porosity	eps_gdl	0.5
GDL Permeability (m ²)	kappa_gdl	3e-12
GDL Electric Conductivity (S/m)	sigma_gdl	687.5
Inlet H ₂ Mass Fraction	wH2_in	0.99
Inlet H ₂ O Mass Fraction	wH2O_in	0.001
Inlet O ₂ Mass Fraction	wO2_in	0.231
Anode Inlet Flow Velocity (m/s)	U_in_anode	0.133
Cathode Inlet Flow Velocity (m/s)	U_in_cathode	0.8
Anode Viscosity (Pa.s)	mu_anode	1.152e-5
Cathode Viscosity (Pa.s)	mu_cathode	2.505e-5

Table 3.2 Continuation of Table 3.1

Parameter	Symbol	Value
Hydrogen Molar Mass (kg/mol)	MH2	0.002
Nitrogen Molar Mass (kg/mol)	MN2	0.028
Water Molar Mass (kg/mol)	MH2O	0.018
Oxygen Molar Mass (kg/mol)	MO2	0.032
H ₂ -H ₂ O Binary Diffusion Coef.(m ² /s)	D_H2_H2O	$9.15e-5*(T/307.1)^{1.75}$
N ₂ - H ₂ O Binary Diffusion Coef.(m ² /s)	D_N2_H2O	$2.56e-5*(T/307.15)^{1.75}$
O ₂ -N ₂ Binary Diffusion Coef.(m ² /s)	D_O2_N2	$2.2e-5*(T/293.2)^{1.75}$
O ₂ -H ₂ O Binary Diffusion Coef.(m ² /s)	D_O2_H2O	$2.82e-5*(T/308.1)^{1.75}$
Cell Temperature (K)	T	433
Reference Pressure (Pa)	p_ref	120e3
Cell Voltage (V)	V_cell	0.55
Oxygen Reference Concen. (mol/m ³)	cO2_ref	40.88
Hydrogen Reference Concen. (mol/m ³)	cH2_ref	40.88
Open Volume Fraction for Gas Diffusion in Porous Electrodes	eps_cl	0.5
Porous Electrode Permeability	kappa_cl	kappa_gdl/5
Membrane Conductivity (S/m)	sigma_m	10

3.3. HT-PEMFC Model Development having Multiple Flow Channels

Modeling of isothermal HT-PEMFC having multiple flow channels is performed in the scope of this study. The model has 25 cm² active area with mixed serpentine flow channel geometry. For this modeling, PPA doped PBI membrane is not considered. Instead, PBI based composite membrane is considered. Chemical and physical properties of the membrane are based on PBI/SiO₂ membrane which is prepared by FCRC group.

Figure 3.49 shows HT-PEMFC model domain having multiple flow channels in mixed serpentine geometry.

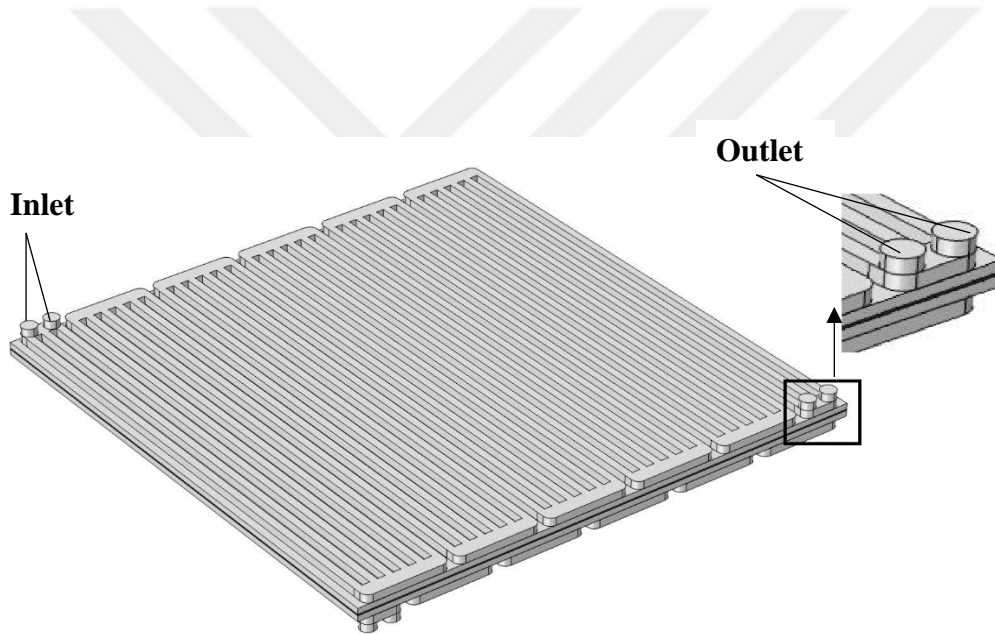


Figure 3.49 3-D, isothermal HT-PEMFC model domain having multiple flow channels

In table 3.3, all parameters required for isothermal HT-PEMFC modeling with PBI/SiO₂ membrane are listed by considering multiple flow channel geometry. Table 3.4 represents the continuation of Table 3.3.

Table 3.3 Parameters list embedded in Comsol Multiphysics for HT-PEMFC modeling having multiple flow channel

Parameter	Symbol	Value
Cell Length (m)	L	0.04
Channel Height (m)	H_ch	7.5e-4
Channel Width (m)	W_ch	7.5e-4
Rib Width (m)	W_rib	0.0015
GDL Width (m)	H_gdl	180e-6
Porous Electrode Thickness (m)	H_electrode	100e-6
Membrane Thickness (m)	H_membrane	100e-6
GDL Porosity	eps_gdl	0.5
GDL Permeability (m ²)	kappa_gdl	3e-12
GDL Electric Conductivity (S/m)	sigma_gdl	687.5
Inlet H ₂ Mass Fraction	wH2_in	0.99
Inlet H ₂ O Mass Fraction	wH2O_in	0.001
Inlet O ₂ Mass Fraction	wO2_in	0.231
Anode Inlet Flow Velocity (m/s)	U_in_anode	0.884
Cathode Inlet Flow Velocity (m/s)	U_in_cathode	3.494
Anode Viscosity (Pa.s)	mu_anode	1.135e-5
Cathode Viscosity (Pa.s)	mu_cathode	2.464e-5

Table 3.4 Continuation of Table 3.3

Parameter	Symbol	Value
Hydrogen Molar Mass (kg/mol)	MH2	0.002
Nitrogen Molar Mass (kg/mol)	MN2	0.028
Water Molar Mass (kg/mol)	MH2O	0.018
Oxygen Molar Mass (kg/mol)	MO2	0.032
H ₂ -H ₂ O Binary Diffusion Coef.(m ² /s)	D_H2_H2O	$9.15e-5*(T/307.1)^{1.75}$
N ₂ -H ₂ O Binary Diffusion Coef.(m ² /s)	D_N2_H2O	$2.56e-5*(T/307.15)^{1.75}$
O ₂ -N ₂ Binary Diffusion Coef.(m ² /s)	D_O2_N2	$2.2e-5*(T/293.2)^{1.75}$
O ₂ -H ₂ O Binary Diffusion Coef.(m ² /s)	D_O2_H2O	$2.82e-5*(T/308.1)^{1.75}$
Cell Temperature (K)	T	438
Reference Pressure (Pa)	p_ref	120e3
Cell Voltage (V)	V_cell	0.55
Oxygen Reference Concen. (mol/m ³)	cO2_ref	40.88
Hydrogen Reference Concen. (mol/m ³)	cH2_ref	40.88
Open Volume Fraction for Gas Diffusion in Porous Electrodes	eps_cl	0.5
Porous Electrode Permeability	kappa_cl	kappa_gdl/5
Membrane Conductivity (S/m)	sigma_m	8.66

CHAPTER 4

MODELING AND SENSITIVITY ANALYSIS OF HIGH TEMPERATURE PEM FUEL CELLS BY USING COMSOL MULTIPHYSICS¹

4.1. Introduction

A fuel cell is an energy conversion device that directly converts chemical energy of a fuel into electrical energy through an electrochemical reaction. Fuel cells are generally classified based on the electrolyte they use. Polymer Electrolyte Membrane (PEM) fuel cells are one of the most commonly used type of fuel cells. PEM fuel cells are based on a polymer membrane as the electrolyte. This membrane should be permeable to protons but should not conduct electrons. The polymer electrolyte membrane is placed between two catalyst layers. Hydrogen is fed to the anode side and air to the cathode side [43]. The catalyst layers are the regions where chemical reaction takes place. The hydrogen molecules are split into protons and electrons on the anode catalyst and produce intermediate products of protons and electrons. The protons are transported across the PEM and the electrons pass through an external circuit. The protons reacts oxygen at the cathode side and form water.

¹ Sezgin B, Caglayan DG, Devrim Y, Steenberg T, Eroglu I.
Int J Hydrogen Energy 2016; 41: 10001-9

Each catalyst layer facilitates a half reaction: oxidation or reduction. Hydrogen oxidation occurs at the anode side:



Oxygen reduction takes place at the cathode side:



The catalyst layer is supported by a gas diffusion layer (GDL). A good GDL must possess effective transportation of gaseous reactants to the catalyst layers and low electronic resistivity. High temperature PEM fuel cells are considered as next generation fuel cells. The electrochemical kinetics for electrode reactions are enhanced by operation between 160-180°C (as compared to low temperature PEM fuel cells, which operate at 80°C). A phosphoric acid doped polybenzimidazole (PBI) membrane is used as electrolyte. This electrolyte shows good proton conductivity, excellent oxidative and thermal stability, low gas permeability, almost zero water electro-osmotic drag and good mechanical properties [8]. The conductivity of PBI membrane depends on the temperature, relative humidity, molecular weight, acid doping level and method of preparation of the membrane. Having a high temperature operation has some advantages over a low temperature operation. For example, gases do not need to be humidified and the produced water is in gas phase. This helps to simplify the fuel cell system because transport limitations related with the presence of liquid water are precluded. Moreover, CO tolerance is higher for high temperature operation and this simplifies the reformer system [4], [9], [21]. In addition, external humidification is not required. Therefore system cost, weight, and size can be reduced. For these reasons, modeling of a high temperature PEM fuel cell gains importance, because it may help to detect possible problems which actual experimental techniques cannot reach and even to decrease number of experiments [24]. In addition, modeling can help to understand the processes and effects occurring under different design parameters and operating conditions. This requirement is also critical for industrial applications in

terms of developing, designing, optimizing and ensuring quality and safety. For this modeling, Comsol Multiphysics 5.0 is an advantageous commercial software package because it is a finite element analysis software platform that can be applied to a wide range of physics and engineering problems. Moreover, existence of Fuel Cells & Batteries module is another advantage for specific reasons.

High temperature PEM fuel cells (HT-PEMFC) are relatively new field and less modeling work has been performed as compared to low temperature PEM fuel cells. Among these studies, a few of them use Comsol Multiphysics program. There is a similar work performed by Lobato et al. [24]. They studied influence of flow channel geometry for HT-PEMFC. However, they only studied the cathode side of the cell. They changed the flow rate of oxygen/air and kept constant the hydrogen flow rate, meaning that they modeled the half-cell of the HT-PEMFC.

In the present work, three-dimensional modeling of a high temperature PEM fuel cell with single flow channel is studied. The model includes the transport of gases in anode and cathode gas flow channels, diffusion in the catalyst layers, the transport of water and hydronium ion in the polymer electrolyte and in the catalyst layers, and the transport of electrical current in the solid phase. The purpose is to investigate the effect of inlet velocity of air fed to the cathode side, inlet velocity of hydrogen fed to the anode side and proton conductivity of acid doped PBI membrane on the fuel cell performance. The originality of this study comes from the investigation of the influence of inlet velocity of hydrogen on the cell performance. The flow rate of hydrogen is a critical parameter because when flow rate of hydrogen increases, oxygen may not be sufficient for the electrochemical reaction.

4.2. Experimental

Electrodes with an active surface of 25 cm² were prepared by spraying the catalytic ink over the microporous layer of the GDL using an ultrasonic spraying machine (Sonotec Exactacoat). The Pt loadings on cathode/ anode (in mgPt cm⁻²): 1.5/1.5 for Pt/C.

For the MEA preparation, a commercial PBI membrane (Dapozol[®], Danish Power Systems) was used. The membrane was doped with PA by immersing it in 85% H₃PO₄ during an hour at a temperature of 40°C. The acid doping level, defined as the number of mole of PA per mole repeat unit of PBI, was 10, enough to provide PA from the membrane to the catalytic layer by diffusion. The electrodes and the membrane were assembled by hot-pressing at a temperature of 200°C and a pressure of 4 MPa applied for 3 min. The conductivity measurements were carried out by using a four probe conductivity cell under air without humidification. The details are given elsewhere [10].

4.3. Modeling Approach

4.3.1. Modeling Instructions

Modeling of a high temperature PEM fuel cell has an essential role for the optimization of parameters affecting the performance of the fuel cell. Three dimensional model is developed because 1D model fails to predict the mass transportation effects and 2D model does not account all the transport phenomena in a fuel cell [23]. The model is developed as having a single flow channel, operating temperature as 160°C and operating voltage as 0.6 V. Other model parameters are given in Table 4.1.

Table 4.1 Parameter list for high temperature PEM fuel cell modeling

Parameters	Value
Cell length (m)	0.04
Channel height (m)	7.5×10^{-4}
Channel width (m)	7.5×10^{-4}
Rib width (m)	0.0015
GDL width (m)	550×10^{-6}
Porous electrode thickness (m)	25×10^{-6}
Membrane thickness (m)	75×10^{-6}
GDL Porosity	0.5
GDL Electric Conductivity(S/m)	687.5
Inlet H ₂ Mass Fraction	0.99
Inlet H ₂ O Mass Fraction	0.002
Inlet O ₂ Mass Fraction	0.208
Cell Temperature (K)	433
Reference Pressure (Pa)	120×10^3
Cell Voltage (V)	0.6

In the x-direction, the model includes one half of one channel to one half of a rib. The y-direction spans the entire length of the gas channels. The z-direction includes anode gas channel and rib to cathode gas channel and rib [22]. The z-direction also includes membrane electrode assembly (MEA). The cell is modeled at different inlet velocities of reactant gases including the velocity values used for the experiment. The reactant gas at the anode contains 99% hydrogen by mass. The reactant gas at the cathode is dry air as oxygen source. As another critical parameter, effect of protonic conductivity of the membrane on the cell performance is studied under the assumption that the membrane thickness is same for all conditions.

4.3.2. Assumptions

The main assumptions for the model are [44]:

- Operation is assumed to be isothermal
- Steady state operation is assumed
- All reactants and products are in gaseous phase
- All gases and water obey ideal gas law
- The flow is assumed to be laminar
- All material parameters are constant
- There is no crossover of gases and water through the membrane

4.3.3. General Equations

For gas flow channels, Navier-Stokes equation is used in order to describe momentum transfer and gas flux is assumed to be incompressible and laminar [24]. In addition, continuity equation is applied to insure the mass conservation.

$$\rho(\mathbf{u} \cdot \nabla)\mathbf{u} + \nabla p - \nabla \cdot \eta(\nabla\mathbf{u} + (\nabla\mathbf{u})^T) = 0 \quad \text{Equation 4.3}$$

$$\nabla \cdot (\rho\mathbf{u}) = 0 \quad \text{Equation 4.4}$$

For multi-component diffusion, Maxwell-Stefan equation is used. It solves for the fluxes in terms of mass fraction. The general form of the equation is:

$$\nabla \cdot \left(-\rho\omega_i \sum_j (D_{ij}\nabla x_j + (x_j - \omega_j)\frac{\nabla p}{p}) + \rho\omega_i\mathbf{u} \right) = 0 \quad \text{Equation 4.5}$$

For the porous media (GDLs and catalyst layers), Darcy's Law can be used in order to get the velocity distribution [45].

$$\rho(\mathbf{u} \cdot \nabla)\mathbf{u} + \nabla p - \nabla \cdot \eta(\nabla\mathbf{u} + (\nabla\mathbf{u})^T) = -\frac{\eta}{k_p}\mathbf{u} \quad \text{Equation 4.6}$$

For the current transport, the continuity of current in a conducting material is described as follows [46]:

$$\nabla \cdot i = 0 \quad \text{Equation 4.7}$$

However, there are two kinds of current in a PEM fuel cell: ionic current and electrical current. Ionic current is obtained by the travel of protons through the membrane while electrical current is obtained by transfer of electrons through the solid matrix of electrodes. Therefore, the continuity of current becomes:

$$\nabla \cdot i = \nabla \cdot i_e + \nabla \cdot i_s = 0 \quad \text{Equation 4.8}$$

Charge balance is necessary for the electrolyte.

$$\nabla \cdot (\kappa_e \nabla \phi_e) = 0 \quad \text{Equation 4.9}$$

4.3.4. Boundary Conditions

Boundary conditions are stated as follows:

- Continuity at all internal boundaries
- No slip boundary condition for all channel walls
- All initial values are set to zero
- No backpressure at channel outlet, convective flux boundary conditions
- Constrain outer edges set to zero for both inlet and outlet
- Bipolar plates on the both side of the cell set to electric ground and cell operation potential
- HTPEMFC is insulated from the environment

4.3.4. 3D Comsol Multiphysics Model

In order to model the system, Comsol Multiphysics 5.0 and its Fuel Cells & Batteries module is used. This program is a powerful tool that allows the user to solve PDE systems by finite element method.

For high temperature PEM fuel cell modeling, Electrochemistry> Secondary Current Distribution (siec) physics is added. This physics is used for modeling the electrochemical currents by using Ohm's law and in order to get to potential distributions in the electrolyte [47]. Besides Ohm's law, Butler-Volmer equation and Tafel equation are used while running the program. By using this physics, polarization plot and distribution of current density through the membrane can be obtained. Then, Chemical Species Transport> Reacting Flow in Porous Media> Transport of Concentrated Species (rfcs) is added in order to analyze the mass transfer of the cell. This physics is added for two times for mass transport of both anode and cathode gas compartments because hydrogen and water are present at the anode side while oxygen, water and nitrogen are present at the cathode side. Maxwell-Stefan equation is used in order to solve for mass transfer of the gaseous species in the gas diffusion layer (GDL) and catalyst layer. Moreover, Navier-Stokes equation and Brinkman equations are used for the porous GDLs and electrodes in this physics. By using this physics, concentration profiles for anode and cathode can be obtained.

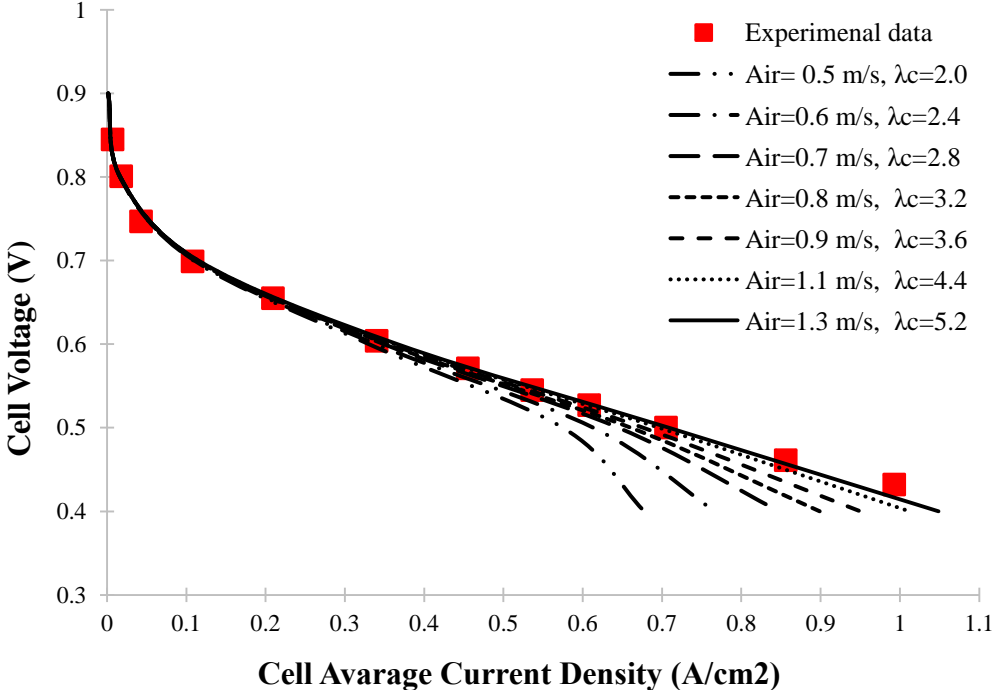
4.4. Results and Discussions

In this present work, experimental data are compared with the modeling results for a single HT-PEM fuel cell, operating at 160°C. We investigate the effect of three critical design parameters on fuel cell performance and the concentration profiles of species in the anode and cathode compartments. Those parameters are inlet velocity of hydrogen to the anode side, inlet velocity of air to the cathode side and proton conductivity of the PBI membrane. The cell performances are predicted at ambient pressure using 99% hydrogen by weight (remaining is water) and air as reactants. Other modeling parameters are given in Table 4.1. For all models, the mass flow rates of the reactants for current densities equal to or greater than 0.5 A/cm² are taken as predefined values of the stoichiometric excesses λ . At lower current densities the gas flow rates are fixed to the respective values for 0.5 A/cm² [48]. Models predict open circuit voltage (OCV) of 0.9 V.

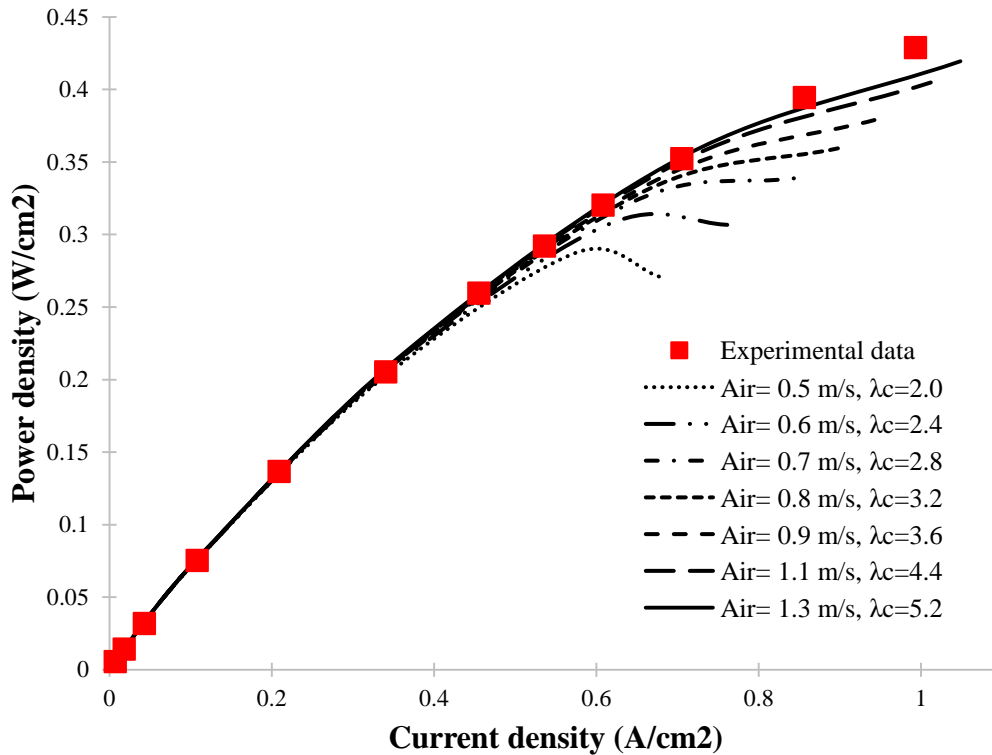
4.4.1. Effect of Inlet Air Velocity on Performance of HT-PEMFC

At the first set of runs, inlet velocity of hydrogen gas is kept constant at 0.1 m/s while inlet velocity of air is changed as 0.5, 0.6, 0.7, 0.8, 0.9, 1.1 and 1.3 m/s. Figure 4.1-(a) illustrates the impact of air inlet velocity on the cell performance. The model results are compared with experimental data for cases that the inlet velocity of the hydrogen gas is taken as 0.1 m/s. For the ohmic and activation regions, modeling results match with the experimental data well. As seen from the figure, the model underestimates the performance for low air velocities. Therefore, inlet velocity of air should be increased to at least 1.1 m/s or 1.3 m/s in order to achieve the best fit with experimental data. Higher stoichiometric excess values of air ($2.0 \leq \lambda_c \leq 5.2$) are considered here since fuel cell tests are usually performed aiming at evaluation of the fuel cell materials not for optimization of the cell operation [10]. Figure 4.1-(b) illustrates the power density curves of the cell with different inlet air velocities at 160°C. As inlet air velocity increases, power density curves of models approach to experimental data. As air inlet velocity increases higher peak power densities are obtained. However, the voltage corresponding to

the peak power density decreases causing a decrease in the efficiency of the cell. In order to keep the efficiency high, fuel cell is operated at 0.5-0.6 V. It is interesting to note that experimental data implies a continuous power increase as the current density increases.



(a)



(b)

Figure 4.1 Comparison of experimental polarization data with model predictions for varying air velocities; (a) Fuel cell polarization behavior, voltage vs current density, (b) Power density vs current density. Modeling conditions; 160°C, ambient pressure, H₂ inlet velocity= 0.1 m/s, $\lambda_A=1.0$, $\kappa = 10$ S/m.

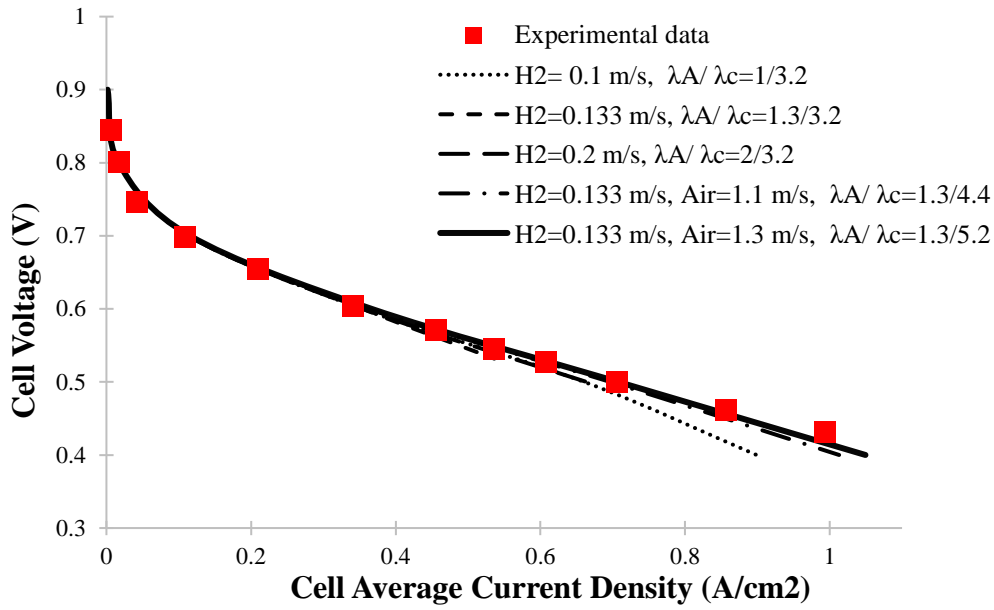
Similar studies including comparison of experimental data obtained in single HT-PEM fuel cell and modeling results with different air flowrates are present in the literature [22], [23] Cheddie and Munroe [22] compared their 3D non-isothermal model results with experimental data given by Wang et al. [49]. For the ohmic and activation regions, their model curves match the experimental polarization data well. Shamardina et al. [23] changed the stoichiometric excess from 1.5 to 6, while stoichiometric excesses λ specified corresponded to the current density of 0.4 A/cm². Their 2D model polarization curves were in good agreement with their experimental data obtained for 5 cm² MEA.

One of the main factors affecting the cell performance is the inlet velocity of air fed to the cathode gas channels. Inlet velocity of a reactant is directly related with the flow rate by multiplying inlet velocity with the cross sectional area. However, cross sectional area can be various for different channel dimensions and channel geometries which leads to different velocities for the reactants. It is known that different channel dimensions and geometries affect the fuel cell performance [19], [50]. For this particular reason, we based the model parameters on velocities of the reactants instead of their flow rates for simulations.

4.4.2. Effect of Inlet Hydrogen Velocity on Performance of HT-PEMFC

The effect of the hydrogen flow rate on the fuel cell performance is not taken into account in most of the models published in literature [22]–[24]. Lobato et al. [24] assumed that hydrogen concentration in anode side is always enough so that it never effects cathode performance. Anode was not modeled, its corresponding potential was associated to the lower electrolyte boundary. Despite that opposite to low temperature PEM fuel cells, in the case of high temperature ones the anode overpotentials are not completely negligible [51]. In the present work, change in the inlet hydrogen velocity has been accounted in the model equations. Therefore, anode is also included in the full-cell modeling. Figure 4.2-(a) shows the comparison between the model results with experimental data for cases that the inlet velocity of the air is taken as 0.8 m/s, and considering that hydrogen gas velocity is changed as 0.1, 0.133 and 0.2 m/s. As it can be seen from this figure, there is a good match between the model and the experimental performance data except for the last two data points for hydrogen inlet velocity 0.133 m/s and air inlet velocity is 0.8 m/s where these flow rates correspond to the experimental values ($\lambda_{A/C}=1.3/3.2$). It is unforeseen that the model cannot predict current densities below 0.53 V at these conditions and also at higher hydrogen inlet velocities (i.e. $\lambda_A \geq 1.3$). This may suggest that the air stream is unable to supply enough oxygen for the electrochemical reaction to take place for $\lambda_C \leq 3.2$, which causes distinct concentration over potential regions [22]. However, models fit well

with the experimental data for the ohmic and activation regions above 0.53 V. In order to see the best match with modeling results and experimental data, inlet air velocity is increased to 1.1 and 1.3 m/s, while inlet hydrogen velocity is taken as its experimental value, 0.133 m/s. Performance curves for both cases show good agreement with the experimental data even in mass transport region. The best fit with the experimental data is attained at the inlet velocities of hydrogen and air as 0.133 m/s and 1.3 m/s, respectively. In Figure 4.2-(b), power density curves corresponding the conditions in Figure 4.2-(a) are illustrated. Power density curves show that there is a continuous increase in the power in the range 0.9-0.4 V; thus, there exists no peak in the curves. The maximum power density experimentally obtained is 430 mW/cm². This value is greater than the peak power density values obtained by Yang et al. [10]. They reported that the peak power density values were varying from 195 to 300 mW/cm². Their HT-PEM fuel cell had catalyst loading of 0.6 mg Pt/cm² for each electrode and no humidification was applied for either hydrogen or air. It should be emphasized that an outstanding performance is reported in the present work which might be due to the higher Pt loading of the MEA (1.5 mg Pt/cm² for each electrode) and the properties of the PBI membrane. Therefore, the present experimental performance data attain higher power density values.



(a)

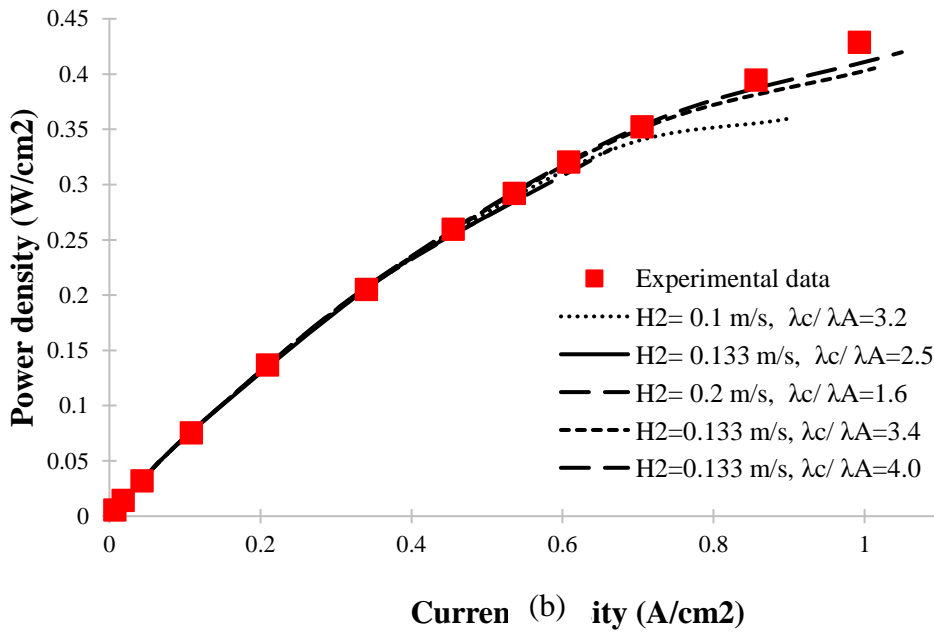


Figure 4.2 Comparison of experimental polarization data with model predictions for varying hydrogen and air velocities; (a) Fuel cell performance based on acid doped PBI membrane voltage vs current density, (b) Power density vs current density. Modeling conditions; 160°C, ambient pressure, Air inlet velocity= 0.8 m/s, $\lambda_c = 3.2$, $\kappa = 10$ S/m.

4.4.3. Effect of Proton Conductivity of PBI Membrane on Performance of HT-PEMFC

The influence of the proton conductivity of PBI membrane on the fuel cell performance is significant especially in the ohmic region. Therefore, it can be considered as a critical parameter affecting the fuel cell performance. The proton conductivity of phosphoric acid doped PBI membrane highly depends on the molecular weight of PBI, acid doping level (ADL) of the membrane and the operating conditions such as relative humidity and temperature. Yang et al. had studied the effect of proton conductivity on fuel cell performance experimentally [10]. They tried to minimize molecular weight effect on conductivity of PBI membrane by manipulating acid doping level (ADL) of the membrane. PBI membranes with different molecular weights exhibited comparable conductivities when they have similar ADLs. Experimental in-plane conductivity of the acid doped PBI membrane used in the present work was measured as 10 S/m at 160°C. In a previous work, the proton conductivity of similar PBI membranes were reported as 14 S/m at 160°C [10]. Wannek et al. reported the conductivity of the PBI membrane as 8 S/m at 140°C [48].

The conductivity of phosphoric acid doped PBI electrolyte changes with the proton transport direction (i.e. in-plane vs. through-plane). Higher proton conductivity values can be obtained by in-plane measurements. Hjuler et al. reported in-plane and through-plane proton conductivities of the PBI membranes at 100 and 180°C as a function of relative humidity and ADL. Their results showed that proton conductivity increases with temperature and relative humidity. Through-plane proton conductivity is lower compared to the in-plane proton conductivity [11]. It is difficult to measure in-situ proton conductivity therefore; here the sensitivity of the model results on conductivity value has been investigated. Figure 4.3 shows the impact of proton conductivity of acid doped PBI membranes on the fuel cell performance at 160°C under ambient pressure without humidification. For this case, inlet velocity of hydrogen and air are taken as 0.133 m/s and 0.8 m/s; respectively, same as the experimental conditions. The models predict the performance curves for four different proton conductivity values such as 10, 12, 14

and 20 S/m. As seen from the figure, increasing proton conductivity shifts the performance curves upwards. The model is unable to obtain last two data points (0.5 V and 0.4 V) at the proton conductivity of 10 S/m. However, polarization curves where proton conductivity of the membrane is taken as 12 and 14 S/m fit well with the experimental performance data. In fact, the best fit with the experimental data is obtained when proton conductivity is 14 S/m. On the other hand, higher proton conductivities (i.e. 20 S/m) overestimate the current densities obtained by experiments which causes a deviation especially in the ohmic region from the experimental data.

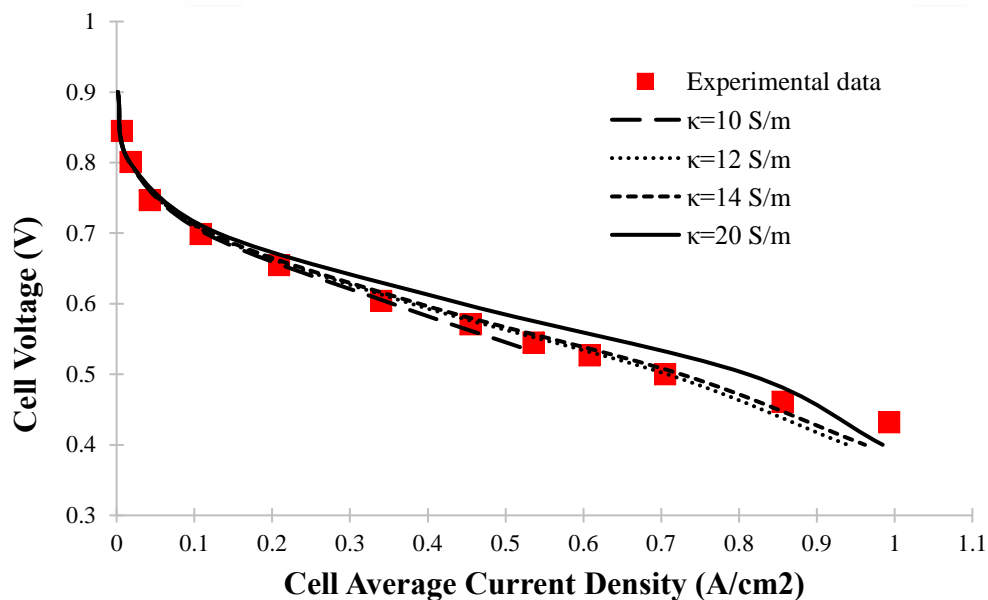


Figure 4.3 Comparison of experimental polarization data with model results obtained with acid doped PBI membrane having different proton conductivities. Modeling conditions; 160°C, ambient pressure, H₂ inlet velocity= 0.133m/s and Air inlet velocity= 0.8 m/s, $\lambda_{AC}=1.3/3.2$ and mass fraction of hydrogen=0.99

4.4.4. Channel Concentration Profiles of Reactants and Products along a Single Channel

Modeling results can show hydrogen and water concentration profiles of anode compartment. Corresponding concentration profiles are obtained where inlet velocities of hydrogen and air are same with the experimental values ($\lambda_A=1.0$ and $\lambda_C=3.0$). In addition, proton conductivity of the acid doped PBI membrane is chosen as 10 S/m in order to keep all experimental parameters in the model. Therefore, operating temperature is 160°C and the model assumes that cell is operated at ambient pressure. Figure 4.4-(a) illustrates hydrogen concentration profile of anode gas channel at 0.6 V. At the inlet, hydrogen concentration is 33.2 moles/m³. When the model progresses through the outlet, hydrogen concentration decreases up to 33.0 moles/m³ since hydrogen is consumed by the reaction. The reactant fed to the anode gas channel is assumed as containing 99% hydrogen (by weight). Therefore, water content in the reactant and its concentration is too low. Figure 4.4-(b) illustrates water concentration profile of anode gas channel at 0.6 V. Water concentration at the anode gas channel changes from 0.11 moles/m³ to 0.36 moles/m³ from the inlet toward outlet.

As same with the anode compartment, concentration profiles of cathode compartment are obtained by using experimental parameters for modeling. Figure 4.5-(a) illustrates the oxygen concentration profile of cathode gas channel at 0.6 V. Concentration of oxygen at the inlet is 6.22 moles/m³ and it decreases to 3.82 moles/m³ at the outlet because oxygen is consumed in order to form water. Produced water concentration profile is illustrated in Figure 4.5-(b). At the inlet, water concentration is 0.11 moles/m³. When the reaction takes place, water is produced and its concentration increases. At the outlet, concentration of produced water reaches to 9.84 moles/m³.

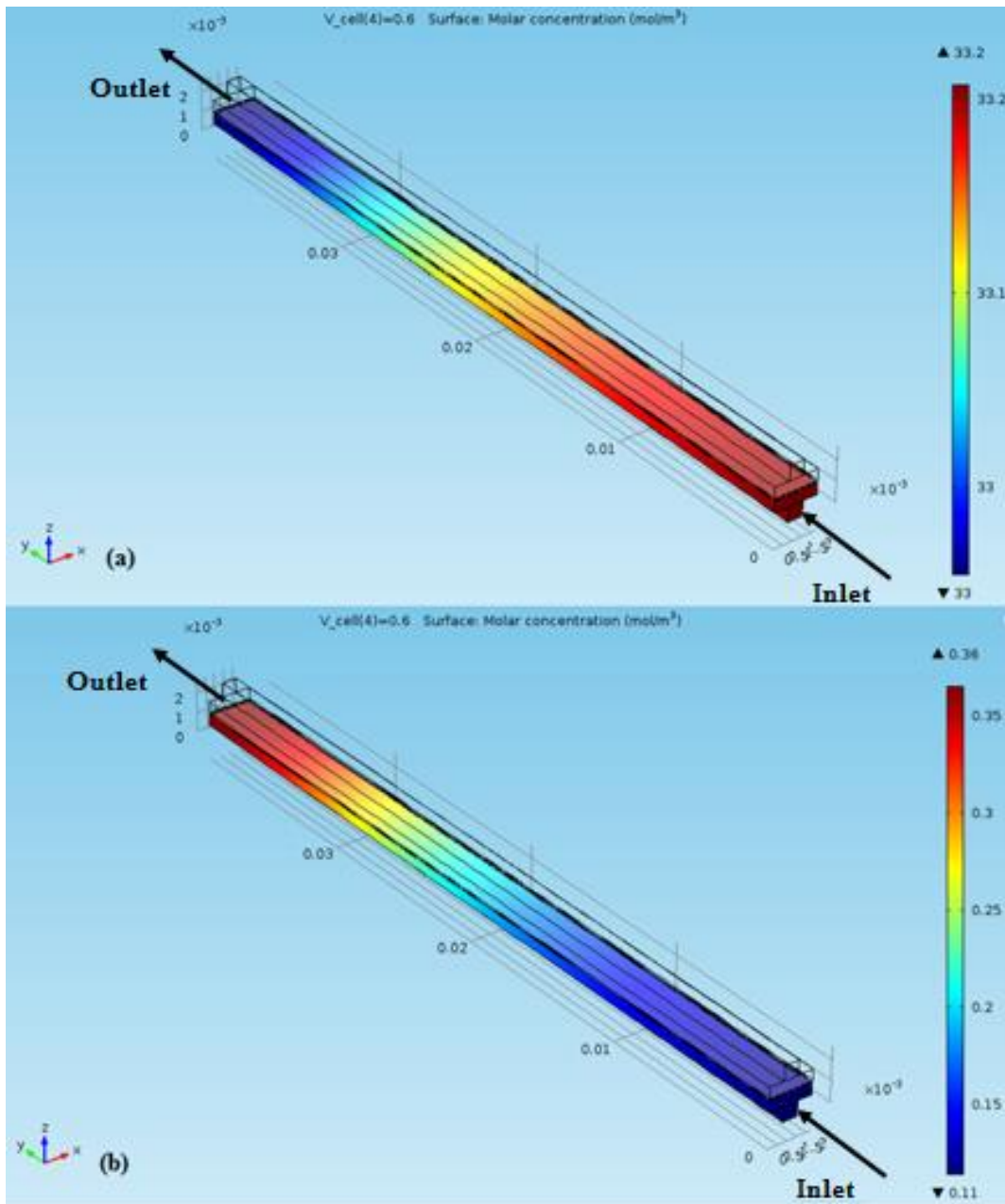


Figure 4.4 Concentration profiles along anode gas channel predicted for 0.6V and $\kappa = 10$ S/m. (a) Hydrogen concentration profile, (b) Water concentration profile. Modeling conditions are same as Figure 4.3.

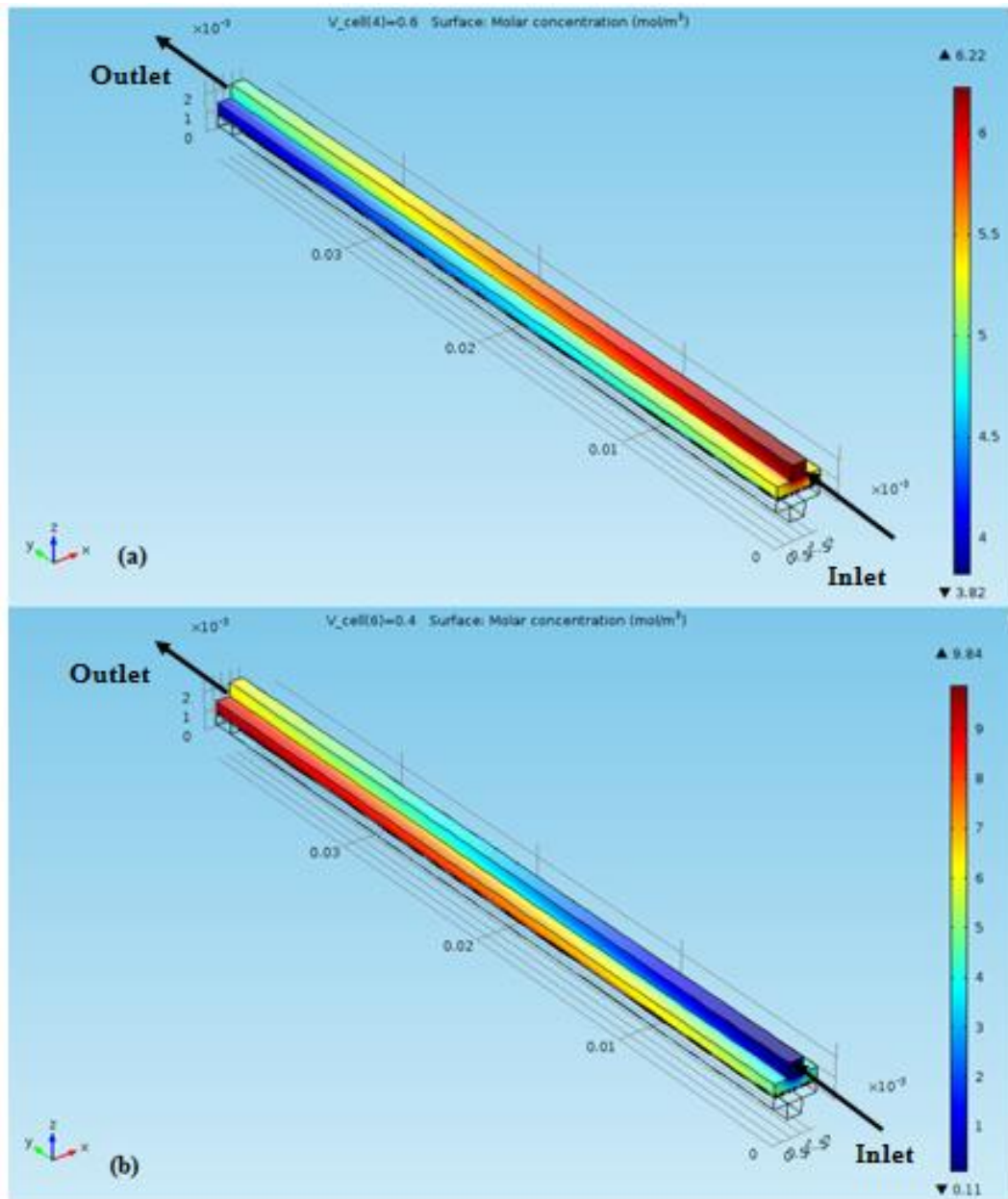


Figure 4.5 Concentration profiles along cathode gas channel predicted for 0.6V and $\kappa = 10 \text{ S/m}$. (a) Oxygen concentration profile, (b) Water concentration profile. Modeling conditions are same as Figure 4.3.

4.5. Conclusion

The effect of inlet velocities of air and hydrogen, and the effect of proton conductivity of acid doped PBI membrane are investigated for a high temperature PEM fuel cell. A model, having an operating temperature as 160°C and operating voltage as 0.6 V, is developed. This 3D model is simulated by using Comsol Multiphysics 5.0 with Fuel Cells & Batteries Module. The model shows good match with the experimental data for ohmic and activation regions at experimental conditions ($\lambda_A=1.0$, $\lambda_C=3.0$ and $\kappa=10$ S/m) but not for mass transport region because air is unable to supply enough oxygen to the cell for the electrochemical reaction to take place at lower velocities and therefore lower flow rates. At sufficiently high flow rates for air (where $\lambda_C \geq 4.4$), the model also shows good match for mass transport region. The best match with the experimental data is obtained when the inlet hydrogen gas velocity is 0.133 m/s whereas inlet air velocity is 1.3 m/s, keeping hydrogen content of the gas fed to the anode side at 99% by weight. For other cases, the difference between experimental data and modeling results are primarily evident at limiting conditions. Moreover, different proton conductivities lead to different cell performances. The best match with the experimental data is obtained where proton conductivity is 14 S/m, instead of experimental proton conductivity value, 10 S/m. Further increase in conductivity results overestimation of the polarization behavior in ohmic region.

CHAPTER 5

SENSITIVITY ANALYSIS OF HT-PEMFC

In this chapter, sensitivity analysis which is performed for three dimensional HT-PEMFC model having multiple flow channels in mixed-serpentine geometry will be given in details. For this analysis, chemical and physical properties of PBI membrane are based on the PBI membrane prepared by our research group. While PPA doped PBI membrane is taken as basis for the study reported in Chapter 4, PBI composite membrane is preferred for this part. SiO₂ inorganic materials are used to make PBI composite membranes.

For PBI/SiO₂ composite membrane preparation, PBI polymer is solved in 10mL DMAc, at 80°C under continuous stirring. Once the PBI polymer is dissolved completely, the SiO₂ (2.5 wt. %) is added and the mixture is stirred for 10-15 minutes until the particles disperse in mixture. For further mixing, ultrasonic bath is used. Mixtures are kept in the ultrasonic bath for an hour. Finally, when they become good suspensions, they are poured into petri dishes and the solvent DMAc is removed as much as possible by drying the membranes at 80°C for 24 hours. Later, membranes are soaked in 85% phosphoric acid and doped for a long time, till the doping level does not change with time anymore. The composite membranes fabricated and doped with PPA then tested for their acid leaching ratios and conductivity. The prepared membrane is fabricated by using Ultrasonic Coating Machine. Pt catalyst is used for both anode and cathode electrodes. Catalyst loading is determined as 1.0 mg/cm² Pt for both sides. Electrodes are hot-pressed onto both sides of the membrane at 150°C and 172 N/m² for 5 min. After the MEA preparation is completed, HT-PEMFC tests are performed with the usage of test station (TECHSYS HYGO FCTS-H2ME 500). The cell with prepared

MEA is conditioned for 24 h at 0.7 V, before starting performance tests. After the system comes to steady-state, current-voltage data has been recorded starting from OCV by changing the load. The stoichiometric ratio of hydrogen to air are taken as 1.5/2.5 [14]. The pictures of the experimental set-up are given in Appendix B.

In this chapter verification of the model results with the experimental data for PBI/SiO₂ membrane, effect of proton conductivity of the membrane (PBI and PBI/SiO₂), effect of inlet velocities of the reactants (hydrogen and air) and effect of meshing strategy on the HT-PEMFC performance, including concentration distribution profiles of reactants and products, will be presented.

5.1. Model Validation

Experiments of the HT-PEMFC, operated at 165°C, are performed by our research group. In order to compare modeling results with the experimental data, operating conditions and all parameters including dimensions, chemical and physical properties are taken same with the experimental parameters in order to make the comparison analogous. The parameters are given in Table 5.1. At this point, experiments are performed by using PBI/SiO₂ membrane as PBI composite membrane and it has the proton conductivity as 8.66 S/m at the operating temperature. Hydrogen and air are fed to the system as reactant at 1.5/2.5 stoichiometric ratio. According to this ratio, hydrogen has the inlet velocity of 0.884 m/s to the anode side, while air has the inlet velocity of 3.494 m/s to the cathode side.

Table 5.1 Parameter list for HT-PEMFC modeling

Parameters	Value
Cell length (m)	0.04
Channel height (m)	7.5×10^{-4}
Channel width (m)	7.5×10^{-4}
Rib width (m)	0.0015
GDL width (m)	180×10^{-6}
Porous electrode thickness (m)	100×10^{-6}
Membrane thickness (m)	100×10^{-6}
GDL Porosity	0.5
GDL Electric Conductivity(S/m)	687.5
GDL Permeability (m ²)	3×10^{-12}
Inlet H ₂ Mass Fraction	0.99
Inlet H ₂ O Mass Fraction	0.002
Inlet O ₂ Mass Fraction	0.208
Reference Pressure (Pa)	120×10^3
Cell Voltage (V)	0.6

The comparison is based on polarization curves obtained by experiment and model. Figure 5.1 shows the comparison of experimental data with model result on performance curves for the HT-PEMFC. The figure shows that model results have a good agreement with the experimental results. This means that model is validated with the experiment.

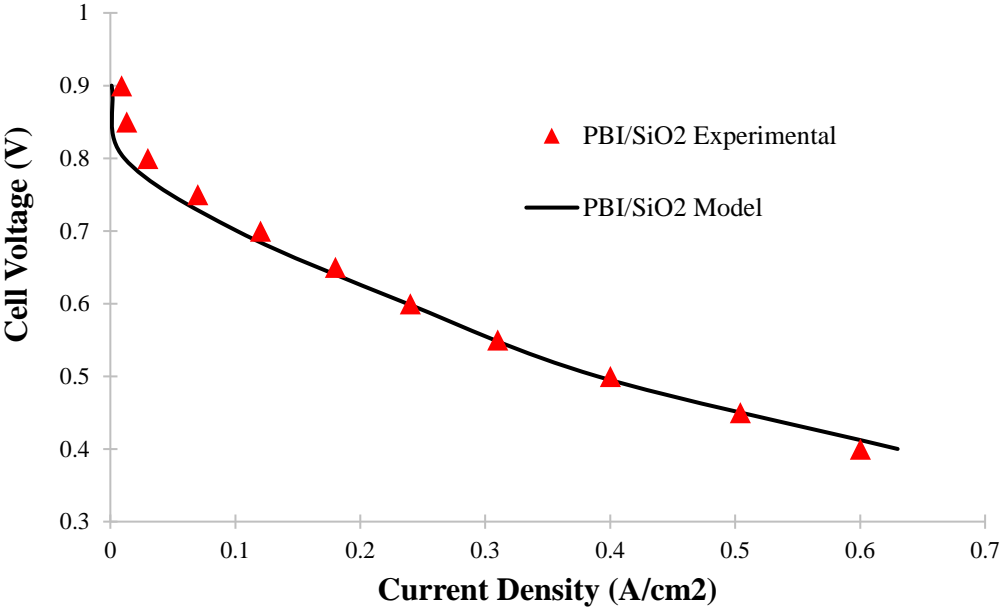


Figure 5.1 Comparison of experimental polarization data with model result for PBI/SiO₂ membrane

The current density distribution at 0.6 V, operating voltage, is given in Figure 5.2. The distribution is uniformly changed along the channel. The color changes from red to blue, which represents that the red parts have highest current densities while blue parts have the lowest.

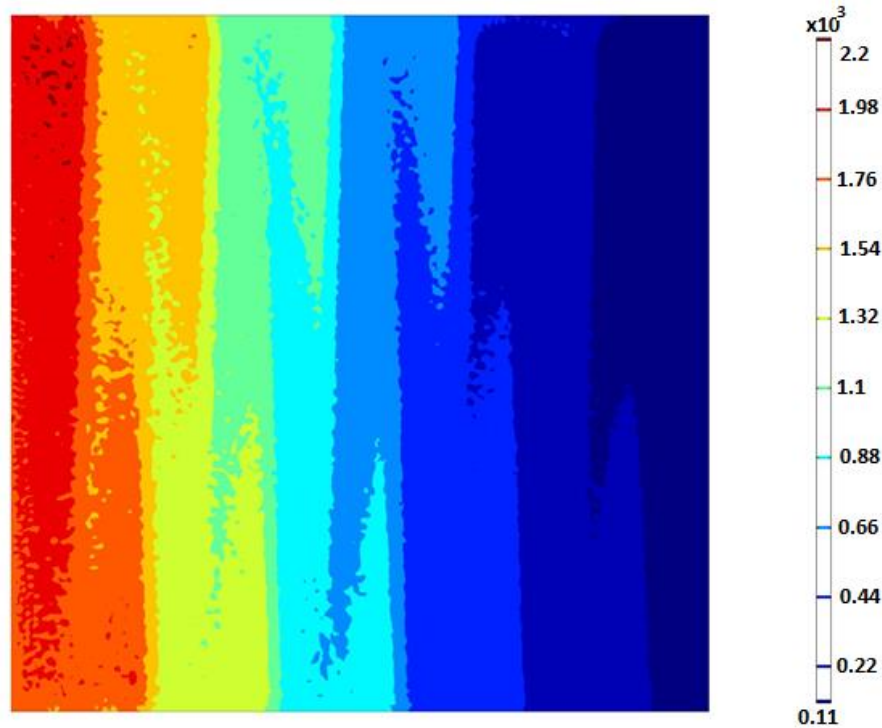


Figure 5.2 Membrane current density distribution at 0.6 V

Figure 5.3, 5.4 and 5.5 show concentration distributions of hydrogen at the anode, oxygen at the cathode and generated water at the cathode side. These profiles are also obtained at the operating voltage, 0.6 V. These concentration profiles, as well as current density distribution, are obtained where inlet velocities of hydrogen and air are same with the experimental values. In Figure 5.3, hydrogen concentration is 32.9 moles/m^3 at the inlet, and it decreases up to 32.8 moles/m^3 toward to outlet since hydrogen is consumed by the reaction. In Figure 5.4, concentration of oxygen at the inlet is 3.9 moles/m^3 and it decreases to 0.05 moles/m^3 at the outlet because oxygen is consumed in order to form water. Produced water concentration profile is illustrated in Figure 5.5. At the inlet, water concentration is 0.05 moles/m^3 , while concentration of produced water reaches to 6.5 moles/m^3 at the outlet.

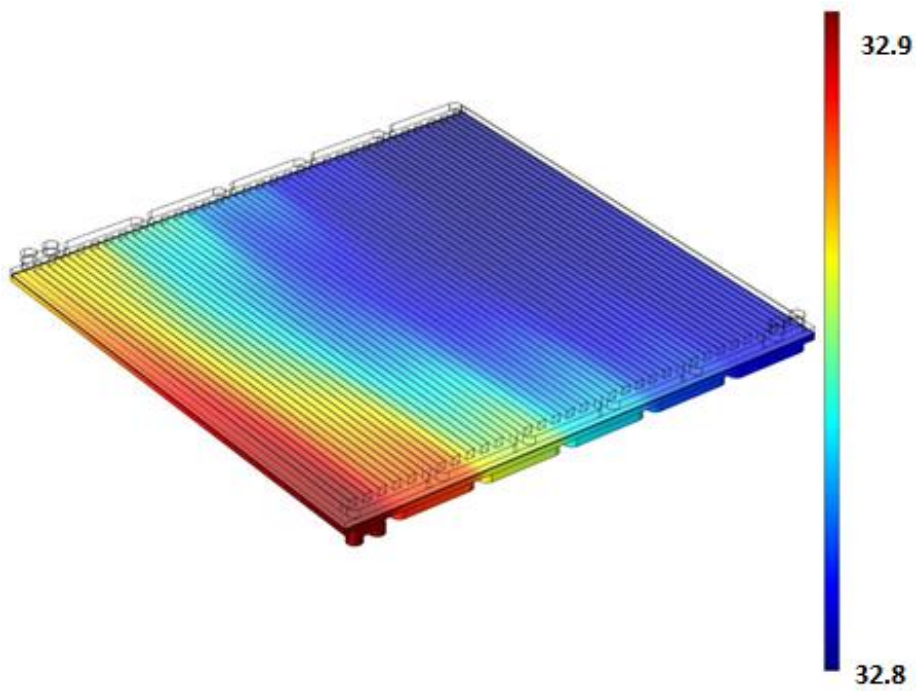


Figure 5.3 Concentration profile for hydrogen at anode, predicted for 0.6 V with PBI/SiO₂ membrane (mol/m³)

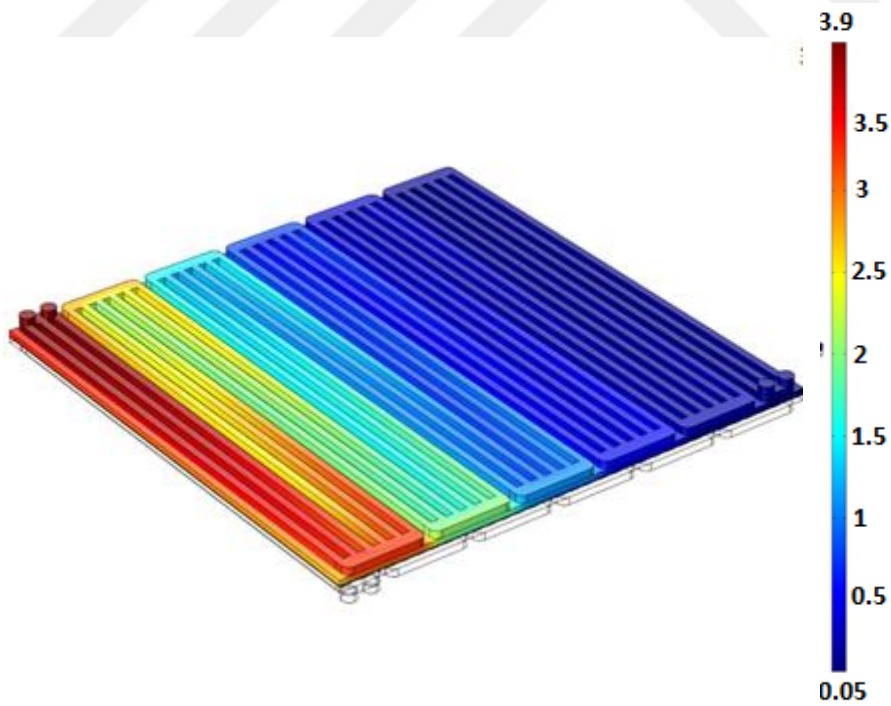


Figure 5.4 Concentration profile for oxygen at cathode, predicted for 0.6 V with PBI/SiO₂ membrane (mol/m³)

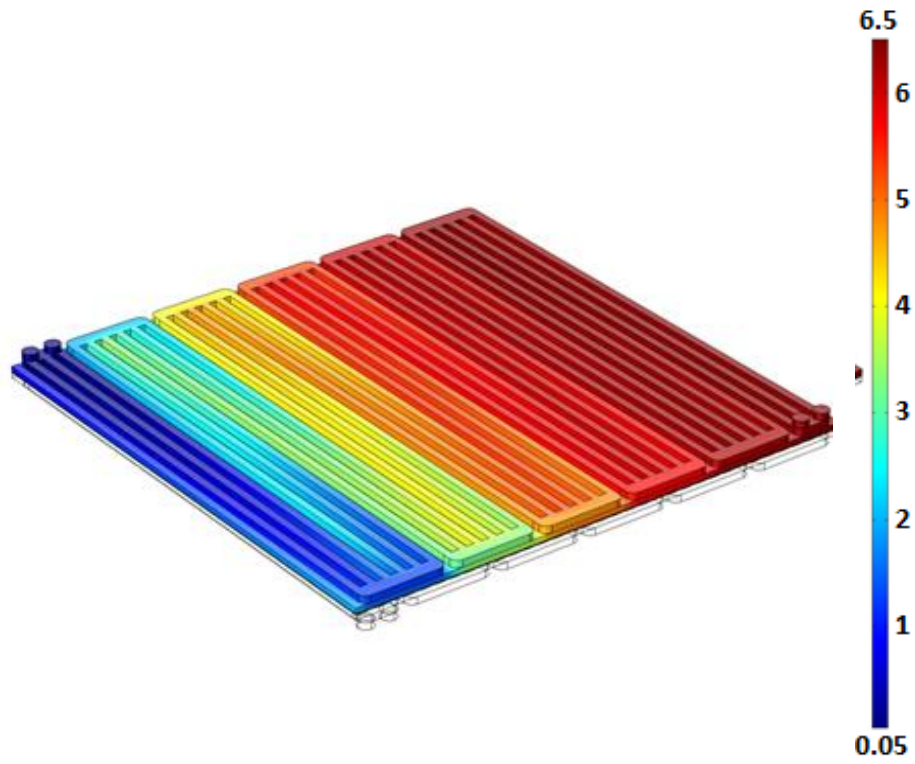


Figure 5.5
Concentration profile for produced water at cathode, predicted for 0.6 V with
PBI/SiO₂ membrane (mol/m³)

5.2. Effect of Proton Conductivity of the Membrane

The influence of the proton conductivity of PBI membrane on the fuel cell performance is significant especially in the ohmic region. Therefore, it can be considered as a critical parameter affecting the fuel cell performance. For this case, comparison of PEM fuel cell performances at different PBI conductivities is pre-estimated by only model results. This comparison is performed for PBI membrane and PBI/SiO₂ membrane and it is shown in Figure 5.6. It can be seen from the figure that lower proton conductivity results lower performance for HT-PEMFC. This low proton conductivity may be resulted due to acid leaching during the process. Therefore, it makes sense that composite PBI membrane has higher proton conductivity than the other and higher fuel cell performance, consequently [52].

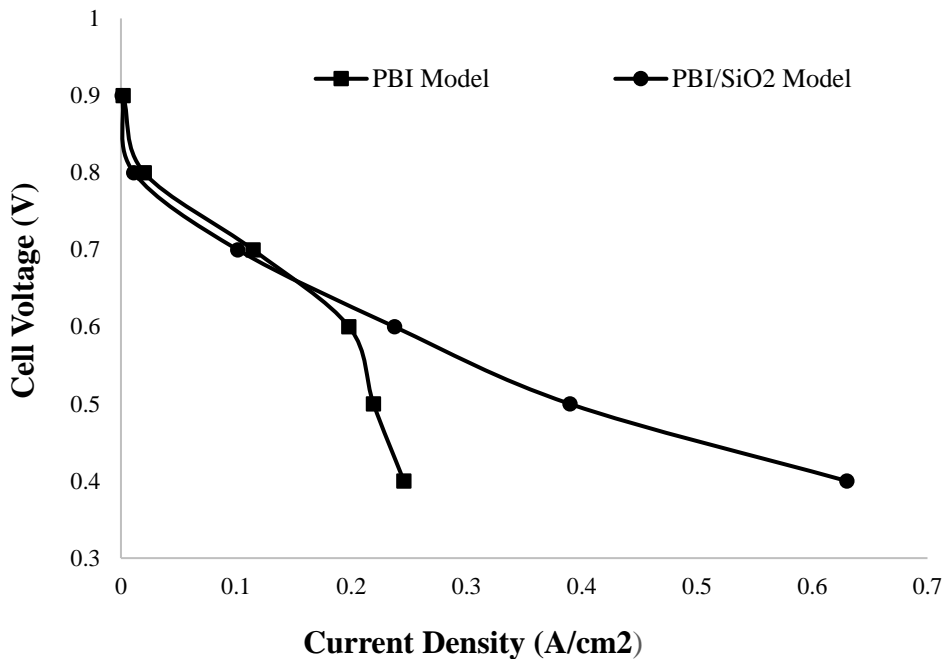


Figure 5.6 Comparison of polarization curves obtained by model for PBI ($\kappa=7.11$ S/m) and PBI/ SiO₂ ($\kappa=8.66$ S/m)

5.3. Effect of Inlet Velocities of Reactants (Hydrogen and Air)

Another critical parameter that affects the fuel cell performance is inlet velocities of hydrogen and air to the anode and cathode sides. In fact, inlet velocities of reactants are directly related with the volumetric flowrates of reactants (by multiplying the cross-sectional area). Dimensions and geometries, and therefore cross-sectional areas can differ for each study. Thus, inlet velocities of reactants also differ from one geometry to another. For this reason, instead of considering volumetric flowrates, consideration of inlet velocities for hydrogen and air would be more accurate for modeling.

Apart from the experimental data, which has 1.5/2.5 stoichiometric ratio (corresponding H₂ inlet velocity=0.884 m/s, Air inlet velocity=3.494 m/s), four different rate of stoichiometric ratios are studied in order to investigate the velocity effect on the performance. Table 5.2 shows the chosen stoichiometric ratios and corresponding inlet velocities for both hydrogen and air. Moreover, the table includes the values used in experiments.

Table 5.2 Different stoichiometric ratios and corresponding inlet velocities of reactants

Stoichiometric Ratio	H₂ Inlet Velocity (m/s)	Air Inlet Velocity (m/s)
1.1/2.0	0.648	2.80
1.5/2.5	0.884	3.494
3.0/5.0	1.764	6.988
3.8/6.3	2.21	8.735
6.0/10.0	3.536	17.47

For the ratio below than 1.5/2.5, the performance of the fuel cell shows significant decrease. However, for further increases above 1.5/2.5, the performance curves starts to shift upward. This can be explained that even if hydrogen flowrate is increased by four times larger, higher performances can be obtained at the presence of enough oxygen to complete the electrochemical reaction. Figure 5.7 shows the effect of inlet velocities on the HT-PEMFC performance.

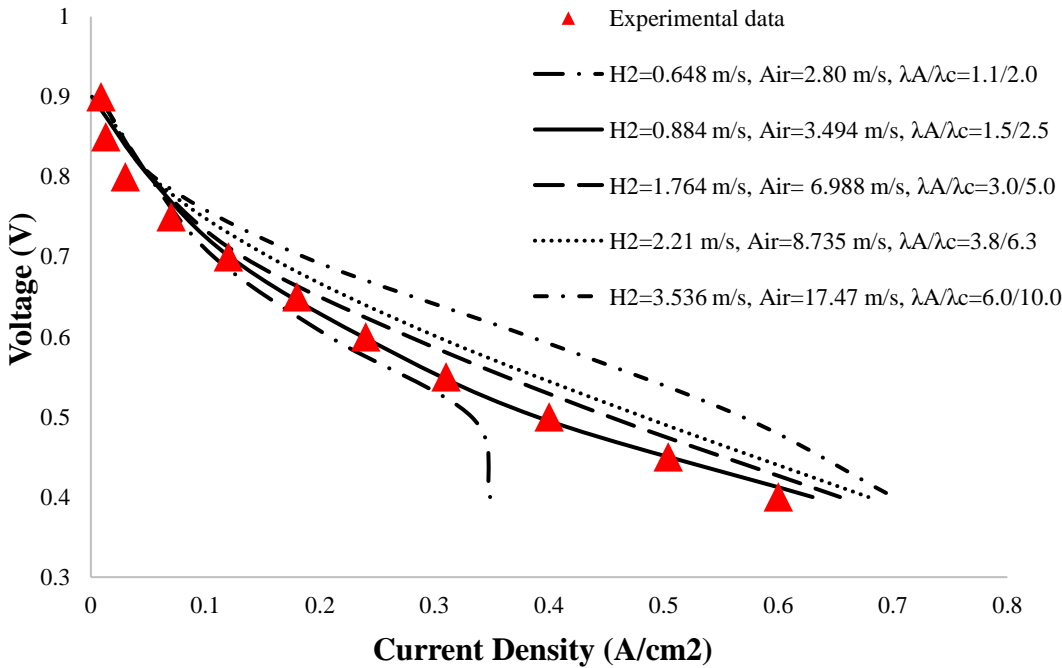


Figure 5.7 Effect of different inlet velocities of hydrogen and air on the high temperature PEM fuel cell performance

5.4. Effect of Meshing Strategy

For modeling, an effective mesh strategy is very important because the computational mesh has a strong influence on the accuracy of the solution. Therefore, meshing strategy should be generated carefully. It is important that the balance of creating enough computational meshes to capture the geometry without creating so many is hard to redress. Number of meshes should not exceed the available memory of meshing computer. In Comsol Multiphysics 5.0, physics controlled meshing strategies is listed as follows: Extremely Coarse< Extra Coarse< Coarser< Coarse< Normal< Fine< Finer< Extra Fine< Extremely Fine. An extremely fine mesh will have small individual elements which may require good hardware and long computational time. Using an extremely coarse mesh can reduce the computational time but it may produce inaccurate simulation results. This balance between mesh detail and computational time must be carefully considered.

In this part of the study, meshing strategy is performed from extremely coarse to extremely fine. For extremely coarse and extra coarse meshes, the meshing process produces meshes with such poor quality that the simulation fails to converge. Therefore, there are no model results for these meshing strategies. However, for coarser, coarse and normal meshing strategies, simulations are able to converge and give results. For further strategies coming after normal mesh cannot be proceeded in the present study because of limited available memory of the meshing computer.

Figure 5.8 shows the effect of meshing strategy on the fuel cell performance. For coarser meshing, computational time takes 1 hr 45 min, while coarse meshing takes 4 hr 30 min and normal meshing takes 8 hrs. As it can be seen from the Figure 5.8, increasing the number of mesh elements makes the results more accurate. In this study, experimental data are compared with the model results. This is an advantage to be able to decide the most effective meshing strategy. Normal meshing strategy is adequate to fit model results with the experimental data. Therefore, it can be said that the most effective mesh strategy is not always

extremely fine, extra fine or finer since the required computation time is too long. It is important keeping number of mesh elements minimum while taking accurate results.

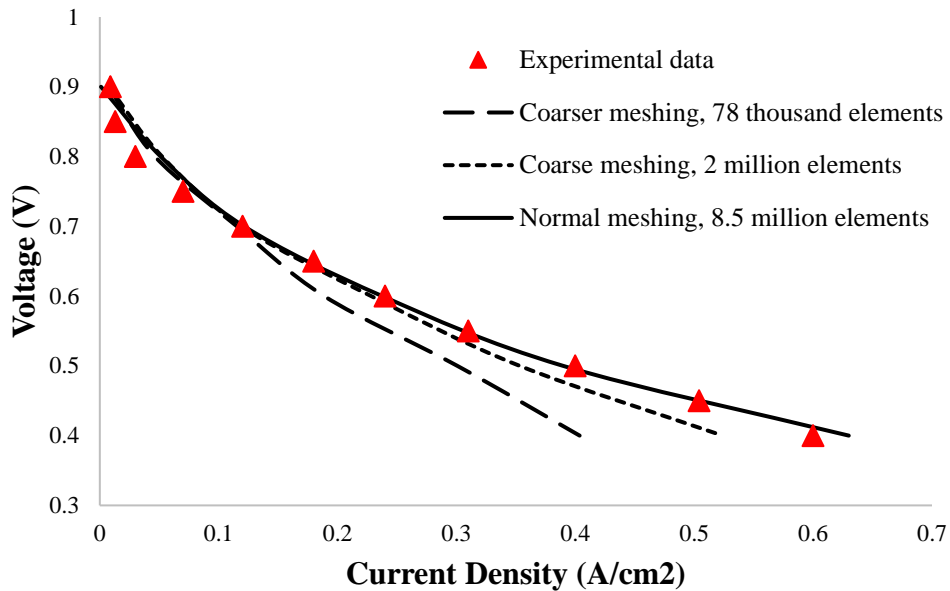


Figure 5.8 Effect of mesh strategy on the HT-PEMFC performance

This meshing strategy fits well with the experimental data between 0.5-0.9 V. For lower voltages, “Coarse” meshing results in lower current densities than “Normal” meshing. Therefore, for the prediction of the current densities at lower voltages, “Normal” meshing should be preferred. All model results, Figure 5.1-5.7, are obtained by “Normal” meshing strategy.

Researchers preferred “Coarse” meshing because of the lower computational time and due to their computer capacity. In a similar study, Çağlayan, has selected “Coarse” mesh size in 3-D modeling of a HT-PEMFC at different operating temperatures. The triple mixed serpentine model consists of 1.3 million elements and the serpentine model consists of 1.6 million elements [25].

Lobato et al. has also concluded that the final solution is very sensitive to the number of mesh elements [19]. They also carried out a sensitivity analysis aiming to determine the best number that balances the calculation time and the solution accuracy in a reasonable calculation time for three different flow channel geometries. They have solved the partial differential equation (PDE) system by Comsol Multiphysics 3.5. However, they did not make a sensitivity analysis for meshing because of their computer specifications. Therefore, it is recommended that for higher accuracies, computational time should be increased on the latest version of the Comsol Multiphysics.





CHAPTER 6

CONCLUSIONS

In this thesis, modeling of HT-PEMFCs is conducted. 3-D, isothermal and steady-state model is developed for two different geometries; single flow channel and multiple flow channel geometries. For multiple flow channel domain, model domain geometry is built in mixed serpentine type. For HT-PEMFC model having single flow channel, properties of PBI membrane which is commercialized by Danish Power Systems are taken as modeling parameter of the polymer membrane. On the other hand, for HT-PEMFC model having multiple flow channels, properties of PBI composite membrane (PBI/SiO₂) are taken as modeling parameter. This PBI based composite membrane is prepared by our research group.

For single flow channel HT-PEMFC modeling at 160°C operating temperature, effects of hydrogen and air inlet velocities on the cell performance are studied, separately. The study has shown that model results are fit with the experimental data especially for ohmic and activation regions. It is seen that increasing inlet velocity of air enhances the cell performance, but at low air inlet velocities, the model underestimates the cell performance. The effect of hydrogen inlet velocity is generally neglected for the previous studies in the literature; however, for high temperature operation it should be taken into account because not all the anode overpotentials are negligible. The model results have revealed that increasing inlet velocity of hydrogen yields increase in the performance if sufficient oxygen is supplied to the system. Moreover, increasing proton conductivity of the membrane shifts the performance curve upward. However, the model result underestimates the performance compared with the experimental data. It is suggested that proton

conductivity of the membrane should be increased in order to obtain best match with the experimental result.

For multiple channel HT-PEMFC modeling at 165°C operating temperature, effects of hydrogen and air inlet velocities on the performance are studied simultaneously by increasing stoichiometric ratios. The model is validated with the experimental data where all the model parameters kept same with the experimental parameters for PBI/SiO₂ membrane. The stoichiometric ratio of the experiment is determined as 1.5/2.5 (H₂/Air) and the model results showed that ratios below 1.5/2.5 has a dramatic increase on the performance curve. On the other hand, higher ratios than 1.5/2.5 show increasing cell performances. In addition, the effect of proton conductivity of the membrane is studied for PBI and PBI/SiO₂ membrane. These two membranes are compared by modeling and it is seen that PBI/SiO₂ gives better performance since it has higher proton conductivity. Effect of meshing strategy is also studied for multiple channels HT-PEMFC modeling. Size of mesh elements affect the accuracy of the obtain results. Mesh study reveals that when the domain is meshed with small size elements, the model results get closer to the experimental results. For the case of this study, “*Normal*” mesh size is determined as the best mesh strategy to catch experimental results.

REFERENCES

- [1] F. Barbir, *PEM fuel cells: theory and practice*. Academic Press, 2013.
- [2] J. T. Pukrushpan, “Modeling and Control of Fuel Cell Systems and Fuel Processors,” *ResearchGate*, Jan. 2003.
- [3] Q. Li, J. O. Jensen, R. F. Savinell, and N. J. Bjerrum, “High temperature proton exchange membranes based on polybenzimidazoles for fuel cells,” *Prog. Polym. Sci.*, vol. 34, no. 5, pp. 449–477, May 2009.
- [4] J. Zhang *et al.*, “High temperature PEM fuel cells,” *J. Power Sources*, vol. 160, no. 2, pp. 872–891, Oct. 2006.
- [5] Y. Shao, G. Yin, Z. Wang, and Y. Gao, “Proton exchange membrane fuel cell from low temperature to high temperature: Material challenges,” *J. Power Sources*, vol. 167, no. 2, pp. 235–242, May 2007.
- [6] D. Feroldi and M. Basualdo, “Description of PEM Fuel Cells System,” in *PEM Fuel Cells with Bio-Ethanol Processor Systems*, M. S. Basualdo, D. Feroldi, and R. Outbib, Eds. London: Springer London, 2012, pp. 49–72.
- [7] Z. Jiang and Z.-J. Jiang, *Carbon Nanotubes Supported Metal Nanoparticles for the Applications in Proton Exchange Membrane Fuel Cells (PEMFCs)*. INTECH Open Access Publisher, 2011.
- [8] Y.-L. Ma, J. S. Wainright, M. H. Litt, and R. F. Savinell, “Conductivity of PBI Membranes for High-Temperature Polymer Electrolyte Fuel Cells,” *J. Electrochem. Soc.*, vol. 151, no. 1, pp. A8–A16, Jan. 2004.
- [9] M. Mamlouk and K. Scott, “The effect of electrode parameters on performance of a phosphoric acid-doped PBI membrane fuel cell,” *Int. J. Hydrog. Energy*, vol. 35, no. 2, pp. 784–793, Jan. 2010.

- [10] J. S. Yang *et al.*, “High Molecular Weight Polybenzimidazole Membranes for High Temperature PEMFC,” *Fuel Cells*, vol. 14, no. 1, pp. 7–15, Feb. 2014.
- [11] H. A. Hjuler, T. Steenberg, C. Terkelsen, T. Holst, H. R. Garcia, and K. Cooper, “Performance of the HT-PEM Membrane Electrode Assembly,” *ECS Trans.*, vol. 50, no. 2, pp. 1127–1135, Mar. 2013.
- [12] S. Subianto, “Recent advances in polybenzimidazole/phosphoric acid membranes for high-temperature fuel cells: Recent advances in polybenzimidazole/phosphoric acid membranes,” *Polym. Int.*, vol. 63, no. 7, pp. 1134–1144, Jul. 2014.
- [13] A. A. Lysova, I. I. Ponomarev, and A. B. Yaroslavtsev, “Composite materials based on polybenzimidazole and inorganic oxides,” *Solid State Ion.*, vol. 188, no. 1, pp. 132–134, Apr. 2011.
- [14] Y. Devrim, H. Devrim, and I. Eroglu, “Polybenzimidazole/SiO₂ hybrid membranes for high temperature proton exchange membrane fuel cells,” *Int. J. Hydrog. Energy*, vol. 41, no. 23, pp. 10044–10052, Jun. 2016.
- [15] S. Litster and G. McLean, “PEM fuel cell electrodes,” *J. Power Sources*, vol. 130, no. 1–2, pp. 61–76, May 2004.
- [16] S. Park, J.-W. Lee, and B. N. Popov, “A review of gas diffusion layer in PEM fuel cells: Materials and designs,” *Int. J. Hydrog. Energy*, vol. 37, no. 7, pp. 5850–5865, Apr. 2012.
- [17] H. Tawfik, Y. Hung, and D. Mahajan, “Metal bipolar plates for PEM fuel cell—A review,” *J. Power Sources*, vol. 163, no. 2, pp. 755–767, Jan. 2007.
- [18] A. Hermann, T. Chaudhuri, and P. Spagnol, “Bipolar plates for PEM fuel cells: A review,” *Int. J. Hydrog. Energy*, vol. 30, no. 12, pp. 1297–1302, Sep. 2005.
- [19] J. Lobato, P. Cañizares, M. A. Rodrigo, F. J. Pinar, and D. Úbeda, “Study of flow channel geometry using current distribution measurement in a high temperature polymer electrolyte membrane fuel cell,” *J. Power Sources*, vol. 196, no. 9, pp. 4209–4217, May 2011.

- [20] H. Ju and C.-Y. Wang, "Experimental Validation of a PEM Fuel Cell Model by Current Distribution Data," *J. Electrochem. Soc.*, vol. 151, no. 11, p. A1954, 2004.
- [21] D. Cheddie and N. Munroe, "Mathematical model of a PEMFC using a PBI membrane," *Energy Convers. Manag.*, vol. 47, no. 11–12, pp. 1490–1504, Jul. 2006.
- [22] D. F. Cheddie and N. D. H. Munroe, "Three dimensional modeling of high temperature PEM fuel cells," *J. Power Sources*, vol. 160, no. 1, pp. 215–223, Sep. 2006.
- [23] O. Shamardina, A. Chertovich, A. A. Kulikovsky, and A. R. Khokhlov, "A simple model of a high temperature PEM fuel cell," *Int. J. Hydrog. Energy*, vol. 35, no. 18, pp. 9954–9962, Sep. 2010.
- [24] J. Lobato, P. Cañizares, M. A. Rodrigo, F. J. Pinar, E. Mena, and D. Úbeda, "Three-dimensional model of a 50 cm² high temperature PEM fuel cell. Study of the flow channel geometry influence," *Int. J. Hydrog. Energy*, vol. 35, no. 11, pp. 5510–5520, Jun. 2010.
- [25] D. G. Caglayan, B. Sezgin, Y. Devrim, and I. Eroglu, "Three-dimensional modeling of a high temperature polymer electrolyte membrane fuel cell at different operation temperatures," *Int. J. Hydrog. Energy*, vol. 41, no. 23, pp. 10060–10070, Jun. 2016.
- [26] T. E. Springer, T. A. Zawodzinski, and S. Gottesfeld, "Polymer electrolyte fuel cell model," *J. Electrochem. Soc.*, vol. 138, no. 8, pp. 2334–2342, 1991.
- [27] M. Wöhr, K. Bolwin, W. Schnurnberger, M. Fischer, W. Neubrand, and G. Eigenberger, "Dynamic modelling and simulation of a polymer membrane fuel cell including mass transport limitation," *Int. J. Hydrog. Energy*, vol. 23, no. 3, pp. 213–218, Mar. 1998.
- [28] V. Gurau, H. Liu, and S. Kakac, "Two-dimensional model for proton exchange membrane fuel cells," *AIChE J.*, vol. 44, no. 11, pp. 2410–2422, 1998.
- [29] N. P. Siegel, M. W. Ellis, D. J. Nelson, and M. R. von Spakovsky, "A two-dimensional computational model of a PEMFC with liquid water transport," *J. Power Sources*, vol. 128, no. 2, pp. 173–184, Apr. 2004.

- [30] M. Hu, A. Gu, M. Wang, X. Zhu, and L. Yu, "Three dimensional, two phase flow mathematical model for PEM fuel cell: Part I. Model development," *Energy Convers. Manag.*, vol. 45, no. 11–12, pp. 1861–1882, Jul. 2004.
- [31] P. T. Nguyen, T. Berning, and N. Djilali, "Computational model of a PEM fuel cell with serpentine gas flow channels," *J. Power Sources*, vol. 130, no. 1–2, pp. 149–157, May 2004.
- [32] R. Sousa and E. R. Gonzalez, "Mathematical modeling of polymer electrolyte fuel cells," *J. Power Sources*, vol. 147, no. 1–2, pp. 32–45, Sep. 2005.
- [33] A. D. Le and B. Zhou, "A general model of proton exchange membrane fuel cell," *J. Power Sources*, vol. 182, no. 1, pp. 197–222, Jul. 2008.
- [34] K. Scott, S. Pilditch, and M. Mamlouk, "Modelling and experimental validation of a high temperature polymer electrolyte fuel cell," *J. Appl. Electrochem.*, vol. 37, no. 11, pp. 1245–1259, Oct. 2007.
- [35] E. U. Ubong, Z. Shi, and X. Wang, "Three-Dimensional Modeling and Experimental Study of a High Temperature PBI-Based PEM Fuel Cell," *J. Electrochem. Soc.*, vol. 156, no. 10, p. B1276, 2009.
- [36] M. Kvesić, U. Reimer, D. Froning, L. Lüke, W. Lehnert, and D. Stolten, "3D modeling of a 200 cm² HT-PEFC short stack," *Int. J. Hydrog. Energy*, vol. 37, no. 3, pp. 2430–2439, Feb. 2012.
- [37] A. Su, Y. M. Ferng, J. Hou, and T. L. Yu, "Experimental and numerical investigations of the effects of PBI loading and operating temperature on a high-temperature PEMFC," *Int. J. Hydrog. Energy*, vol. 37, no. 9, pp. 7710–7718, May 2012.
- [38] P. Chippar and H. Ju, "Numerical modeling and investigation of gas crossover effects in high temperature proton exchange membrane (PEM) fuel cells," *Int. J. Hydrog. Energy*, vol. 38, no. 18, pp. 7704–7714, Jun. 2013.
- [39] B. Sezgin, D. G. Caglayan, Y. Devrim, T. Steenberg, and I. Eroglu, "Modeling and sensitivity analysis of high temperature PEM fuel cells by using Comsol Multiphysics," *Int. J. Hydrog. Energy*, vol. 41, no. 23, pp. 10001–10009, Jun. 2016.

- [40] D. Ouellette, C. O. Colpan, E. Matida, and C. A. Cruickshank, “A single domain approach to modeling the multiphase flow within a flowing electrolyte – direct methanol fuel cell,” *Int. J. Hydrog. Energy*, vol. 40, no. 24, pp. 7817–7828, Jun. 2015.
- [41] D. Ouellette, C. O. Colpan, E. Matida, C. A. Cruickshank, and F. Hamdullahpur, “A comprehensive 1D model of a flowing electrolyte-direct methanol fuel cell with experimental validation: A comprehensive 1D model of a FE-DMFC with experimental validation,” *Int. J. Energy Res.*, vol. 39, no. 1, pp. 33–45, Jan. 2015.
- [42] O. F. Atacan, D. Ouellette, and C. O. Colpan, “Two-dimensional multiphase non-isothermal modeling of a flowing electrolyte – Direct methanol fuel cell,” *Int. J. Hydrog. Energy*, Jul. 2016.
- [43] M. Khakpour and K. Vafai, “Analysis of transport phenomena within PEM fuel cells – An analytical solution,” *Int. J. Heat Mass Transf.*, vol. 51, no. 15–16, pp. 3712–3723, Jul. 2008.
- [44] “Modeling of HTPEM Fuel Cell Start-Up Process by Using COMSOL Multiphysics.” [Online]. Available: <https://www.comsol.com/paper/modeling-of-htpem-fuel-cell-start-up-process-by-using-comsol-multiphysics-13474>. [Accessed: 07-Oct-2016].
- [45] N. Zamel and X. Li, “Non-isothermal multi-phase modeling of PEM fuel cell cathode,” *Int. J. Energy Res.*, vol. 34, no. 7, pp. 568–584, Jun. 2010.
- [46] Z. Shi and X. Wang, “Two-Dimensional PEM Fuel Cells Modeling using COMSOL Multiphysics,” in *Modelling and Simulation*, G. Petrone and G. Cammarat, Eds. I-Tech Education and Publishing, 2008.
- [47] “Mass Transport Analysis of a High Temperature PEM Fuel Cell.” [Online]. Available: <https://www.comsol.com/model/mass-transport-analysis-of-a-high-temperature-pem-fuel-cell-8550>. [Accessed: 07-Oct-2016].
- [48] C. Wannek, W. Lehnert, and J. Mergel, “Membrane electrode assemblies for high-temperature polymer electrolyte fuel cells based on poly(2,5-benzimidazole) membranes with phosphoric acid impregnation via the catalyst layers,” *J. Power Sources*, vol. 192, no. 2, pp. 258–266, Jul. 2009.

- [49] J.-T. Wang, J. S. Wainright, R. F. Savinell, and M. Litt, “A direct methanol fuel cell using acid-doped polybenzimidazole as polymer electrolyte,” *J. Appl. Electrochem.*, vol. 26, no. 7, pp. 751–756.
- [50] T. Henriques, B. César, and P. J. C. Branco, “Increasing the efficiency of a portable PEM fuel cell by altering the cathode channel geometry: A numerical and experimental study,” *Appl. Energy*, vol. 87, no. 4, pp. 1400–1409, Apr. 2010.
- [51] D. F. Cheddie and N. D. H. Munroe, “A two-phase model of an intermediate temperature PEM fuel cell,” *Int. J. Hydrog. Energy*, vol. 32, no. 7, pp. 832–841, May 2007.
- [52] Y. Özdemir, N. Üregen, and Y. Devrim, “Polybenzimidazole based nanocomposite membranes with enhanced proton conductivity for high temperature PEM fuel cells,” *Int. J. Hydrog. Energy*, May 2016.

APPENDIX A

COMPUTER SPECIFICATIONS

Brand/Model Information Dell XPS 8700

Processor Specifications

Processor
Intel

Processor Cache
8 MB

Processor Speed
4.00 GHz

Processor Model
Intel Core i7-4790

Processor Type
4. Generation Intel Core i7

Operating System

Licensed
Windows 8.1 64-Bit

Display Card	Display Card Memory
	4GB
	Display Card Model
	nVidia GeForce GTX 745
	Display Card Type
	External Display Card

Memory Properties	Memory Frequency
	1600Mhz
	Memory Capacity
	16GB
	Memory Type
	DDR3
	Memory Bank
	4 Slot

Disk Properties	Disk Speed
	7200 rpm
	Disk Capacity
	2TB
	Disk Type
	SATA

Extension Slot Properties	PCI
	Mini-PCIe : 2 Slot
	PCI Express x1
	x1: 2 slot
	PCI Express x16
	PCIe x16 (Graphics): 1 slot

Link Properties	Bluetooth
	Yes
	Display Output
	VGA, HDMI
	Ethernet
	10/100/1000

Wireless Card
Dell Wireless 1703

Card Reader
Yes

Other Properties	Keyboard & Mouse
	Dell KM632 Wireless Mouse and Keyboard
	Optical Reader
	Yes
	Power Supply
	460W up to 85 Efficient



APPENDIX B

EXPERIMENTAL SET-UP

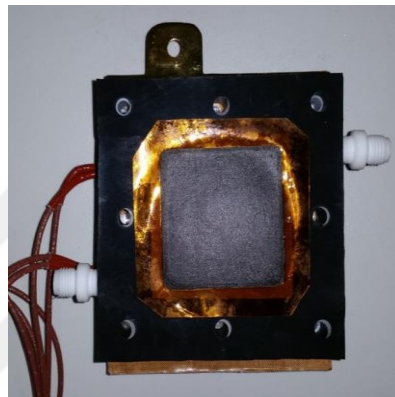


Figure B.6.1 Prepared MEA including PBI/SiO₂ membrane

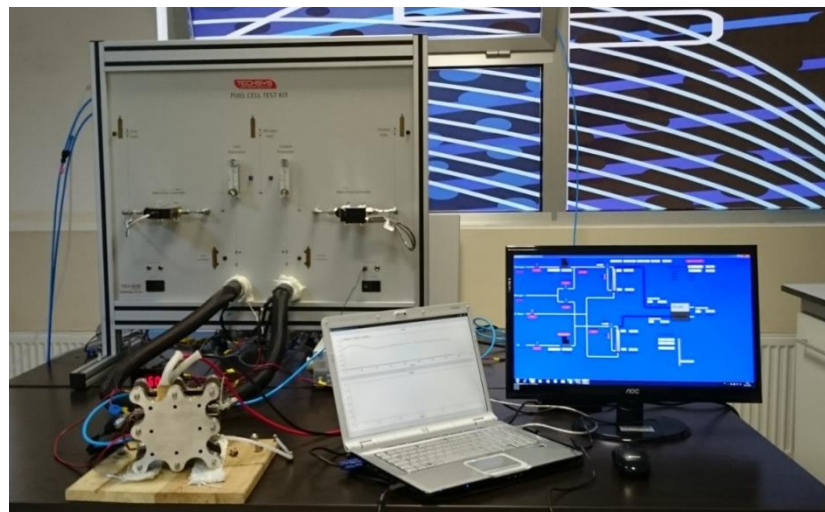


Figure B.2 PEMFC test station